TECHNISCHE UNIVERSITÄT MÜNCHEN
TUM School of Engineering and Design

Uncertainties due to river boundary conditions during extreme events

Pablo Alejandro Merchán-Rivera

Vollständiger Abdruck der von der TUM School of Engineering and Design der Technischen Universität München zur Erlangung des akademischen Grades eines

Doktor der Ingenieurwissenschaften (Dr.-Ing.)

genehmigten Dissertation.

Vorsitz:	Prof. Dr.-Ing. Michael Manhart
Prüfer*innen der Dissertation:	1. Prof. Dr. rer. nat. habil. Gabriele Chiogna
	2. Prof. Dr.-Ing. Markus Disse
	3. Prof. Dr. Giovanni Porta (Polytechnic University of Milan)

Die Dissertation wurde am 27.04.2022 bei der Technischen Universität München eingereicht und durch die TUM School of Engineering and Design am 15.06.2022 angenommen.

"… but your ignorance should worry you far more
than the unknown, my dear."

– A WISE 3D RENDERING –

Contents

Abstract

The interactions between rivers and aquifers play a fundamental role in the fate, transport, and transformation of solutes, pollutants, and nutrients in the subsurface. Fluctuating stream stages and peak-flow episodes associated with extreme events, such as groundwater flooding and hydropeaking, can significantly influence the dynamics between streams and aquifers, modifying hydraulic gradients, flux exchange, and the subsurface flow paths. The usual practice to study what occurs under the hood is the application of numerical groundwater models, where the streams and rivers are expressed as boundary conditions. However, uncertainties associated with input data, model parameters, numerical implementation, process conceptualization, scale, and discretization may lead to a poor understanding. This dissertation investigates the interaction between rivers and aquifers during two types of extreme events, e.g., groundwater flooding and hydropeaking. The main objective is to characterize flow and transport processes in the groundwater under uncertain river boundary conditions and quantify the propagation of uncertainty using formal stochastic techniques. In addition, the research also aims to propose a series of methodological frameworks for the quantification of uncertainty to be applied in similar modeling exercises. Four scientific publications are part of this cumulative dissertation. A broad spectrum of sensitivity and uncertainty analysis techniques is applied, including scenario modeling, linear uncertainty analysis, screening sensitivity analysis, Bayesian inference, spectral expansions, and discrete collocation projections. The investigations include the spatiotemporal quantification of flow field features as efficient alternatives for describing transport processes and mixing in groundwater. Overall, the results of this dissertation include the quantification of uncertainty employing deterministic scenario modeling and formal stochastic approaches; the detailed quantification of spatial and temporal responses of the groundwater flow and the flow field to the dynamics of the river boundary conditions, and the description of the spatiotemporal evolution of the uncertainty; and, the characterization of flow and transport processes in the subsurface in probabilistic terms by identifying non-trivial flow features (i.e., stagnation zones, reverse flow, and Okubo-Weiss metric). Relevant contributions include the development of a Bayesian framework for assessing the risk of groundwater flooding and a framework based on polynomial chaos expansions for identifying elusive and non-trivial flow features in probabilistic terms.

Zusammenfassung

Die Wechselwirkungen zwischen Flüssen und Grundwasserleitern spielen eine grundlegende Rolle für den Verbleib, den Transport und die Umwandlung von gelösten Stoffen, Schadstoffen und Nährstoffen im Untergrund. Schwankende Wasserstände und Abflussspitzen im Zusammenhang mit Extremereignissen (z. B. Grundwasserüberschwemmungen und Schwallbetrieb) können die Dynamik zwischen Fließgewässern und Grundwasserleitern erheblich beeinflussen und die hydraulischen Gradienten, den Flussaustausch und die unterirdischen Fließwege verändern. Um zu untersuchen, was unter der Wasseroberfläche geschieht, werden in der Regel numerische hydrologische Modelle eingesetzt, und Flüsse werden als Randbedingungen dargestellt. Allerdings können Unsicherheiten im Zusammenhang mit den Eingangsdaten, den Modellparametern, der numerischen Implementierung, der Prozesskonzeption, der Skala und der Diskretisierung zu einem unzureichenden Systemverständnis führen. In dieser Dissertation wird die Wechselwirkung zwischen Flüssen und Grundwasserleitern bei Grundwasserüberflutungen und Schwallereignissen untersucht. Das Hauptziel besteht darin, die Strömungs- und Transportprozesse im Grundwasser unter unsicheren Flussrandbedingungen zu charakterisieren und die Ausbreitung der Unsicherheit mit Hilfe formaler stochastischer Techniken zu quantifizieren. Darüber hinaus zielt diese Arbeit darauf ab, eine Reihe von methodischen Frameworks für die Quantifizierung von Unsicherheiten vorzuschlagen, die bei ähnlichen Modellierungsaufgaben angewendet werden können. Vier wissenschaftliche Veröffentlichungen sind Teil dieser kumulativen Dissertation. Es wird ein breites Spektrum von Sensitivitäts- und Unsicherheitsanalysetechniken angewandt, darunter Szenarienmodellierung, lineare Unsicherheitsanalyse, Screening-Sensitivitätsanalyse, Bayes'sche Inferenz, spektrale Erweiterungen und diskrete Kollokationsprojektionen. Die Untersuchungen umfassen die raum-zeitliche Quantifizierung von Strömungsfeldmerkmalen als effiziente Alternativen zur Beschreibung von Transportprozessen und Vermischung im Grundwasser. Insgesamt umfassen die Ergebnisse dieser Dissertation die Quantifizierung der Unsicherheit unter Verwendung deterministischer Szenarienmodellierung und formaler stochastischer Ansätze, die detaillierte Quantifizierung der räumlichen und zeitlichen Reaktionen der Grundwasserströmung und des Strömungsfeldes auf die Dynamik der Flussrandbedingungen und die Beschreibung der räumlich-zeitlichen Entwicklung der

Unsicherheit sowie die Charakterisierung von Strömungs- und Transportprozessen im Untergrund in probabilistischer Hinsicht durch die Identifizierung nicht-trivialer Strömungsmerkmale (d.h. Stagnationszonen, Rückströmung und Okubo-Weiss-Metrik). Zu den relevanten Beiträgen gehören die Entwicklung eines Bayes'schen Frameworks für die Bewertung des Risikos von Grundwasserüberschwemmungen und eines auf polynomialen Chaos-Erweiterungen basierenden Frameworks für die Identifizierung schwer fassbarer und nicht-trivialer Strömungsmerkmale unter probabilistischer Betrachtung.

Affidavit

I hereby declare that the work presented in this Doctoral thesis is authentic and original unless clearly indicated otherwise, and in such instances full reference to the source is provided. I further declare that no unethical research practices were used. This dissertation was not submitted in the same or in a substantially similar version to another examination board.

Munich, April 4th, 2022

Pablo Merchán-Rivera

Acknowledgments

This dissertation represents a snapshot of knowledge and theories in the field of uncertainty quantification in hydrology. It is also a snapshot of four years of doctoral research. A path that I enjoyed but that was not free of challenges, glitches, and virus variants. Fortunately, I was not alone, and I would like to acknowledge all the people without whom I would not have made it through these years.

First, I owe my deepest gratitude to Prof. Dr. Gabriele Chiogna. Thank you for providing friendly guidance and support throughout this project. I am glad and grateful for having such a great supervisor. Thank you also for trusting me since my master's degree began. Special thanks to Prof. Markus Disse for the opportunity to be part of this fantastic research group and for the friendly support during these years.

I would like to thank Prof. Dr. Giovanni Porta for his kind willingness to take part in the Examination Board. Thank you as well to Prof. Dr.-Ing. Michael Manhart for accepting to participate as Chairman of my doctoral defense.

I want to acknowledge the support of my dear country, reflected in the grant CZO2-11621 of the Secretaría Nacional de Educación, Ciencia y Tecnología de Ecuador (SENESCYT), which back a significant part of my doctoral research.

Thank you to the UNMIX and Hydromix team (Mónica Basilio Hazas, Daniel Bittner, Giorgia Marcolini, Steven Mattis, Tanu Singh, Mario Texeira Parente, and Francesca Ziliotto) for the great discussions and feedback. Furthermore, thanks to Prof. Dr. Barbara Wohlmuth for her support and contribution, which help me to explore the mathematical techniques of this dissertation with much more confidence.

I want to say thank you to the Chair of Hydrology and River Basin Management staff, which made this a pleasant and welcoming workplace. Particularly, thanks to Christiane Zach-Cretaine for her incredible support and patience.

I would also like to thank all of the persons who contributed to my work in different ways during the last four years: Danika Ahoor, Mohammad Alqadi, Punit Bhola, Alexandra

Elbakyan, Alexandra Geist, Wesley Henson, Florentin Hofmeister, Jingshui Huang, Fabian Merk, Soukaina Mourchid, Santiago Osorio, Teresa Pérez Ciria, Francesca Perosa, Rebecca Schill, Claire Sembera, Michael Tarantik. I sincerely apologize to everyone I forgot on this list.

I want to include in this acknowledgment all the authors and contributors of the various Python libraries used in this work for their enormous contribution to science and education.

To close with a flourish, I want to thank my family for their love and unconditional support. María Elena, Iván, Jorge, and Daniel, all this work belongs to you because all I am is thanks to you. Thanks to all my big family in Ecuador. I felt your support in every step. Thanks to Mounia Lahmouri for walking on my side. Her motivation and encouragement are the reason why you are reading this work. Thank you, Mounia, for sharing the good and the bad during these last years. Thank you for making me feel that you are always there for me.

Scientific contributions

Research articles

Title:	Propagation of Hydropeaking Waves in Heterogeneous Aquifers: Effects on Flow Topology and Uncertainty Quantification
Authors:	**Merchán-Rivera, P.[(1)]**, Basilio Hazas, M.[(2)], Marcolini, G.[(3)], Chiogna, G.[(4)]
Journal:	International Journal on Geomathematics (submitted)
Contributions:	(1) conceptualization, data curation, formal analysis, funding acquisition, investigation, methodology, software, validation, visualization, and writing - original draft, writing - review & editing; (2) conceptualization, data curation, formal analysis, investigation, methodology, writing - original draft; (3) conceptualization, data curation, formal analysis, investigation, methodology, writing - original draft; (4) conceptualization, methodology, investigation, supervision, project administration, writing - original draft, writing – review & editing

Title:	A Bayesian Framework to Assess and Create Risk Maps of Groundwater Flooding
Authors:	**Merchán-Rivera, P.[(1)]**, Geist, A.[(2)], Disse, M.[(3)], Huang, J.[(4)], Chiogna, G.[(5)]
Journal:	Journal of Hydrology (published)
Contributions:	(1) conceptualization, data curation, formal analysis, investigation, methodology, software, visualization, and writing - original draft, writing - review & editing; (2) validation, formal analysis, investigation, writing - original draft; (3) conceptualization, resources, writing - review & editing, supervision; (4) conceptualization, writing – review & editing; (5) conceptualization, methodology, project administration, supervision, investigation, writing – review & editing

Title:	Identifying Stagnation Zones and Reverse Flow Caused by River-Aquifer Interaction: An Approach Based on Polynomial Chaos Expansions
Authors:	**Merchán-Rivera, P.[(1)]**, Wohlmuth, B.[(2)], Chiogna, G.[(3)]
Journal:	Water Resources Research (published)
Contributions:	(1) conceptualization, data curation, formal analysis, funding acquisition, investigation, methodology, resources, software, validation, visualization, writing - original draft, writing - review & editing; (2) conceptualization, formal analysis, methodology, project administration, validation, supervision, writing - review & editing; (3) conceptualization, formal analysis, methodology, supervision, project administration, writing - original draft, writing – review & editing

Title:	Surface Water and Groundwater Interaction During Flood Events in the Alz Valley: Numerical Modeling and Solute Transport Simulations
Authors:	**Merchán-Rivera, P.**[(1)], Chiogna, G.[(2)], Disse, M.[(3)], Bhola, P.[(4)]
Journal:	Agua Subterránea (published)
Contributions:	(1) conceptualization, data curation, formal analysis, funding acquisition, investigation, methodology, software, visualization, and writing - original draft, writing - review & editing; (2) conceptualization, funding acquisition, investigation, methodology, project administration, supervision, investigation, writing – review & editing; (3) resources, supervision, writing - review & editing, supervision; (4) data curation, formal analysis, investigation, writing – review & editing

Conferences and talks

Title:	Polynomial Chaos Expansions for Identifying Stagnation Zones and Reverse Flow Caused by River-Aquifer Interactions
Authors:	**Merchán-Rivera, P.**, Wohlmuth, B., Chiogna, G.
Event:	SIAM Conference on Mathematical and Computational Issues in the Geosciences
Place and date:	Milan (Italy), 23.06.2021

Title:	Numerical Models: Theory, applications and implementation
Authors:	**Merchán-Rivera, P.**
Event:	Ministry of Environment of Ecuador
Place and date:	Quito (Ecuador), 23.12.2019

Title:	Uncertainties due to boundary conditions in predicting mixing in groundwater
Authors:	Chiogna, G., **Merchán-Rivera, P.**, Basilio Hazas, M., Bittner, D., Texeira Parente
Event:	IGSSE Martini Colloquium
Place and date:	Munich (Germany), 08.11.2019

Title:	Comparative Analysis of Groundwater Modeling Software to Describe the Interaction Between Surface Water and Groundwater During Floods
Authors:	**Merchán-Rivera, P.**, Chiogna, G., Disse, M.
Event:	SIAM Conference on Mathematical and Computational Issues in the Geosciences
Place and date:	Houston (USA), 11.03.2019

Title:	Conceptual and numerical models for groundwater contamination
Authors:	**Merchán-Rivera, P.**
Event:	Hidrogeocol Ecuador Cía. Ltda,
Place and date:	Quito (Ecuador), 07.11.2018

Title:	Interaction between surface water and groundwater during flood events
Authors:	**Merchán-Rivera, P.**, Disse, M., Bhola, P., Chiogna, G.
Event:	Ciclo de Conferencias EPN
Place and date:	Quito (Ecuador), 31.10.2018

Title:	Surface water and groundwater interaction during flood events in the Alz Valley: Numerical modeling and solute transport simulations
Authors:	**Merchán-Rivera, P.**, Chiogna, G., Disse, M., Bhola, P.
Event:	XIV Congreso Latinoamericano de Hidrogeología
Place and date:	Salta (Argentina), 23.10.2018

Posters

Title:	UNMIX – Uncertainties due to boundary conditions in predicting mixing in groundwater
Authors:	Basilio Hazas, M., **Merchán-Rivera, P.**, Bittner, D., Texeira Parente, M., Mattis, S., Wohlmuth, B., Chiogna, G.
Event:	IGSSE Forum 2019
Place and date:	Raitenhaslach (Germany), 25.06.2019

Title:	Effect of river boundary conditions on groundwater flow and solute transport during a flood event
Authors:	**Merchán-Rivera, P.**, Disse, M., Bhola, P., Chiogna, G.,
Event:	Annual Doctoral Seminar - Karlsruher Institut für Technologie, TU Dresden, Universität Stuttgart, TU München
Place and date:	Saldenburg (Germany), 16.05.2019

Title:	Effect of river boundary conditions on groundwater flow and solute transport during a flood event
Authors:	**Merchán-Rivera, P.**, Disse, M., Bhola, P., Chiogna, G.,
Event:	EGU General Assembly 2019
Place and date:	Vienna (Austria), 08.04.2019

Title:	Uncertainties predicting subsurface mixing due to river boundary conditions during flood events
Authors:	**Merchán-Rivera, P.**
Event:	TUM-GS Kick-off seminar
Place and date:	Raitenhaslach (Germany), 24.07.2018

1 Introduction

From sanitary functions to the critical role for sustaining the proliferation of life, the occurrence, distribution, and movement of water are essential for a plethora of activities and processes in the Earth (Dingman, 2015; Ward et al., 2016). It is under this veil that hydrology, the science of water, has been developed and, day by day, it receives more attention due to the depleting and scarcer water resources. Hydrological systems are composites of continuously interrelated elements with dynamics that span within numerous temporal and spatial scales. In fact, our conception of the hydrologic systems and our capabilities to manage water resources evolve with our knowledge about the interrelation mechanisms of these constitutive components. In this line of thought, a growing body of literature recognizes the importance of the interactions between surface water and groundwater (Brunner et al., 2017; Krause et al., 2014; Lewandowski et al., 2020). It comes with no surprise given their significance in a wide range of scientific and engineering subjects, such as ecohydrology, water supply, and water quality (Winter, 1998). Aquatic environments depend on the relatively stable influx of groundwater that provides water and nutrients (Kløve et al., 2011). The water and energy exchange between surface water and groundwater are also important for ecosystem restoration due to their effect on the distribution and abundance of microbial activity (Arrigoni et al., 2008; Daniluk et al., 2013). Furthermore, the integration of large-scale interactions of groundwater and surface water bodies can be relevant for the operation of water reservoirs (Tian et al., 2018), watershed planning (Khan and Khan, 2019) and the assessment and management of flood risk (Abboud et al., 2018). Similarly, due to the dynamic interconnection between water bodies, the investigation of contamination and the understanding of solute transport often require to explicitly focus on assessing the transfers between surface water and groundwater (Andrade et al., 2018; Hintze et al., 2020). Within the context of the river-aquifer systems, the transport and fate of solutes and contaminants have been major areas of interest and debate (Brunner et al., 2017; Krause et al., 2014). A large number of studies explains the possible implications of the interactions between rivers and aquifers in the biogeochemical transformations for nutrient cycling and ecosystem metabolism (Boano et al., 2014; Boulton et al., 2010; Findlay, 1995; Pinay et al., 2015), and it has also been observed that the continuous flux exchange influences the thermal dynamics

in rivers and aquifers, which is also related to reactive transformations (Marzadri et al., 2016; Master et al., 2005).

The interaction between rivers and aquifers is a complex matter that happens at different spatiotemporal scales that can be affected by the occurrence, magnitude and distribution of hydrologic controls and anthropogenic impacts (Ascott et al., 2017; Lewandowski et al., 2019; Woessner, 2000). Extreme events, such as groundwater flooding and hydropeaking, can modify the usual behavior of the hydrological regime and the dynamics of rivers and aquifers (Abboud et al., 2018; Macdonald et al., 2008; Pérez Ciria et al., 2019). Although, there are various definitions are used for extreme event in physical sciences, there are some generic points of consensus in the interpretation. A natural or anthropogenic event is considered extreme when it is unexpected, i.e., when the event was unforeseen, or disruptive, i.e., when some process or activity in the evaluated system faces some disorder or upheaval (Coles, 2001; McPhillips et al., 2018; Sharma et al., 2013). Following the classifications presented in McPhillips et al. (2018), groundwater flooding and hydropeaking can be defined as extreme events within the context of hazards in earth science and ecological disturbance, respectively. On one hand, groundwater flooding occurs when the groundwater rises to the surface level or into underground civil infrastructure (Macdonald et al., 2012, 2008) and can yield significant economic and social damages and disruptions (Abboud et al., 2018; Colombo et al., 2018; Gattinoni and Scesi, 2017; Morris et al., 2018; Oyedele et al., 2009; Yu et al., 2019). On the other hand, hydropeaking refers to downstream fluctuations in discharge and water levels from the activities of high-head storage hydropower plants (Bruder et al., 2016; Meile et al., 2011), which can greatly exceed the natural behavior of the hydrological system and modify the hydraulic conditions of the streams (Hauer et al., 2017; Meile et al., 2011). Overall, rapid fluctuating stages and peak-flow conditions from these extreme events can affect the water flux, the residence time of solutes, and flow paths in the subsurface flow (Bernard-Jannin et al., 2016; Boano et al., 2013; Malzone et al., 2016a; Singh et al., 2020; Trauth and Fleckenstein, 2017; Wu et al., 2018; Ziliotto et al., 2021). For instance, recent findings point out the influence of transient conditions and turbulent flow on mixing and transport processes in aquifers (Baioni et al., 2021; Singh et al., 2019; Ziliotto et al., 2021).

Numerical models are frequently used to understand the river-aquifer interactions, in which the river stage fluctuations are described as transient boundary conditions in the groundwater system (Anderson et al., 2015). Numerical models based on finite-difference or finite-element techniques are regularly applied because they allow us to approximate the complex geometry of the surface streams (Peyrard et al., 2008). Accordingly, to simulate solute transport and reactive solute transport in the subsurface, models solve formulations of the advection-dispersion-reaction equation using the flow terms computed by the numerical groundwater flow models (Bedekar et al., 2016). A frequent concern in this practice is that transport simulations can easily become a computationally expensive matter (Lykkegaard et al., 2021;

Smith, 2013). For this reason, the characterization of the flow field has become an attractive method to identify the origin and fate of fluids and solutes and describe the mechanisms that control the dissolution, dissipation, and mixing in the subsurface (Bresciani et al., 2019; Hidalgo et al., 2015; Hidalgo and Dentz, 2018; Jiang et al., 2014). For instance, stagnation points provide information about the origin and fate of fluids and solutes (Bresciani et al., 2019) and the location of mixing and highly reactive regions. Multi-directional variations in the flow field, such as reverse flow, give insights about the circulation of nutrients (Dudley-Southern and Binley, 2015), infiltration depth of solutes and reaction rates in the subsurface (Trauth and Fleckenstein, 2017). Topological flow properties are a good alternative to the solution of the transport problem due to their relation with mixing processes in aquifers (Bresciani et al., 2019; de Barros et al., 2012) and porous media (de Anna et al., 2014a; Engdahl et al., 2014; Wright et al., 2017). One of them is the Okubo-Weiss metric (Okubo, 1970; Weiss, 1991) that has been used to describe mixing potential and characterize subsurface flow in terms of dominant forces, such as vorticity, shear strain, and normal strain (de Barros et al., 2012; Wallace et al., 2021; Wright et al., 2017).

On top of the physical complexity of hydrological system and the resources required for modeling them, there is a chaotic nature in the actual predictive modeling process. Uncertainties associated with input data, model parameters, model scale and discretization, numerical implementation, and process conceptualization may lead to a poor understanding of these systems and, consequently, trigger wrong decisions (Carroll and Carroll, 2006; Smith, 2013). Besides the fundamental uncertainty from transient properties of the river stage and groundwater flow, extreme events, such as the aforementioned, introduce further ambiguity in the interpretation of the physical processes and new sources of error (Colombo et al., 2018; Hester et al., 2021; Jimenez-Martinez et al., 2015; Ziliotto et al., 2021). The accuracy and reliability of measurement devices is compromised during extreme scenarios due to design limitations (Mahecha et al., 2017; Saidi et al., 2014). Also, a lack of data is often accompanying the study of extreme events because of their inherent disruptiveness or unexpected quality (Barker and Haimes, 2009). A quantitative assessment of the uncertainties associated to these events is hence essential but also challenging. The challenges have been thoroughly acknowledged in the field of hydrology (Brunner et al., 2010; Di Baldassarre and Montanari, 2009; Götzinger and Bárdossy, 2008) and probability theory tools to address aleatory and epistemic uncertainties have been developed to respond (Beven and Freer, 2001; Ghaith and Li, 2020; Merz and Thieken, 2009; Rajabi and Ataie-Ashtiani, 2016; Ross et al., 2009; Vrugt, 2016). Nevertheless, the effect of the uncertainty in the dynamics of flow, transport and mixing in river-aquifer systems in such extreme conditions indeed remains broadly unexplored (Deman et al., 2016; Ghaith and Li, 2020; Morris et al., 2018). Precisely, research gaps appear due to the lack of investigations that addressed these issues from a comprehensive perspective (Morris et al., 2018; Valocchi et al., 2019). Moreover, although numerical models have been broadly used for understanding hydrological systems, the proper

application of formal stochastic approaches for quantifying model uncertainty and sensitivity is not as extensive or rigorous as required (McMillan et al., 2018; Pfister and Kirchner, 2017; Saltelli et al., 2019).

In a nutshell, the previous paragraphs describe two debates that have thrived in parallel in the field of hydrology: the discussion about techniques to progress in the mechanistic understanding and predictability of the river-aquifer dynamics (Conant et al., 2019; Krause et al., 2014), and the development effective methods to characterize the transport and mixing processes in aquifers (Chow et al., 2020; Fiori and de Barros, 2015; Valocchi et al., 2019). Both of them surrounded by the halo of uncertainty (Brunner et al., 2017; Cirpka and Valocchi, 2016; Di Baldassarre and Montanari, 2009; Sanchez-Vila and Fernàndez-Garcia, 2016; Zhou et al., 2014). The objective of this dissertation is to characterize the uncertainty in the groundwater flow and subsurface transport processes due to the river boundary conditions during groundwater flooding and hydropeaking events. Also, the research aims to create methodological frameworks for the quantification of uncertainty to be applied in similar modeling exercises. The research pays special attention in understanding flow field features, such as stagnation points, reverse flow and Okubo-Weiss metric, as efficient alternatives for quantifying transport process and describe mixing in groundwater. The dissertation is divided into four different components and four academic publications were written correspondingly, addressing not only assessment and formal quantification of uncertainty but also mechanisms of communication of model uncertainty. Along these studies, a broad spectrum of sensitivity and uncertainty analysis techniques were evaluated and applied, including scenario modeling (Anderson et al., 2015), linear uncertainty analysis (Doherty et al., 2010), screening sensitivity analysis (Campolongo et al., 2007; Morris, 1991), Bayesian inference (Kaipio and Somersalo, 2005), spectral expansions (Xiu and Karniadakis, 2002), and discrete projections (Le Maitre and Knio, 2010; Xiu, 2007). While the optimization of these methods was beyond the scope of the study, two rationales guided the design and construction of the proposed frameworks: non-intrusiveness and reduction of computational demand. These motivations imply to work with no solver modifications (i.e., no changes in the underlying hydrological model) and to assemble techniques that are efficient for the computational demand of typical distributed hydrological models. To make a meaningful contribution to research on applied stochastic hydrology, the proposed mechanisms are designed to be straightforwardly applied into pre-existing models and similar predictive modeling exercises.

This document has been organized in the following way. Chapter 2 begins by explaining the outline and components of the investigation, the interrelation between articles, as well as the extreme events of interest and their representations. Chapter 3 presents the theory and concepts that support this dissertation. This chapter links the formal representation of the governing principles and the emergence of uncertainties in the description of river-aquifer

interactions. In addition, the general concepts behind the quantification of uncertainty are explained. Chapter 4, 5, 6, and 7 include the four academic papers of the collection. The dissertation concludes with Chapter 8, where major findings are restated, and the implications of the research outcomes are discussed. To close, the latter also looks at what can be investigated in the future.

2 Research framework

2.1 Research scope and research questions

The practical and theoretical matters of research have been explained and reviewed in the previous section but, broadly, we can summarize them in three interconnected subjects (see Figure 2.1):

- **a)** Interaction between rivers and aquifers during extreme events, specifically groundwater flooding and hydropeaking
- **b)** Effect of transient river boundary conditions in the dynamics of flow and transport in the subsurface in such extreme environments
- **c)** Quantification of uncertainty using formal stochastic approaches such as spectral expansions and Bayesian methods

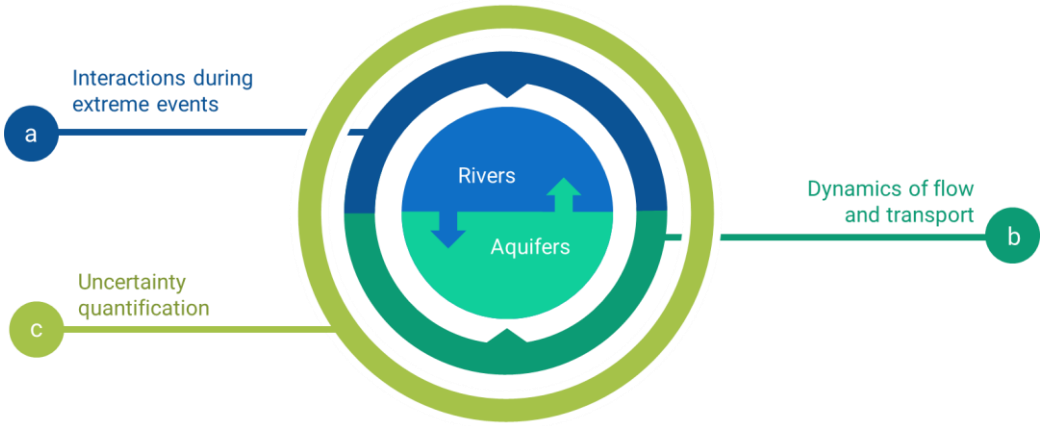

Figure 2.1. Graphical representation of the dissertation scope and main addressed subjects

Three research question derive from the mentioned three-fold issue and are set to answer as part of this dissertation:

Q1. What is the role of highly transient river boundary conditions during extreme events, such as groundwater flooding and hydropeaking, on the responses of the flow and transport processes in the subsurface?

Q2. How can uncertainties during extreme events, such as groundwater flooding and hydropeaking, propagate and affect the flow and transport processes in the subsurface?

Q3. How can stochastic approaches be used to identify the spatial distribution and temporal variability of relevant flow conditions in the subsurface?

2.1.1 Research components and specific objectives

To answer these research questions, the investigations of this dissertation were divided in four components, which are associated to different scientific articles. Although every component explores each of the research questions at a certain degree, some articles spot them in detail and aim to explicitly contribute to answer some specific questions. Figure 2.2 includes a summary of these relationships and the sections within the dissertation where they are presented.

2.1.1.1 Groundwater flow and solute transport simulations (Chapter 4)

The first part of the research was the identification of changes in the solute concentration due to the effect of transient river boundary conditions during the flooding event. A three-dimensional groundwater model was developed to describe the groundwater flow in the aquifer of the Alz valley and transport simulations of a conservative solute were performed to evaluate the advective and dispersive processes during the flood event. The transport simulation involved a single injection of a conservative tracer close to the river. To observe the effect of the river boundary conditions, various scenarios were created in which all the parameters and hydrologic conditions from the base model were fixed except for the stage and the riverbed conductance. In line with Q1 and Q2, the objective of this research component was:

- To identify in a real case model if the temporal dynamics of the river-aquifer interactions during groundwater flooding can affect the advective and dispersive transport of solutes.

2.1.1.2 Bayesian inference in groundwater flood risk assessment (Chapter 5)

The second component aimed to formally quantify and decomposed in spatial and temporal terms the sensitivity and uncertainty from the different input variables and parameters that

describe the groundwater flooding event. The model used in the previous research was updated based on additional observational data. Also, the spatial dimension of the model were reduce given that the two-dimensional model structure was sufficient to represent the groundwater flow, keeping the same accuracy level and largely improving the computational efficiency. Hence, a two-dimensional numerical model was built to describe the event and the role of river-aquifer interactions was described as head-dependent flux boundary conditions. The elementary effects method and Bayesian inference were coupled for this purpose. The DiffeRential Evolution Adaptive Metropolis (DREAM) algorithm was used as Markov Chain Monte Carlo technique for the estimation of the predictive distributions of the groundwater heads and the estimation of the relevant parameters. The objectives of this study were related to Q1 and Q3 and included:

- To understand the spatial distribution and temporal variability of groundwater flood events and the effect of parameter interactions.
- To identify in probabilistic terms the regions susceptible to groundwater flooding acknowledging the uncertainty in the model inputs.

2.1.1.3 Polynomial chaos expansions to understand flow field dynamics (Chapter 6)

The third part of this dissertation is the application of polynomial chaos expansions and pseudo-spectral discrete collocation to understand the effect of river boundary conditions. In this research, a framework was proposed not only for the quantification of the uncertainty but also for the identification of stagnation zones and reverse flow caused by the interactions between rivers and aquifers in the previously calibrated model. It involves a set of classification criteria and kernel density estimations at every element of the numerical models for the temporal and spatial mapping of the aforementioned flow features. The result was a non-intrusive framework that can be straightforwardly applied in pre-existing models. The effect of the uncertain river boundary condition during the flood event is evaluated in a two-dimensional numerical model and the hotpots of stagnation and reverse flow were identify and the influence of the river-aquifer interactions were also identified. This work thoroughly addresses Q1, Q2, and Q3. The following are the goals of this research:

- To map the occurrence of complex flow processes, such as reverse flow and stagnation points hotspots, caused by stream-aquifer interactions in terms of temporal dynamics and spatial patterns.
- To quantify the propagation of uncertainty in the groundwater flow field due to the uncertain river boundary conditions during a flood event.

2.1.1.4 Effect of hydropeaking waves in the flow topology (Chapter 7)

The last research component of this dissertation was the exploration of uncertainty from different hydropeaking waves (i.e., triangular wave, sine wave, complex wave, and trapezoidal wave) in heterogeneous aquifers. The wave-shaped highly transient boundary conditions were specified as Dirichlet boundary conditions and a series of deterministic and stochastic scenarios were built to understand the effects of the wave propagation into groundwater flow and the flow topology. A synthetic model was built considering a two-dimensional unconfined aquifer with one single realization of a lognormal heterogeneous isotropic hydraulic conductivity field. Here, once again, the focus of the research was the uncertainty related to highly transient river boundary conditions. The Okubo-Weiss metric was used as topological descriptor to understand the mechanisms controlling transport of solutes in the subsurface and the mixing processes. This work applies polynomial chaos expansions to quantify the propagation of the spatiotemporal uncertainty into the hydraulic head in the aquifer and the Okubo-Weiss. Therefore, the objectives of this research component were aligned as well to Q1, Q2, and Q3 and included:

- To quantify and map the effect of hydropeaking waves in the groundwater heads and the flow field topology described by the Okubo-Weiss metric.
- To quantify the propagation of uncertainty related to the shape of hydropeaking waves in the groundwater heads and the flow field topology described by the Okubo-Weiss metric.

Table 2.1 includes the summary of the objectives that were defined for each component of the research. Various techniques to understand the river-aquifer systems and the associated uncertainties have been revised and used in this dissertation. A brief list of the applied methods is included in Table 2.2. A general introduction to these concepts is included in Chapter 3 to improve the explanation of the relationships of the interactive variables that are part of this research.

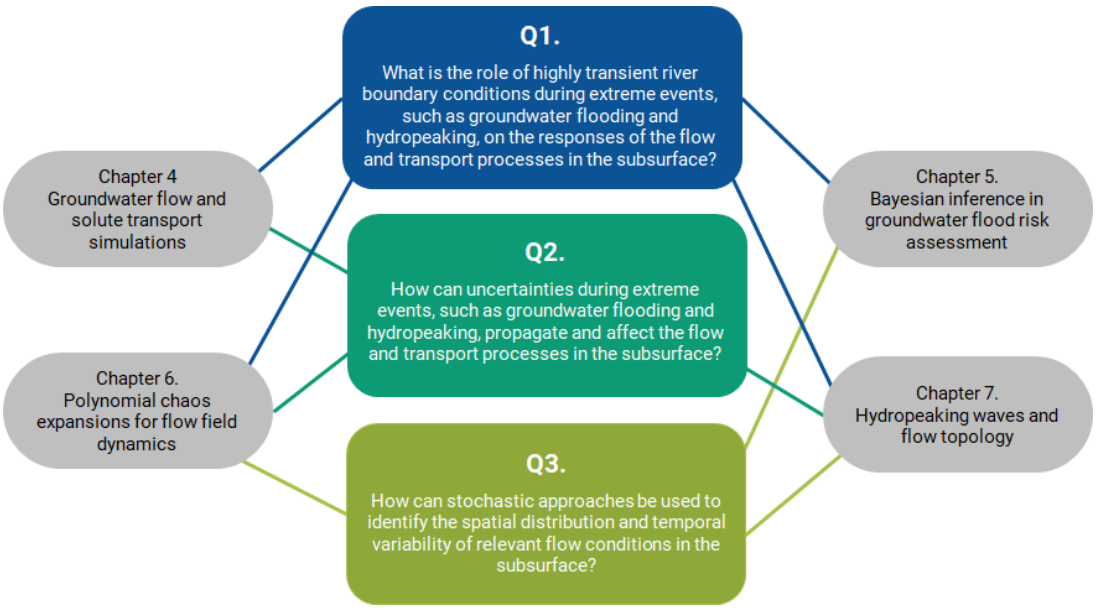

Figure 2.2. Dependencies between research questions and the dissertation chapters that address each of them

Chapter	Related publication	Specific objective	Addressed research question
Chapter 4. Groundwater flow and solute transport simulations	Merchán-Rivera et al. (2018). Surface water and groundwater interaction during flood events in the Alz Valley: Numerical modeling and solute transport simulations.	• To identify in a real case model if the temporal dynamics of the river-aquifer interactions during groundwater flooding can affect the advective and dispersive transport of solutes.	Q1, Q2
Chapter 5. Bayesian inference in groundwater flood risk assessment	Merchán-Rivera et al. (2022). A Bayesian Framework to Assess and Create Risk Maps of Groundwater Flooding.	• To understand the spatial distribution and temporal variability of groundwater flood events and the effect of parameter interactions. • To identify in probabilistic terms the regions susceptible to groundwater flooding acknowledging the uncertainty in the model inputs.	Q2, Q3
Chapter 6. Polynomial chaos expansions for flow field dynamics	Merchán-Rivera et al. (2021). Identifying Stagnation Zones and Reverse Flow Caused by River-Aquifer Interaction: An Approach Based on Polynomial Chaos Expansions.	• To map the occurrence of complex flow processes, such as reverse flow and stagnation points hotspots, caused by stream-aquifer interactions in terms of temporal dynamics and spatial patterns. • To quantify the propagation of uncertainty in the groundwater flow field due to the uncertain river boundary conditions during a flood event	Q1, Q2, Q3
Chapter 7. Hydropeaking waves and flow topology	Merchán-Rivera et al. (2022) Propagation of Hydropeaking Waves in Heterogeneous Aquifers: Effects on Flow Topology and Uncertainty Quantification.	• To quantify and map the effect of hydropeaking waves in the groundwater heads and the flow field topology described by the Okubo-Weiss metric. • To quantify the propagation of uncertainty related to the shape of hydropeaking waves in the groundwater heads and the flow field topology described by the Okubo-Weiss metric.	Q1, Q2, Q3

Table 2.1. Specific objectives of the research components of the dissertation and the associated research questions

Chapter	Keywords	Summary of applied methods
Chapter 4. Groundwater flow and solute transport simulations	surface water-groundwater interaction, flooding, solute transport, river boundary conditions	• Deterministic scenario analysis • 3D groundwater modeling with MODFLOW-2005 (Harbaugh, 2005) • Advective-dispersive transport modeling with MT3DMS (Zheng and Wang, 1999) • Parameter Estimation and Uncertainty Analysis with PEST (Doherty et al., 2010)
Chapter 5. Bayesian inference in groundwater flood risk assessment	groundwater flooding, Bayesian inversion, probability maps, flood risk, sensitivity analysis, uncertainty quantification	• Probabilistic risk assessment • 2D groundwater modeling with MODFLOW-2005 (Harbaugh, 2005) • Elementary effects method (Campolongo et al., 2007; Morris, 1991) • Bayesian inversion using DREAM algorithm (Vrugt, 2016) • Kernel density estimation (Silverman, 1998)
Chapter 6. Polynomial chaos expansions for flow field dynamics	stagnation points, reverse flow, surface water-groundwater interaction, polynomial chaos expansions, probability maps, uncertainty quantification	• 2D groundwater modeling with MODFLOW-2005 (Harbaugh, 2005) • Polynomial chaos expansions (Xiu, 2010; Xiu and Karniadakis, 2002) • Pseudo-spectral collocation approach (Xiu, 2007) • Development of flow criteria classification • Kernel density estimation (Silverman, 1998) • Quasi-Monte Carlo sampling (Halton, 1964)
Chapter 7. Hydropeaking waves and flow topology	uncertainty quantification, hydropeaking, flow field topology, Okubo-Weiss, periodic waves	• Deterministic and stochastic scenario modeling • 2D groundwater modeling with MODFLOW-2005 (Harbaugh, 2005) • Polynomial chaos expansions (Xiu, 2010; Xiu and Karniadakis, 2002) • Pseudo-spectral collocation approach (Xiu, 2007) • Okubo-Weiss metrics (Okubo, 1970; Weiss, 1991)

Table 2.2. Description of methodological contents of the articles

2.2 Extreme events of interest

This dissertation addresses two types of extreme events: groundwater flooding and hydropeaking. As mentioned in the introduction, while groundwater flooding can be defined as extreme events unexpected occurrence and hazard, hydropeaking is an extreme event for the associated ecological disturbance. A primary inclusion criterion for these events was the associated disruptive fluctuations of the stream stages, which can be represented as river boundary conditions in a numerical model. Groundwater flooding and hydropeaking are occasionally referred as extreme events along this dissertation for simplicity.

2.2.1 Groundwater flooding

Groundwater flooding occurs when groundwater rises above the ground surface or into underground civil infrastructure (Macdonald et al., 2012, 2008). It can yield to a flood hazard and produce significant economic and social damages (Abboud et al., 2018; Colombo et al., 2018; Gattinoni and Scesi, 2017; Morris et al., 2018; Oyedele et al., 2009; Yu et al., 2019). The elements that define the severity and duration of groundwater floods differ from other type of events. For instance, fluvial and pluvial floods can occur due to short and intense climatic conditions, such as storm events. In contrast, groundwater floods can occur due to the accumulation of water in the subsurface over long periods of time and, therefore, they often require different approaches for identification, assessment and mitigation (Kreibich et al., 2009; McKenzie et al., 2010; Yu et al., 2019). Previous studies have shown that the high stage of rivers can cause groundwater flooding due to the propagation of the wave and the rapid rising of the groundwater table (Abboud et al., 2018; Joo and Tian, 2021) and, consequently, affect the flow field at the meter-scale (Cardenas, 2008; Woessner, 2000). Figure 2.3 explains the interactions between surface water and groundwater and their effects on the occurrence of groundwater flooding.

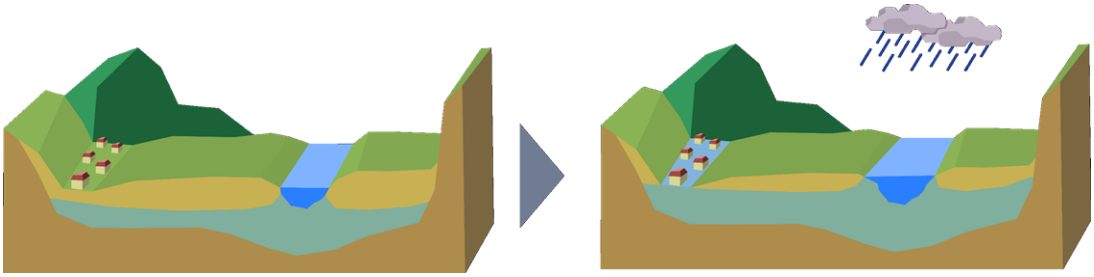

Figure 2.3. Schematics of a groundwater flooding in a river valley. River stage effects in the wave propagation in the aquifer. Groundwater flooding events can be prompted by the accumulation of water in the aquifer as well as by rainfall events.

The analysis of this type of event is introduced in this work by studying a real case occurred in the valley of the Alz River located in southeastern Bavaria, Germany. In May and June 2013 the region was affected by heavy rainfall events that yield flood events and several property damages were reported due to the rise of groundwater into basements and underground infrastructure (Disse et al., 2015; Keilholz et al., 2015). Figure 2.4 presents a map of the study area and some of the most relevant morphological and hydraulic features of the zone.

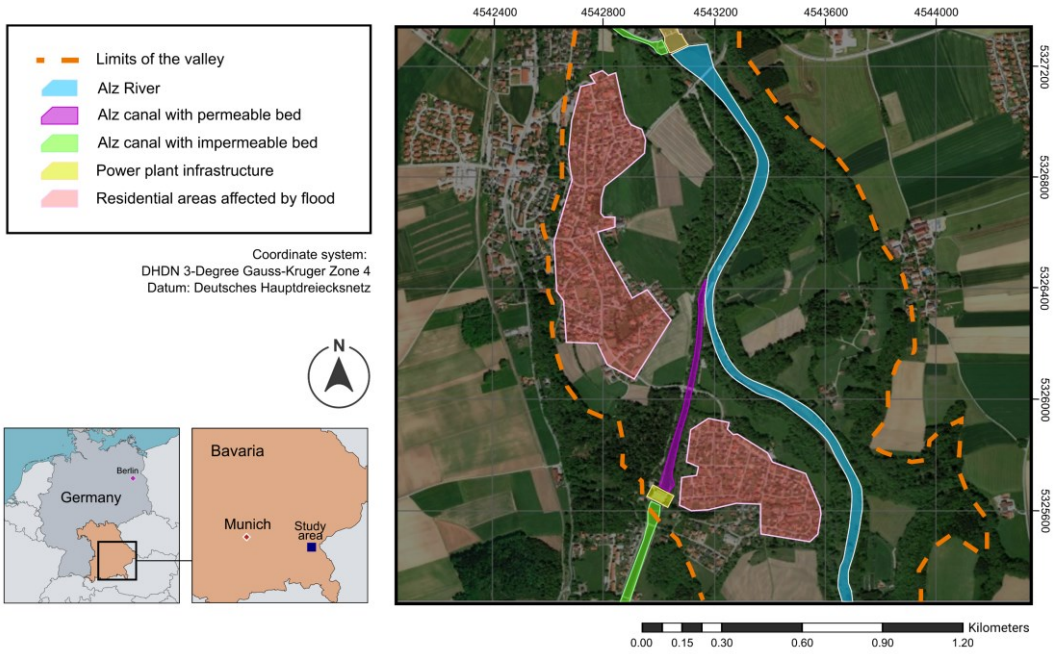

Figure 2.4. Study area. Valley of the Alz River.

2.2.2 Hydropeaking

Energy demand increases rapidly around the world and hydropower plants provide is the most common source of renewable energy (BP p.l.c., 2021). Water from reservoirs is released to flows through turbines and generate energy, which produces frequent and short-term variations in discharge and water levels known as hydropeaking (Bruder et al., 2016; Chiogna et al., 2018). Figure 2.5 includes a graphical representation of hydropeaking. Various studies have assessed hydropeaking and explore the relationships between the affected rivers and the aquifers (Francis et al., 2010; Singh et al., 2019; Song et al., 2020). The hydropeaking fluctuations can significantly exceed the natural behavior of the hydrological regimes and modify the hydraulic conditions of the streams (Hauer et al., 2017; Meile et al., 2011) and mixing and transport processes in aquifers (Singh et al., 2019; Ziliotto et al., 2021).

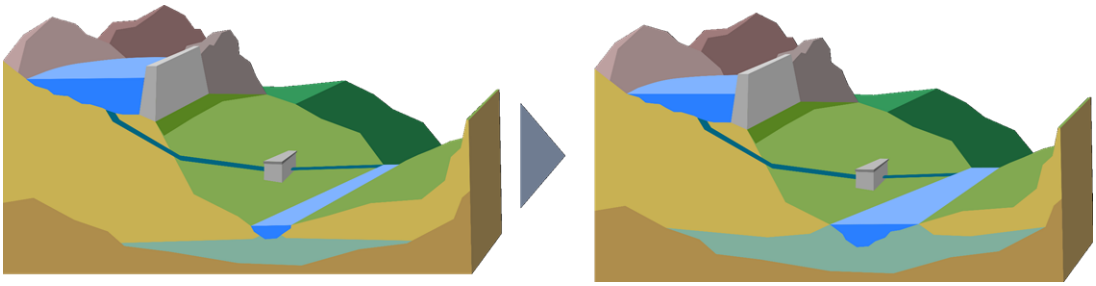

Figure 2.5. Graphical representation of hydropeaking. The operation of the hydropower plants depends on the electricity demand. Water is released from the reservoirs according to the demand leading to fluctuating discharges and water levels in the rivers.

In this research, a synthetic case is constructed to represent the transient river stage using river boundary conditions and the uncertainty associated to the peak amplitude and temporal occurrence of the event is evaluated. The fluctuating boundary conditions are built on the basis of real hydropeaking scenarios occurred in numerous catchments around the world (e.g., the Adige catchment in Italy and the Colorado catchment in the United States), and include: a triangular wave, a sine wave, a complex wave (built by the superposition of two sine waves), and a trapezoidal wave (Chiogna et al., 2018; Ferencz et al., 2019; Li and Pasternack, 2021; Sawyer et al., 2009).

3 Governing principles and uncertainty

This chapter introduces some of the fundamental concepts that govern the saturated fluid flow and transport of solutes in the subsurface and the corresponding mathematical representations. The components of these representations are analyzed first from the mathematical notion and then from the practical point of view. Since the physical principles that control the river-aquifer interactions cannot be entirely denoted by assigning mathematical interpretations, this section is hereafter to highlight the propagation of the uncertainty into the groundwater flow field and the ambiguous character of the predictive process.

3.1 Groundwater flow model and solute transport

Flow in a porous medium can be described by Darcy's law (Darcy, 1856)

$$q = \mathbf{K} \cdot \nabla h \ , \qquad \textit{Eq. 3.1}$$

where $q = (q_x, q_y, q_z)$ is a vector of the specific discharge (i.e., Darcy velocity), **K** is the second-order tensor of hydraulic conductivity, and ∇h is the gradient of hydraulic head. Hence, the transient groundwater flow can be described by a differential equation

$$S_s \frac{\partial h}{\partial t} \pm W = \nabla \cdot q \ , \qquad \textit{Eq. 3.2}$$

where S_s the specific storage, t is the time, and W describes the volumetric flux from source and sink terms (Bear, 1972; Fetter, 1999).

Similar to the fluid flow equations, the mass transport in groundwater can be described by partial differential equations. The concentration of N reactive species c_n is given by

$$\frac{\partial c_n}{\partial t} = -\nabla \cdot J_n \pm R_n(c_1, \dots, c_N) \ , \qquad n = 1, \dots, N \ , \tag{Eq. 3.3}$$

where R_n represent chemical reactions (i.e., transformation, retardation or attenuation), and J_n are mass fluxes given by dispersive and advective processes to be

$$J_n = -D\nabla c_n + \frac{q}{\eta_e} c_n \ , \tag{Eq. 3.4}$$

with $D = \left(D_x, D_y, D_z\right)$ being the hydrodynamic dispersion coefficient vector that involves molecular diffusion and mechanical dispersion (longitudinal and transverse), and η_e denoting the effective porosity (Fetter et al., 2017). For a three-dimensional flow parallel to the x axis, the longitudinal hydrodynamic dispersion coefficient is

$$D_x = \alpha_L^{(x)} v_x + D^*, \tag{Eq. 3.5}$$

and the transverse hydrodynamic dispersion coefficients are

$$D_y = \alpha_T^{(y)} v_x + D^*, \qquad D_z = \alpha_T^{(z)} v_x + D^* \tag{Eq. 3.6}$$

where $\alpha_L^{(x)}$ is the dynamic dispersivity in the x direction, $\alpha_T^{(y)}$ and $\alpha_T^{(z)}$ are respectively the dynamic dispersivity in the y and z directions, $v_x = q_x/\eta_e$ is the average linear velocity in the x direction, and D^* is the effective diffusion coefficient (Fetter et al., 2017; Kitanidis and McCarty, 2012).

The heterogeneous nature of the porous material comprises fundamental uncertainty in S_s, **K**, η_e, and D. But also, uncertainties can propagate from the representation of rivers because, to solve Eq. 3.2 as a boundary value problem, we need to impose information about h and/or q along the boundaries Γ of the model domain. The representation of river-aquifer interactions and the associated uncertainties are discussed immediately below.

3.2 Boundary conditions and the representation of rivers

The interaction between rivers and streams can be described by various types of boundary conditions. The choice of boundary type and its characterization depends on the contact between aquifer and the river (Carabin and Dassargues, 2000) and have important effects in the model solution (Franke et al., 1987). This is significant for river boundary conditions and the regions close to the boundaries because, as exposed in the introduction of this document, they are frequently regions of hydrological, ecological and biogeochemical relevance.

The first-type is the Dirichlet boundary Γ_D, when the boundary imposes a value to the dependent variable (Liu, 2018). This means it is used to directly define the hydraulic heads h [L] from the elevation of the water level in the river on the groundwater system, so that

$$h = g(t,s)\,, \qquad t,s \in \Gamma_D\,, \tag{Eq. 3.7}$$

being h the groundwater head, $g(t,s)$ a continuous function and $\{t,s\}$ are the spatiotemporal dependencies.

Neumann boundary conditions Γ_N, also known as second-type, entails that the derivative of the dependent variable is known (Cheng and Cheng, 2005). Mathematically, it can be represented by

$$\frac{\partial h}{\partial n} = g(t,s)\,, \qquad t,s \in \Gamma_N\,, \tag{Eq. 3.8}$$

where n is the outward normal of the boundary. In practical terms, the normal derivative of the head relates to the concept of Darcy velocity, being $\partial h/\partial n = q$ [LT^{-1}]. Hence, this type of boundary condition is used to define a known specific discharge in or out of the system.

The third-type of boundary conditions Γ_R, known as Robin boundary condition[1], is a linear combination of Dirichlet and Neumann conditions (Jazayeri and Werner, 2019; Liu, 2018),

$$\frac{\partial h}{\partial n} + \omega h = g(t,s)\,, \qquad t,s \in \Gamma_R\,, \tag{Eq. 3.9}$$

being ω a non-zero constant weight factor. Eq. 3.9 raises once again the notion of Darcy Law and brings up the formulation of the conductance of the riverbed material (also referred as leakage coefficient). Let $g(t,s)$ have the explicit value ωh_r, to express the volumetric flux q_v [L^3T^{-1}] as

$$q_v = -\omega h + \omega h_r\,, \tag{Eq. 3.10}$$

[1] A common misconception in the field of hydrogeology is the notion of the third-type as Cauchy boundary conditions. Cauchy boundary conditions refer to imposing both Dirichlet and Neumann boundary conditions simultaneously. Hence, the function $f(t,s)$ and the normal derivative $\partial h/\partial n$ must be specified. The reader can find a more extensive treatment of this topic in Jazayeri and Werner (2019) and Liu (2018).

where h_r is a reference hydraulic head. The weighting factor can be used to represent the riverbed conductance, such that $\omega \coloneqq c_r$. Given that $c_r = -K_r A/L$ [L^2T^{-1}] (Harbaugh, 2005), Eq. 3.10 yields

$$q_v = c_r(h - h_r) = -\frac{k_r A}{L}(h - h_r)\,, \qquad \textit{Eq. 3.11}$$

where k_r is the hydraulic conductivity of the riverbed [LT^{-1}], A is the cross-sectional area [L^2], and L is the length between the two hydraulic heads [L]. This boundary condition is broadly used for the description of rivers and surface water bodies because one can describe the flux q_v as a function of an imposed head h.

3.3 The emergence of uncertainty

Dirichlet and Neumann boundary conditions face similar limitations for the practical implementation. The application of Dirichlet boundary conditions (Eq. 3.7) to represent rivers requires to assume strong connectivity between surface water and groundwater and stable flow rates despite groundwater fluctuations (Bear, 2012). Rapid or frequent variations in the river stage requires to use short intervals and, therefore, numerous time steps (Dassargues, 2020). In practice, water level data is not always available in such short intervals and readings are spatially scatter. Likewise, data related to groundwater table are usually sparse for a comprehensive characterization (Bresciani et al., 2016). Therefore, to apply hydrometric information normally a preprocessing exercise is required, which poses new sources of error and discrepancies. To properly apply Neumann boundary conditions, we require information related to Darcy velocity, which is uncommon. Direct methods to estimate groundwater velocity in the field are rarely available. Tracer tests are the most common approach for measuring the velocity in the field but they are still limited by the cost, labor and time requirements (Essouayed et al., 2019). In addition, any point measurement to understand the flux between rivers and aquifers is an incomplete image of the flow field because the flux is scale-dependent and multi-directional (Cardenas, 2015), as well as driven by the spatial variability in the riverbed material and the aquifer (McCallum et al., 2014). In consequence, Neumann boundary conditions are normally used in the determination of the prescribed flux from injection and extraction wells, but they are not commonly used to represent river-aquifer exchanges.

Robin boundary conditions are a popular approach to represent the interaction between rivers and aquifers in coupled surface water-groundwater models. The strength of this representation is that one can incorporate the dynamics of the river although they fall outside the model domain and define the boundary as a semipervious media. This means that it is possible to directly coupled the groundwater domain with a hydraulic model and reduce the assumptions that are required in Dirichlet boundary conditions. But these variations in the conceptual simplifications does not avoid uncertainty. First, hydraulic models contain their own ambiguity for the calculation of flow, water level and velocity in rivers due to uncertainties and errors in the hydraulic inputs, hydraulic geometry, numerical implementation and measurements (Di Baldassarre and Montanari, 2009; Mohd Anuar et al., 2022; Pappenberger et al., 2006). Second, when imposing Robin boundary conditions, a new source of uncertainty is the hydraulic conductivity of the riverbed material. As shown in Eq. 3.11, the concept is often simplified as the riverbed conductance c_r (Harbaugh, 2005). It is a lumped parameter that requires a series of assumptions related to the river-aquifer hydraulic connection and the discretization of the system that can lead to errors and model discrepancies (Brunner et al., 2010). Similar and more sophisticated conceptualizations of the conductivity properties of the riverbed are included in other models, e.g., MIKE SHE (DHI, 2017, 2013) and HydroGeoSphere (Aquanty Inc., 2015). Nevertheless, no matter which type of conceptualization is applied, the flawless definition of the hydraulic conductivity properties of the riverbed and the river-aquifer exchange flux is infeasible. Both the conductivity and the reference head (see Eq. 3.11) vary in space and time. Indeed, the properties of the riverbed material may differ by several orders of magnitude from the properties of the underlying aquifer (Leek et al., 2009; Tang et al., 2017) and involve unknown preferential flow paths (Anderson et al., 2015). On top of this, field measurements of the hydraulic conductivity of the riverbed are sparse and complex to obtain and estimate (Ghysels et al., 2019; Tang et al., 2015).

The estimation of transport processes in the subsurface is also affected by the definition of boundary conditions in the flow model. The propagation of uncertainties is rather obvious in the advective transport (represented by the second term in the righthand side of Eq. 3.4). It describes the bulk motion of dissolved solids carried along with the groundwater flow (Fetter, 1999) and it is thus conditioned by the discharge q and the head gradients ∇h and their uncertainties. But also, the hydrodynamic dispersion D (see Eq. 3.4) is a function of flow direction and magnitude (Dutta, 2013; Fetter, 1999). Flow field direction in the aquifer can be largely affected by the interaction of multiple surface water bodies, e.g., the confluence of two rivers or the two sections in a meandering stream. In addition, there is uncertainty due to the difference between the scale of the physical process to be modeled and the actual model. For instance, the motion of particles occurs in smaller scales than the numerical grid used for transport simulations. Moreover, the representation of spatial and temporal distribution of the

hydraulic and climatic features in the model will contain discrepancies, independent of the chosen discretization method. The motion of the fluid is mathematically described as a vector flow field, and solutes descriptors (e.g., concentration) are described with scalar fields (Chapman, 1981). This means that we associate a value to every discrete element of a domain, which partially captures the physical space of the aquifer, at a very discrete time step, which partially captures the temporal complexity. Hence, the accuracy of the flow field solutions is associated to the spatial and temporal resolutions (Roache, 1997), which is extremely significant when dealing with highly transient river boundary conditions. Although, the notion of improving the accuracy with high grid resolutions and temporal scale is often desirable, it becomes rapidly impractical in applied hydrological models.

3.4 Uncertainty quantification

To summarize what was described in the previous section, the description of the river-aquifer interactions is affected by experimental uncertainties, model and input uncertainties, and numerical errors. In general terms, the uncertainties described in the previous paragraph can be described as epistemic or aleatory (Smith, 2013). While epistemic uncertainty refers to the lack of knowledge, aleatory uncertainty refers to inherent to a variable problem or experiment (Sullivan, 2015). The way we address the modeling problem can vary but, generally, it can be classified within one of these two categories: deterministic and stochastic. The deterministic approach provides one solution to the partial differential equations (e.g., Eq. 3.2 and Eq. 3.3). Hence, there is a critical assumption that considers that the system and its variables are well-known and they will have one specific value at a given time and space (Fetter et al., 2017). This is rather negative for modeling extreme events because the disruptive and unanticipated values characteristics of the events can easily be misestimated. On the other hand, stochastic approaches involve randomness. They have become popular in the study of hydrologic systems that are governed by complex interactions and limited observable variables (Beven, 2016; Sivakumar, 2017). In particular, the methods that include stochasticity are pivotal for this dissertation because they can produce random images of the river-aquifer systems with enough flexibility to reasonably estimate the statistics of extreme conditions.

As the name suggests, any predictive estimation process compromises a series of actions to predict or anticipate some system responses. The process may contain several activities, such as input representation, sensitivity analysis, uncertainty quantification, parameter estimation, model calibration, and surrogate modeling. Nevertheless, the main driving forces are frequently model calibration and uncertainty quantification (Smith, 2013). The quantification of uncertainty often involves the reformulation of epistemic uncertainties as aleatoric uncertainties with the aim of analyzing them in probabilistic terms (Rocchetta et al., 2018;

Smith, 2013). The next lines formally explain the general approach followed in this dissertation to represent the process of uncertainty quantification.

The hydrological problems can be represented as forward process, in which a model f receives a set of inputs $\{t, s\}$ to determine a corresponding output y to be

$$y = f(t, s). \qquad \textit{Eq. 3.12}$$

To introduce the uncertain components of the model (i.e., input variables and parameters), we can consider the representation of the output as a function of d random variables on the probability space $(\Omega, \mathcal{F}, P)$ where Ω is a sample space, $\mathcal{F}$ is a σ-field, and P is a probability measure. Therefore, y is a function of a random vector $\boldsymbol{\Phi}(\varphi) = [\Phi_1(\varphi), \dots, \Phi_d(\varphi)]: \Omega \rightarrow \mathbb{R}^d$ and some deterministic spatiotemporal dependencies $\{t, s\}$ with finite temporal horizon $t \in [0, T]$ within the spatial domain $\mathcal{D} \subset \mathbb{R}$, such that,

$$y \coloneqq f(t, s; \varphi). \qquad \textit{Eq. 3.13}$$

We obtain hence a random process $u\big(t, s, \boldsymbol{\Phi}(\varphi)\big): [0, T] \times \mathcal{D} \times \Omega \rightarrow \mathbb{R}$ with a finite variance, where the multiple random variables $\Phi_1(\varphi), \dots, \Phi_d(\varphi)$ represent the stochasticity of the system due to uncertainty parameters, source terms, initial or boundary conditions. Then, if we consider that the uncertain inputs are mutually independent random variables, the input variables of the river boundary conditions can be represented within the joint probability distribution $\rho_{\boldsymbol{\Phi}}(\varphi)$, so that

$$\rho_{\boldsymbol{\Phi}}(\varphi) = \prod_{i=1}^{d} \rho_{\Phi_i}(\varphi_i). \qquad \textit{Eq. 3.14}$$

This work employs two different types of univariate distributions to describe the uncertain inputs, which are also commonly applied in modeling exercises in hydrology. The first is the normal distribution $\mathcal{N}(\mu, \sigma)$ with probability density function

$$f_{\Phi_i}(\varphi) = \frac{1}{\sigma\sqrt{2\pi}} e^{-(\varphi-\mu)^2/2\sigma^2}, \qquad -\infty < \varphi < \infty, \qquad \textit{Eq. 3.15}$$

where μ denotes the mean and σ denotes the standard deviation. The second is the continuous uniform distribution $\mathcal{U}(a, b)$ distributed in the interval $[a, b]$ and probability density function being

$$f_{\Phi_i}(\varphi) = \frac{1}{b-a} \chi_{[a,b]}(\varphi), \qquad \textit{Eq. 3.16}$$

where χ represents the unity of the interval $[a, b]$ (Smith, 2013).

One of the main drivers of uncertainty quantification will then be to determine the propagation of randomness from the inputs $\mathbf{\Phi}$ to find the push-forward distribution (Kurowicka and Cooke, 2006; Texeira Parente, 2020) of the output of interest (e.g., h, q and C_n in Eq. 3.2 and Eq. 3.3). and obtain the statistical moments or quantity of interest $Q(\mathbf{\Phi})$, such as the expected value and standard deviation. This process is summarized in Figure 3.1.

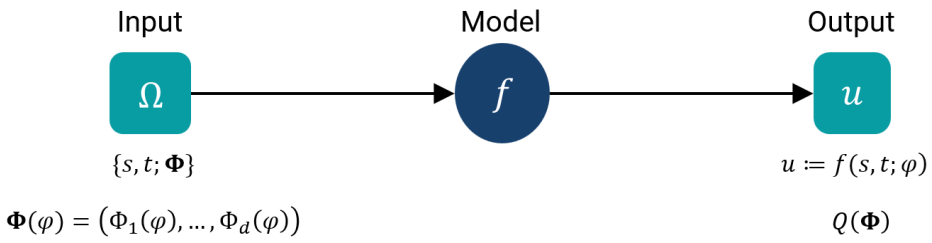

Figure 3.1. Illustration of the setup for the uncertainty quantification process

The components of this dissertation propose a series of schemes with various stochastic techniques to formally propagate the uncertainties through the models. Deterministic modeling is also used to understand the modeled systems and to create a base line for further work (Chapter 4). The most relevant stochastic techniques in the dissertation are those suitable for nonlinear problems and can be classified into two major groups: sampling methods, such as quasi-Monte Carlo sampling and Bayesian inference with Markov Chain Monte Carlo (Chapter 5), and spectral representations, such as polynomial chaos expansions (Chapter 6 and 7). The reader is hence referred to the corresponding article for further detail in the theory and specific notions about the application of the stochastic methods.

4 Groundwater flow and solute transport models

Abstract

Extreme river stage fluctuations occurring during flood events can greatly influence the dynamic of groundwater flow and the interactions between streams and aquifers. In groundwater models, extreme events represent a transient state in the boundary conditions which may affect groundwater flow and transport of solutes. The objective of this research is to understand the influence of river boundary conditions in the interaction between surface water and groundwater during a flood event based on a case study (Alz River, Germany). For describing the groundwater responses under flood conditions, we used MODFLOW-2005 to develop a three-dimensional groundwater numerical model and MT3DMS to simulate the advective and dispersive solute transport. We simulate four additional scenarios to evaluate the influence of the river stage and the riverbed conductance in the groundwater flow and the solute transport. Strong interrelationships were observed between the aquifer and the streams during the simulation period. Changes in both velocity of groundwater flow and hydraulic gradient were detected at different phases of the flood event. The transport simulations showed timing differences in the solute concentrations, giving evidence that the river boundary conditions control the aquifer responses. These responses vary in space and time and affect the transport and concentration of solutes plumes.

Material from:

Merchán-Rivera, P., Chiogna, G., Disse, M., Bhola, P., 2018. Surface water and groundwater interaction during flood events in the Alz Valley: Numerical modeling and solute transport simulations, in: Agua Subterránea. XIV Congreso Latinoamericano de Hidrogeología, Salta, Argentina. ISBN: 978-987-633-536-2.

4.1 Introduction

Interactions between surface water and groundwater (SW-GW) vary at multiple spatial and temporal scales (Boano et al., 2014; Cardenas, 2008; Schmadel et al., 2016) and occur in nearly all landscapes, from small streams, lakes and wetlands to major river valleys and seacoasts (Brunner et al., 2017; Castagna et al., 2015; Winter, 1999). These interactions are important for the management of water resources and the understanding the fate and transport of solutes. However, the mechanisms behind the interactions are complex and dynamic due to geomorphologic, hydrogeologic, and climate controls (Sophocleous, 2002). The physical, chemical and biological mechanisms which intervene in the migration, degradation and remediation of contaminants may be highly affected by these interrelationships (Derx et al., 2010; Jaffe and Kaplan, 2017; Lamontagne et al., 2018).

Extreme events, such as floods or droughts, can greatly influence the dynamic of groundwater flow fields and the interrelationships between streams and groundwater (Liang et al., 2018; Morris et al., 2018). Major floods may dramatically change the spatial extent of hyporheic zone and the direction of subsurface flow paths (Wondzell and Swanson, 1999) and induce both pressure and solute movement into aquifers at different scales (Welch et al., 2013). Moreover, the SW-GW interactions may influence groundwater flooding (Abboud et al., 2018), which are often associated with shallow unconsolidated sedimentary aquifers. These aquifers are susceptible due to the high permeability of the sediments and the high hydraulic connectivity with adjacent river networks (Macdonald et al., 2008).

Flood events are normally characterized by the peak of flow rate, flood elevation, flood volume or flood duration (Raudkivi, 2014), representing transient states in the boundary conditions affecting the water and solute exchange between surface water and groundwater (Brunner et al., 2010; Sophocleous, 2002). Considering that one approach for understanding the responses induced by transient river stages is the use of numerical models (Liang et al., 2018), we used MODFLOW-2005 (Harbaugh, 2005) to develop a three-dimensional (3D) numerical model of the aquifer in the valley at the Alz River, where a flood event was registered in 2013. Groundwater flow and advective and dispersive transport of solutes were also simulated, including four additional scenarios varying river stage and the riverbed conductance. Our aim is to evaluate the impact of river boundary conditions on the SW-GW interaction during flood events and to investigate the effect in the transport of solutes.

4.2 Methods

4.2.1 Site description and dataset

The study area is the Alz valley (Figure 4.1) located in the municipality of Tacherting that is situated in the District of Traunstein, Germany. One of the main features of this village is the Alz River, which borders the eastern edge of the village. It originates in the south from the Chiemsee Lake and falls into the Inn River in the north 63 km downstream. An artificial waterway, the Alz canal, is situated in the southwest of the study area, and it was constructed in order to reroute the water of the Alz to generate electricity through the run-of-river operation. The heavy rainfall at the end of May and the beginning of June 2013 caused great damage in the municipality of Tacherting. The rising water levels and velocities of the streams, and the elevated groundwater levels produced damage to buildings, particularly, due to the seepage of groundwater (Disse et al., 2015).

The starting point of this study is a pre-existing hydrological model developed by Keilholz et al. (2015). This model was developed using MIKE SHE (DHI, 2017) for evaluating the dynamics of the hydrological processes of the flood event. We used the model results and dataset of this research to define the time-variant hydraulic heads and the distribution and the rate of infiltration in our model.

4.2.2 Groundwater flow numerical model

The simulation of the groundwater flow was performed using MODFLOW-2005 (Harbaugh, 2005) as code for solving the finite-difference flow model, and Processing Modflow version 8.0 (Chiang, 2012) as the graphical user interface. The system was subdivided spatially into a finite difference grid of rectangular cells, consisting of eight layers of variable dimensions, 220 rows (5 m each one) and 300 columns (5 m each one). The extension of the modeled area is 1500 m from west to east, and 1100 m form south to north. The model grid encompasses 528000 grid cells, of which 358144 are actively simulated. The discretization in time is established to aim a transient simulation since the solution of the problem is assumed to be time dependent. Therefore, a period of 37 days is divided into 148 stress periods of six hours each. The model domain is delineated based on the surface topography and geological characteristics, which act as physical boundaries and cells out of the perimeter were defined as inactive cells. The bottom of the aquifer (at the bottom of layer 8) is at an elevation of 435 m a.s.l. (above the sea level) (Figure 4.1). The elevations of confining layers were determined from existing geological studies of the region (Bayerisches Landesamt für Umwelt, 2017; Doppler et al., 2011; Traub, 1975).

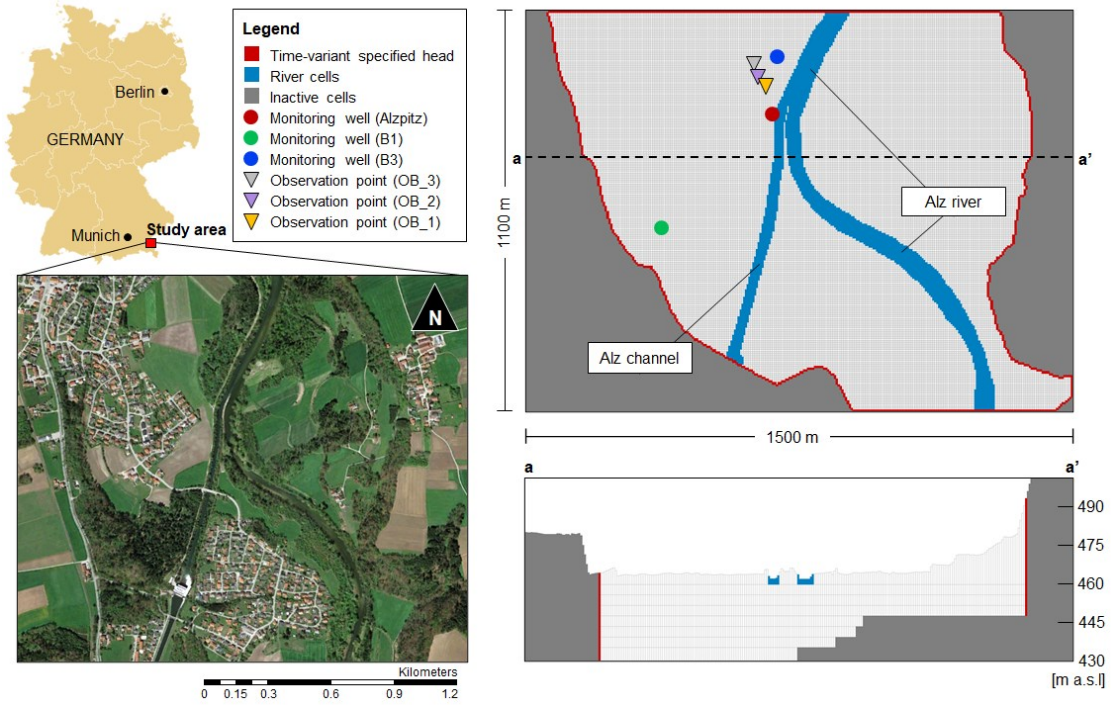

Figure 4.1. Study area and numerical model setup (map source from Google Earth, 2017)

The setup of the model was done by specifying the aquifer properties, which are the horizontal hydraulic conductivity (HK), vertical hydraulic conductivity (VK), specific yield (SY), and specific storage (SS). To extract the concentration changes from the transport simulation, we placed three concentration observation points (OB_1, OB_2 and OB_3) in the model (Figure 4.1). Three MODFLOW packages are used to represent the boundary conditions of the model: the time-variant specified head package (CDH) in the north, west and south part of the model; the river package (RIV) to include the effects of flow between the river and the groundwater regime; and the recharge package (RCH) to simulate specified flux distributed over the top of the model due to infiltration. The stages of both river and canal were obtained interpolating a set of scatter points through the ordinary kriging method with spherical variogram model using ArcGIS (Esri, 2017).

The calibration of the model was done by comparison of the modeled values and observed values of the groundwater head from three monitoring wells: Alzpitz, B1, and B3. The model was calibrated combining manual matching and the regularized inversion process of the parameter estimation code PEST (Doherty, 2010). A supplementary division for the riverbed conductance was done based on the different condition of the natural stream (Alz River) and the artificial canal (Alz canal). Therefore, the parameters included in the calibration were:

HKSA, HKSB, and HKSC (horizontal hydraulic conductivity according to the soil type); VKSA, VKSB, and VKSC (vertical hydraulic conductivities according to the soil type); SS; SY; RCR (riverbed conductance); and, RCC1 and RCC2 (streambed conductance of the canal). Heterogeneous hydraulic conductivity fields were generated for both horizontal and vertical hydraulic conductivity and were applied in each layer for stochastic modeling using the Field Generator of Processing Modflow version 8.0 (Chiang, 2012). The heterogeneity fields are also subdivided according to the three different soil types in the area: younger terraces of sand and gravel (SA), alluvial sand, gravel and marl (SB), and gravel (SC). They are assumed to be lognormally distributed with a standard deviation (log_{10}) of 0.5 and a correlation length (log_{10}) along both rows and columns of 0.1 (the mean values for each soil type are detailed below in the Results section). The parameters were calibrated until the model reached a mean Nash–Sutcliffe coefficient of efficiency and a Pearson correlation coefficient higher than 0.80.

To broadly analyze the influence of river boundary conditions and the sensitivity of the parameters, we performed a series of simulation of scenarios. Four scenarios were executed as a forward run varying the riverbed conductance and the river stage. The rest of the model parameters (HKSA, HKSB, HKSC, VKSA, VKSB, VKSC, SS and SY) were retained constant, using the values from the calibrated model. The scenarios were executed considering variations of ±15% in the water level of the river (as percentage of the height between the water level of the stream and the top of the streambed), and variations ±50% in the riverbed conductance for both the river and the canal. The scenarios were assumed deliberately to observe plausible situations according to the range of variation of both stream stage and riverbed conductance, as well as to avoid the lack of convergence in the simulation.

4.2.3 Solute transport

A constant-density transport simulation was performed to recognize the behavior of a hypothetical solute (Solute A) under flood conditions. The simulation was performed using the modular 3D transport model MT3DMS (Zheng and Wang, 1999). The theoretical approach considered that changes in concentration were caused for advective, dispersive and diffusive transport, and the assumptions do not include any kinetic reactions or sorption. The solute transport simulation is based on the instantaneous injection of Solute A, placed between the monitoring wells B1 and Alzpitz, at an initial concentration of 12500 mg/m^3. For solving the advective transport, Method of Characteristics (MOC), a Eulerian-Lagrangian method, was used as the solution scheme. The solute is placed in one cell (OB_1) on the upper layer to simulate the transport of a solute discharged near to the surface. The simulation began in the first stress period and the concentration changes and distributions were calculated during the 37 days of the flow simulation. Table 4.1 indicates the model parameters for the solute

transport modeling that were assumed based on chlorinated organic compounds and literature review (Davis, 2003).

Table 4.1. Model parameters for solute transport modeling

Model parameters	Unit	Value
Initial concentration	mg/m^3	15000.00
Effective molecular diffusion coefficient	m^2/s	$1e^{-9}$
Longitudinal dispersivity	m	1.70
Transverse dispersivity (horizontal and vertical)	m	0.29
Distribution coefficient	m^3	0.000125
Porosity	-	0.26
Bulk density	kg/m^3	2000.00

4.3 Results and Discussion

4.3.1 Groundwater numerical modeling

The results of the model presented in this section correspond to those after the calibration process. Figure 4.2 shows the comparison between the calculated phreatic level and the observed one in the monitoring wells during the period selected. Figure 4.3 shows the calculated hydraulic heads at different times to illustrate the distribution of the simulated heads and their temporal changes, particularly during the flood event. The results of the quantitative evaluation are summarized in Table 4.2. These statistical measures quantify the error considering the distribution of the residuals rather than to represent a definition of the accuracy of the model. The calibrated parameters are shown in Table 4.3.

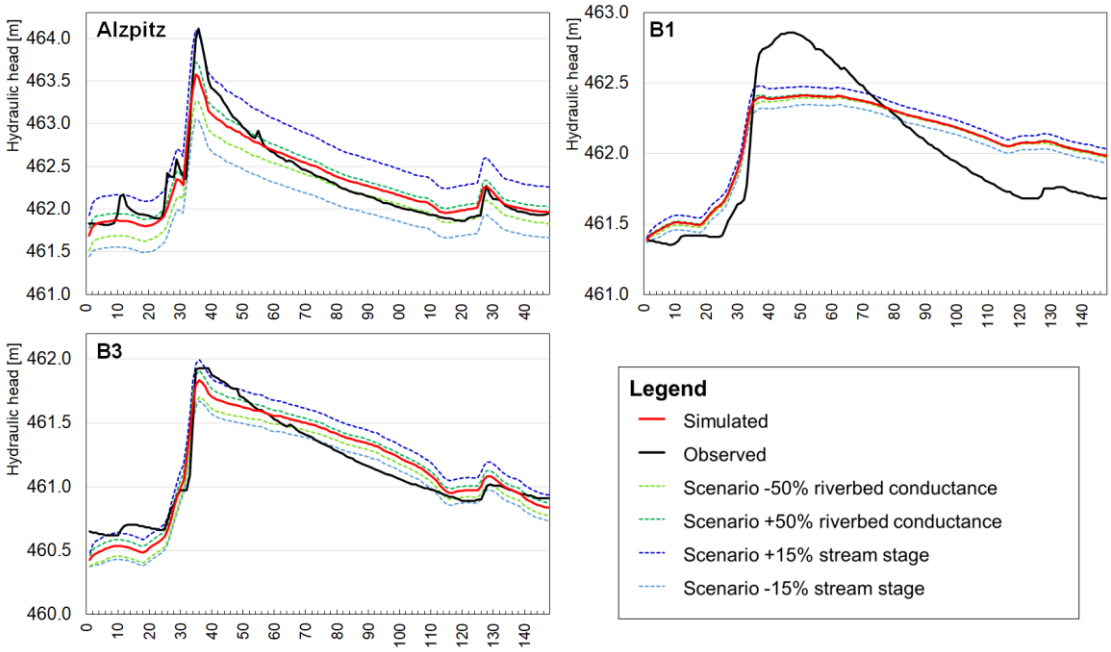

Figure 4.2. Hydraulic head [m] at the different stress periods

The simulated heads were within the calibration objectives and the statistical evaluation suggest that the base model is reliable (Table 4.2). The monitoring wells closer to the streams (Alzpitz and B3) fit better than the monitoring well B1. This may occur because of the influence of the boundaries due to the location of the monitoring well B1 (at approximately 150 m) from the time-variant specified head boundary. We decided to keep the spatial location of the boundaries based on the topography and soil conditions of the area, since the main interest of the model was to evaluate the effect of the river boundary conditions. Calibration of the model would not be possible if we do not consider a strong interconnection between the streams (river and canal) with the aquifer. In other words, to obtain accurate results, we assumed high bed permeability by defining high values of riverbed conductance for the streams. It should be noted that the riverbed conductance at the artificial canal is higher than the riverbed conductance of the river (Table 4.3). According to the simulated water budget, the mean flow into the domain for the period before the flood (20 first stress periods from May 25th to June 30th 2013) is 2.60 m^3/s, whereas during the peak of the flood it is more than 4.83 m^3/s. In average the flow into the system during the whole simulated time is 2.69 m^3/s. The water budget discrepancy was -0.013%.

As shown in Figure 4.2 and Figure 4.3, during the peak of the flood event (stress period 36), the hydraulic head highly increases, particularly in the areas immediate close to the river and the canal. On the other hand, the simulated hydraulic heads slowly decrease from stress period

60 to stress period 148, once the peak time finishes, the influence of the streams on the hydraulic heads highly decline, the hydraulic gradient is lower, and the river effect is less visible in Figure 4.3. Near to the streams, the groundwater heads have similar fluctuation as compared to the stream stages. Near to the river, the peaks of the hydraulic heads decrease faster, which gives evidence of a possible flow back to the river and the canal.

Table 4.2. Results of the statistical evaluation of the calibrated model

Monitoring point	**Mean error**	**Mean absolute error**	**Pearson coefficient**	**Pearson's chi squared**	**Nash-Sutcliffe coefficient**
Alzpitz	-0.001	0.116	0.962	0.007	0.909
B1	0.083	0.238	0.880	0.023	0.686
B3	0.015	0.105	0.951	0.005	0.889
Mean	0.033	0.153	0.960	0.035	0.828

Table 4.3. Calibrated model parameters

Parameter	**Unit**	**Value**
HKSA (mean) and VKSA (mean)	m/s	$7.4131e^{-03}$ and $2.2128e^{-04}$, resp.
HKSB (mean) and VKSB (mean)	m/s	$5.8670e^{-03}$ and $7.5300e^{-04}$, resp.
HKSC (mean) and VKSC (mean)	m/s	$1.2161e^{-02}$ and $8.1611e^{-04}$, resp.
SS	1/m	$3.6625e^{-04}$
EP	-	0.26
SY	-	0.18
RCR, RCC1, and RCC2	m^2/s	$3.8520e^{-04}$, $3.4873e^{-03}$, $6.2461e^{-03}$, resp.

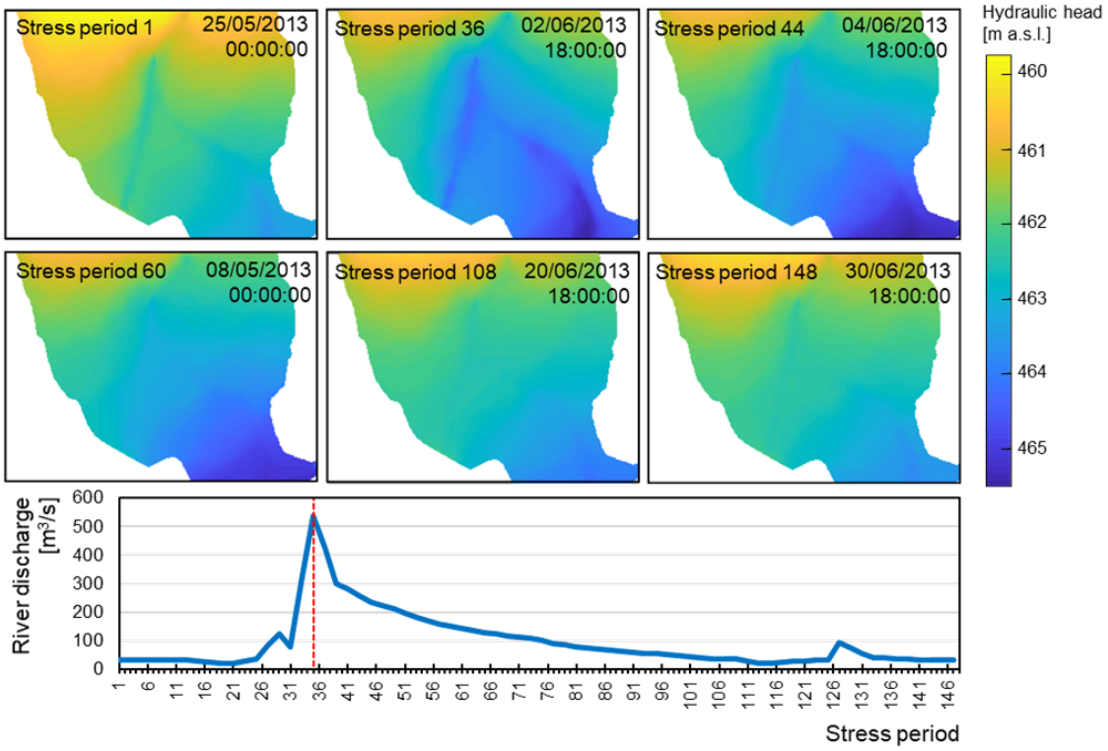

Figure 4.3. Simulated hydraulics heads in the upper layer and river discharge at different stress periods. The vertical red dashed line shows the peak time of the flood event

4.3.2 Solute transport simulation

The change in concentration in the observation points are plotted in Figure 4.4, which includes also the transport modelling of the different scenarios. It is possible to observe that the concentration varies spatially due to the advective and dispersive transport. Besides the solute concentration decreases rapidly, the plume does not travel considerably far from the initial location. The movement of the plume of solute is visible at 15 to 20 m from the initial location. The advective transport decreases considerably after the peak of the flood (from stress period 40) because of the reduction of the groundwater flow velocity. This reduction in the velocity is caused by the decrease in the hydraulic head gradient, which occurs after the peak time, reaching values lower than at the beginning of the simulation period. During the rising flood stage, we observe changes in direction of the groundwater flow caused by the contribution of surface water into the groundwater system. Moreover, the water level of the river and the stream can be two strong hydraulic forces that may induce the groundwater flooding in the southern zone of the region.

The solute moves in the system mainly due to advection in the horizontal direction. Once the gradient is reduced, the horizontal advective transport decreases. However, it is important to consider the increment in the advective movement downwards that may be produced due to the pressure exerted by the river and the canal. Therefore, it is relevant to review the vertical advective transport. On the other hand, dispersion causes the spreading and dilution of the solute plume. Dilution increases faster when more water is introduced in the aquifer, such in the case of scenarios of higher stream stage and higher riverbed conductance. The simulation of the solute shows how low values of dilution mean higher concentration.

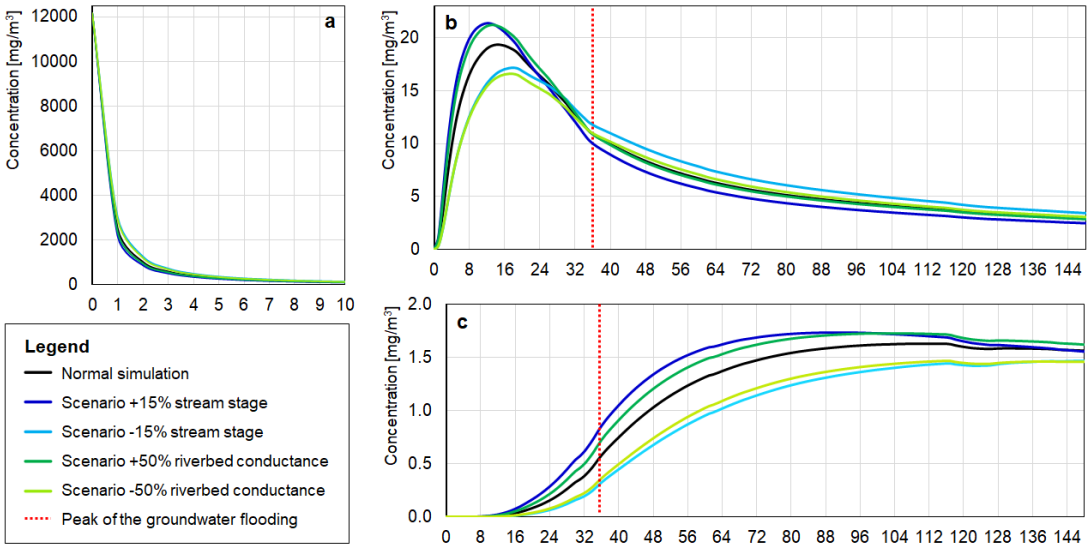

Figure 4.4. Change in concentrations [mg/m^3] for every stress period in the observation points: (a) OB_1, (b) OB_2 and (c) OB_3. The red dashed line shows the peak time of the flood event.

4.4 Conclusions

A 3D numerical model was created to describe the groundwater flow in the aquifer of the Alz valley, and transport simulations were performed to evaluate the solute transport under the flood event. The model accurately represents the conditions of the aquifer during the simulation period, especially in the north-central area of the domain, where the model fits with the calibration targets. The performed simulations give evidence about the temporal and spatial variability of the groundwater flow during the flood event. The groundwater heads near to the rivers and the canals have similar fluctuation patterns to the stream stages.

The medium is pervious and hydraulically conductive as it is mainly composed by gravel and sand, which naturally represent good conditions for allowing groundwater flow. The aquifer is hydraulically connected with both the Alz River and the Alz canal. The aquifer is recharged not only by infiltrated water from precipitation but also by river leakage. This is particularly relevant because it was possible to calibrate the model only if we considered strong hydraulic connection between aquifer and river. During the modeled period, the Alz River and the canal only act as influent streams contributing water to the aquifer. Furthermore, solute transport simulations denote the existence of strong interconnection between the aquifer and the streams, which vary depending on the phase of the flood event. The advective and dispersive transport vary for different scenarios and the influence of the flood event in the aquifer is particularly perceptible when we observe the different timing in the changes in concentration.

The influence of the flood event in the aquifer is particularly noticeable during the higher stages of the flood event and in areas near to the streams. Summing up, the conditions of both the river and the canal affect the groundwater flow velocity and direction. River boundary conditions in the model control the aquifer responses in the proximities of the streams. To evaluate these responses and their temporal variation, it is necessary to evaluate the flood event before, during and after the peak of the event. As this study demonstrate, the aquifer behavior can widely vary from one of these phases to the next one. Certainly, the relative importance and utility of this evaluation will rely on temporal and spatial conditions and the hydrogeological characteristics of the evaluated system.

5 Bayesian inference in groundwater flood risk assessment

Abstract

Groundwater flooding can cause severe damages to homes, utilities, and infrastructure and yield significant economic and social costs. Numerical models are used to understand these events and are the basis to produce imagery products for risk management and communication. However, such maps are generally produced using forward model simulations, and most of the mapping products are still deterministic. In contrast to pluvial and fluvial floods, an open issue in the analysis of susceptibility to groundwater flooding is the lack of probabilistic assessment and mapping products recognizing parametric uncertainty. Hence, we propose a Bayesian-based framework to create probabilistic risk maps and to identify the susceptibility to groundwater flood events. We aim to assess the spatial distribution and temporal variability of groundwater flooding by decomposing the uncertainty and the sensitivity of distributed groundwater numerical models. The scheme involves the use of the elementary effects method, the DiffeRential Evolution Adaptive Metropolis (DREAM) algorithm, and the exploration of the predictive posterior distributions of the groundwater heads to evaluate the susceptibility according to exceedance levels. We use the proposed Bayesian framework with a numerical model that simulates the groundwater flood event that occurred in the valley of the Alz River in 2013. This study developed two types of susceptibility maps based on the exceedance probability of certain groundwater levels and specific cellar depths. The Bayesian inference supports the parameter estimation and thereby increases the spatial confidence of the areas susceptible to inundation. This study shows that maps of susceptibility to groundwater flooding can be built over one single event models and acknowledge the inherent spatial and temporal uncertainty of such events.

Material from:

Merchán-Rivera, P., Geist, A., Disse, M., Huang, J., Chiogna, G., 2022. A Bayesian Framework to Assess and Create Risk Maps of Groundwater Flooding. Journal of Hydrology.

5.1 Introduction

The increasingly frequent occurrence of extreme weather events has raised attention about flood events (Kaiser et al., 2020; Tabari, 2020; Winsemius et al., 2016). Although the focus of flood risk assessment often tends to be on the fluvial and pluvial floods (Ascott et al., 2017; Collins et al., 2020), groundwater flooding can yield significant economic and social damages and disruptions, such as sewer backups (Abboud et al., 2018; Morris et al., 2018), roads and property inundation (Abboud et al., 2018; Keilholz et al., 2015; Morris et al., 2018; Soren, 1976), foundation failures and corrosion (Colombo et al., 2018; Oyedele et al., 2009), damages to underground structures and infrastructure (Gattinoni and Scesi, 2017; Preene and Fisher, 2015), underground pollution transport (González-Quirós and Fernández-Álvarez, 2019), and crop damage (Booth et al., 2016). This type of flood event refers to the groundwater emergence at the ground surface and the rising groundwater level into underground civil infrastructure (Macdonald et al., 2012, 2008). Unlike other types of floods, groundwater flooding can be difficult to identify and assess (Kreibich et al., 2009; McKenzie et al., 2010), and traditional flood protection systems may not be effective (Yu et al., 2019).

Similar to traditional flood risk management, a large number of studies applies numerical modeling at different scales and with a varying degree of complexity to understand groundwater flood events (Abboud et al., 2018; González-Quirós and Fernández-Álvarez, 2019; Morrissey et al., 2020; Yu et al., 2019). These models are typically posed as forward problems, which involve predicting “error-free” model states based on a prior parameterization of the model (Tarantola, 2005). One disadvantage in this type of strategy is that it requires specifying a variety of parameters, which are impossible to characterize exhaustively (Zhou et al., 2014). Another drawback of forward problems is that, once calibrated, the model ignores the equifinality thesis (Beven and Freer, 2001) and the uncertainties, which may imply to adopt strong and questionable assumptions about its forecast reliability (Di Baldassarre et al., 2010). Consequently, probability theory tools, such as inverse methods (Helton et al., 2004; Kaipio and Somersalo, 2005), have evolved to address aleatory and epistemic uncertainties (Merz and Thieken, 2009; Ross et al., 2009). In contrast to forward models, inverse methods were developed to support parameter identification and consequently to improve predictions (Zhou et al., 2014). Bayesian approaches solve inverse problems considering parameters as random variables and providing posterior probabilities by incorporating known data (Smith, 2013). Due to their inferential and predictive properties, Bayesian methods are considered one of the most appropriate techniques for uncertainty analysis (Heße et al., 2019). In spite of the progress in the field of uncertainty quantification, the temporal and spatial uncertainties of the models are often declared but not quantified in groundwater flooding studies. A limited number of studies includes a formal quantification of the uncertainty (Colombo et al., 2018; Fürst et al., 2015; Jimenez-Martinez et al., 2015),

and, to the best of the authors' knowledge, the explicit application of Bayesian inference on groundwater flooding modeling remains unexplored.

Flood risk mapping is a fundamental tool for flood risk management and communication (Demeritt and Nobert, 2014; Henstra et al., 2019). Accordingly, a lot of effort has been made to generate groundwater flood maps for planning, damage assessment, and insurance purposes (Morris et al., 2018). Maps of groundwater flooding susceptibility are regularly constructed on the basis of lumped parameter models (Upton and Jackson, 2011) or by analyzing geological and hydrogeological data (British Geological Survey, 2006; Mancini et al., 2020; Yu et al., 2019). Recent studies employ this type of data with machine learning techniques to create spatially distributed maps of susceptibility to groundwater flood events (Allocca et al., 2021). Still, the lack of probabilistic and inverse methods in groundwater flooding models has been transferred to the groundwater flooding imagery, which often does not include formal likelihood quantification. This partially occurs due to the computational challenge from distributed models and high-dimensional inverse problems (Boyce and Yeh, 2014; Merz and Thieken, 2009; Xu et al., 2017; Zhou et al., 2014), and to limitations derived from data quality and availability (McKenzie et al., 2010; Merz and Thieken, 2009; Morris et al., 2018). Alternatives to overcome these problems are the reduction of the dimension of the input parameter space (Bittner et al., 2021; Boyce and Yeh, 2014; Erdal and Cirpka, 2019; Mara et al., 2017; Stanko et al., 2016; Teixeira Parente et al., 2019), and the optimization of the problem design by changing the spatial and temporal scaling (i.e., simulation period and model extension) and resolution (i.e., time and space discretization) (Guillaume et al., 2016; Scheibe et al., 2015). Assembling these alternatives can be useful to assess groundwater flooding in a probabilistic manner. As explained by Teng et al. (2017) and Di Baldassarre et al. (2010), probabilistic flood risks maps are preferable to single deterministic maps of inundation because they acknowledge the inherent uncertainty. In comparison to pluvial and fluvial flooding, there is less detail for hazard and risk management in groundwater flood mapping (Morris et al., 2018). As the demand for probabilistic maps in pluvial and fluvial flood risk analysis increases (Bhola et al., 2020; Teng et al., 2017), the need for groundwater flooding analysis is not expected to behave differently.

This study introduces a framework to recognize the susceptibility of residential property areas to groundwater flooding acknowledging the uncertainty in the model input parameters. We aim to create mapping products with the estimation of the probability of groundwater flood inundations by targeting one groundwater flood event as the basis of the problem design. We propose to decompose cell-by-cell the uncertainty and the sensitivity of a distributed groundwater numerical model to understand the spatial distribution and temporal variability of groundwater flood events. The framework involves three components: 1) elementary effects method to identify influential input factors and reduce the problem dimensionality, 2) Bayesian inference using the DiffeRential Evolution Adaptive Metropolis (DREAM)

algorithm to estimate statistics of the relevant uncertain parameters and to quantify the output uncertainty incorporating evidence data, and 3) exploration of the predictive posterior distributions to assess the susceptibility to groundwater flooding according to exceedance probability levels. To demonstrate the relevance and feasibility of the application, the framework is applied to evaluate a groundwater flood event that occurred in the valley of the Alz River in Germany in 2013. The event is simulated using a numerical model built on MODFLOW-2005 (Harbaugh, 2005). The posterior probability distributions of the groundwater heads are then explored against groundwater depth thresholds and registered cellar depths.

5.2 Methods

5.2.1 Groundwater flow equation

Groundwater flow in a heterogeneous unconfined aquifer can be described by coupling the continuity equation with Darcy's law (Fetter, 1999), such that

$$\frac{\partial}{\partial x}\left(k_{xx}\frac{\partial h}{\partial x}\right)+\frac{\partial}{\partial y}\left(k_{yy}\frac{\partial h}{\partial y}\right)+\frac{\partial}{\partial z}\left(k_{zz}\frac{\partial h}{\partial z}\right)+W=s\frac{\partial h}{\partial t}\ , \qquad \textit{Eq. 5.1}$$

where h is the piezometric groundwater head [L], k_{xx}, k_{yy}, and k_{zz} denote the hydraulic conductivity values [LT^{-1}] along the x, y, and z coordinate axes, s is the specific storage [L^{-1}], and W represents the sources and sinks [T^{-1}]. MODFLOW-2005 (Harbaugh, 2005) solves the groundwater flow equation in a finite difference form. The rate of change in storage within each cell is equal to the sum of flows into and out of the cell so that

$$\sum Q_i = s\frac{\Delta h}{\Delta t}\Delta V\ , \qquad \textit{Eq. 5.2}$$

where Q_i is the i component of the flow rate into the cell [L^3T^{-1}], ΔV is the cell volume [L^3], and Δh [L] is the change in the groundwater head over a time interval Δt [T]. External sources or stressors, such as the infiltration into the saturated zone and the river-aquifer fluxes, can be

represented as Q_i elements. Hence, the forward problem is driven to predict the groundwater head distributions at successive times as a function of an uncertain set of model inputs θ (i.e., uncertain parameters, source terms, initial or boundary conditions).

5.2.2 Sensitivity analysis

Sensitivity analysis is used to quantify how the uncertainty in the output of a model can be apportioned to the different uncertainties in the model inputs (Saltelli, 2002; Smith, 2013). We use the elementary effects method, also known as Morris method, to identify the sensitive parameters through basic statistical moments (Campolongo et al., 2007; Morris, 1991). Due to its sampling strategy, this technique is advantageous for quantifying the sensitivity in computationally expensive models with many uncertain inputs (Campolongo et al., 2007; Jaxa-Rozen and Kwakkel, 2018; Smith, 2013). In our research, the purpose of its application is to identify which input factors are non-influential and therefore negligible, as well as to recognize the input factors that are non-linear or involved in interactions. Those input factors that are non-influential are fixed to reduce the problem dimensionality, which is an essential step to define an affordable experimental design and proceed with the subsequent Bayesian analysis.

The elementary effect method considers that each model input $q = [q_1, \dots, q_k]$ varies across p selected levels, forming a k-dimensional p-level finite grid of experimentation Γ_p. Then, p represents the number of partitions of the model parameter space at which the model can be evaluated. Assuming that the input terms are scaled to the interval $[0,1]$, the elementary effect associated with the input q_i is defined as

$$d_i(q) = \frac{f(q_1, \dots, q_{i-1}, q_i + \Delta, q_{i+1}, \dots, q_k) - f(q)}{\Delta} = \frac{f(q + \Delta e_i) - f(q)}{\Delta}, \qquad \textit{Eq. 5.3}$$

with a jump size $\Delta \in \{1/(p-1), \dots, 1 - 1/(p-1)\}$ and transformed point $q + \Delta e_i$, where $q = (q_1, \dots, q_k)$ is any selected value in Γ_p, and e_i is a vector of zeros with one in the i^{th} component. Then, $d_i(q)$ quantifies the local sensitivity behavior at the point q. The global sensitivity measure requires to approximate the statistical moments from the associated finite-dimensional distribution G_i by randomly sampling q from the grid points in Γ_p. Morris (1991) proposed the mean μ_i and the standard deviation σ_i of the distribution G_i. By sampling m points, these metrics associated with the i^{th} parameter and j^{th} samples can be expressed as

$$\mu_i = \frac{1}{m}\sum_{j=1}^{m} d_i^j(q) \ , \qquad \textit{Eq. 5.4}$$

$$\sigma_i = \sqrt{\frac{1}{m-1}\sum_{j=1}^{m}\left(d_i^j(q) - \mu_i\right)^2} \ . \qquad \textit{Eq. 5.5}$$

Campolongo et al. (2007) introduced an additional sensitivity metric μ^* to avoid the problems associated to non-monotonic models that may contain effects with opposite signs. This refined version estimates the mean of the absolute values of the elementary effects and can be written as

$$\mu_i^* = \frac{1}{m}\sum_{j=1}^{m}\left|d_i^j(q)\right| \ . \qquad \textit{Eq. 5.6}$$

The elementary effects method proposes to construct μ_i^* and σ_i with m trajectories of $(k+1)$ points in the input space, which provide k elementary effects. The total number of realizations is defined by $(k+1)\times m$. The sampling strategy employs the orientation matrix $\mathbf{B}^*$ to obtain random samples from G_i, so that

$$\mathbf{B}^* = \left(\mathbf{J}_{k+1,1}q^* + \frac{\Delta}{2}\left[\left(2\mathbf{B} - \mathbf{J}_{k+1,k}\right)\mathbf{D}^* + \mathbf{J}_{k+1,k}\right]\right)\mathbf{P}^* \ , \qquad \textit{Eq. 5.7}$$

where q^* is a random initial point, $\mathbf{J}_{k+1,k}$ is a $(k+1)\times k$ matrix of ones, $\mathbf{B}$ is a $(k+1)\times k$ strictly lower triangular matrix of ones, $\mathbf{D}^*$ is a $k\times k$ diagonal matrix formed by randomly chosen elements from the set $\{-1,1\}$, and $\mathbf{P}^*$ is a $k\times k$ random permutation matrix.

5.2.3 Bayesian inference and sampling algorithm

5.2.3.1 Bayesian inference

Bayesian inference is derived from the Bayes' theorem to explicitly introduce in the analysis assumptions about evidence data and prior knowledge of the model inputs (Box and Tiao, 2011; Smith, 2013). Let y represent a given set of observations or evidence data and θ denote a set of parameters. Following the Bayesian formulation, the posterior probability of the parameter set $P(\theta|y)$ can be obtained with the prior probability of the parameter set $P(\theta)$, the observed data $P(y)$, and the likelihood function $P(y|\theta) \equiv L(\theta|y)$, such that

$$P(\theta|y) = \frac{P(y|\theta) \times P(\theta)}{P(y)} \ . \qquad \textit{Eq. 5.8}$$

Given that all statistical inferences of $P(\theta|y)$ can be made from the unnormalized density, $P(y)$ can be omitted (Vrugt, 2016), and the Bayes equation is simplified as

$$P(\theta|y) \propto L(\theta|y) \times P(\theta) \, . \qquad \textit{Eq. 5.9}$$

$L(\theta|y)$ summarizes the distance between the observation and the simulated quantity of interest (groundwater heads for the sake of our research). Our formulation of the Bayesian inference problem assumes that the error residuals are homoscedastic and normally distributed $\varepsilon_t \sim \mathcal{N}(0, \sigma^2)$, and it employs the log-likelihood $\mathcal{L}(\theta|y)$ for numerical stability (Vrugt, 2016). Then, considering n-vector of error residuals at times $t_s = \{1, \dots, n\}$, the log-likelihood function applied in this study can be written as

$$\mathcal{L}(\theta|y) = -\frac{n}{2} \times log\left[\sum_{t_s=1}^{n} \varepsilon_t(\theta)^2\right] . \qquad \textit{Eq. 5.10}$$

For further debate about mathematical definitions of the likelihood function and details in their derivation process, we refer the readers to the corresponding literature (Kaipio and Somersalo, 2005; Schoups and Vrugt, 2010; Vrugt, 2016)

5.2.3.2 Sampling algorithm

To estimate the probability density function of the parameters, Markov Chain Monte Carlo (MCMC) sampling is implemented using the differential evolution adaptive metropolis (DREAM) scheme (Vrugt et al., 2009, 2008; Vrugt and Ter Braak, 2011). In general, MCMC techniques consist of the iterative sampling of a probabilistic space to find areas of a high likelihood of the posterior distribution of the parameter space. The DREAM algorithm is an efficient MCMC-based method. It runs multiple chains of simulations simultaneously and adjusts the scale and orientation of the proposal distribution during the run. Candidate points are created by sampling the prior parameter distribution for each chain, and the Metropolis-Hastings ratio is used to decide if a candidate point is accepted or not. The convergence of each chain is evaluated using the Gelman-Rubin diagnostic (Gelman and Rubin, 1992). Extensive theoretical descriptions of the DREAM algorithm implementation can be found in the literature (Houska et al., 2015; Vrugt, 2016; Vrugt et al., 2009, 2008; Vrugt and Ter Braak, 2011).

5.2.4 Exceedance probability and susceptibility maps

The final step of the framework involves extracting information from the posterior distributions of the groundwater heads at each element of the model and at different time steps to analyze the spatial and temporal conditions of the event. We characterize the associated groundwater flooding risk by computing the probability of the groundwater table of exceeding a certain threshold value (i.e., exceedance probability). For convenience, this can be explained from the cumulative distribution function of the predicted groundwater heads $F(h)$ for $F: \mathbb{R} \rightarrow [0,1]$, that can be described by

$$F(h) \coloneqq P(H \leq h)\,. \qquad \textit{Eq. 5.11}$$

The exceedance probability $\bar{P}$ can then be estimated with the complementary cumulative distribution function of Eq. 5.11, expressed as

$$\bar{P} = P(H > h) = 1 - F(h)\,.$$ *Eq. 5.12*

Consequently, we create the maps of susceptibility to groundwater flooding considering the probability $\bar{P}_{i,j}^{(t)}$ of exceeding a threshold $\mathrm{K}_{i,j}$, computed at the time step $t = [t_1, \ldots, t_n]$ and the discrete point $i = 1, \ldots, n_c$ and $j = 1, \ldots, n_r$, where n_c and n_r are, respectively, the number of columns and rows used for the spatial discretization. Thus,

$$\bar{P}_{i,j}^{(t)} = 1 - F_{i,j}^{(t)}(\mathrm{K}_{i,j})\ .$$ *Eq. 5.13*

We propose two types of thresholds in this work. The first one is the groundwater depth threshold $\kappa_{i,j}$, which represents a specified distance d between the surface elevation and the groundwater table at the cell i, j. Hence, it can be defined according to a two-dimensional array of a digital elevation model $T_{i,j}$, that is,

$$\kappa_{i,j} = T_{i,j} - d\,.$$ *Eq. 5.14*

The second threshold is defined according to the cellar depths $\hat{\kappa}_{i,j}$ at a specific house, property, or building. Hence, $\hat{\kappa}_{i,j}$ is the reported depth of the underground infrastructure located at the cell i, j. Therefore, $\mathrm{K}_{i,j}$ can be equal to $\kappa_{i,j}$ or $\hat{\kappa}_{i,j}$ depending on the assessment.

5.2.5 Practical application

5.2.5.1 Case study

The study area is located in southeastern Bavaria, Germany. During heavy rainfall events at the beginning of June 2013, the region was affected by flood events that caused several damages in the residential properties (Disse et al., 2015; Keilholz et al., 2015). The study

region is characterized by an unconsolidated shallow sedimentary aquifer formed by gravels and sands (Doppler et al., 2011; Keilholz et al., 2015; Merchán-Rivera et al., 2018). The groundwater flow is very dynamic due to the high permeability of the porous material of the aquifer, the relatively rapid groundwater recharge, and the hydraulic connection with the Alz River and the Alz Canal. The flood event in 2013 in the Alz River valley and the hydrogeological features of the region were the subjects of previous studies. Doppler et al. (2011) and Bayerisches Landesamt für Umwelt (2017) describe the geological properties and the morphological features of the valley. Further studies also estimate the uncertainty in the discharge and stage of the Alz River (Willems, 2011; Willems and Stricker, 2012) and quantify the propagation of uncertainty due to the representation of the river boundary conditions (Merchán-Rivera et al., 2021). Figure 5.1 includes details of the study area and the flood event.

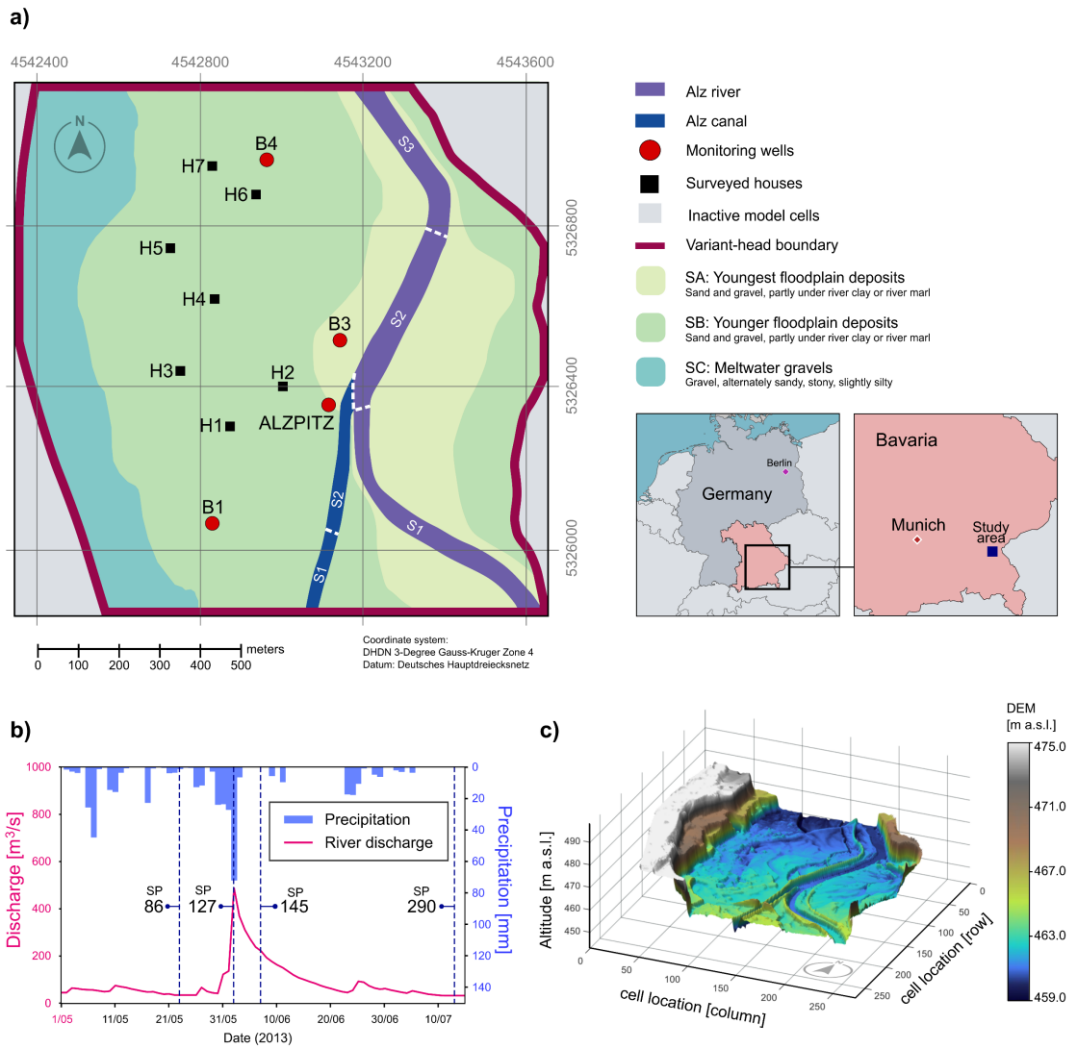

Figure 5.1. Study case implementation: a) study area location and model setting with groundwater monitoring wells (circles) and the selected surveyed houses (squares); b) event description and representative stress periods (SP) for the different event phases; and, c) digital elevation model (DEM) used to represent the surface elevation

5.2.5.2 Model description

A two-dimensional model was built using MODFLOW-2005 (Harbaugh, 2005) to describe the event. The model simulates 300 stress periods at intervals of six hours to cover a total of 75 days (from May 02, 2013 to July 15, 2013). The spatial discretization is a finite-difference grid formed by one layer, 260 rows, and 260 columns. The initial and boundary conditions were defined based on the preexisting regional model built by Keilholz (2015). Three types of boundary conditions are used in the model: 1) specified head boundaries, using time-variant

specified head package (Harbaugh et al., 2000; Leake and Prudic, 1991) to simulate the variation in the water table at the borders of the domain, 2) recharge into the saturated zone, using the recharge package (Harbaugh, 2005; Harbaugh et al., 2000) to simulate the distributed infiltration flux, and 3) river interactions, using the river package (Harbaugh, 2005; Harbaugh et al., 2000) to simulate the interaction between the streams and the aquifer. The spatial distribution of the specified head and river boundaries are illustrated in Figure 5.1a. Given that the initial conditions of the groundwater heads and the specified-head boundaries were extracted from the regional model (Keilholz et al., 2015), which include a larger simulation period, there was no need to include a warm up period. Three hydraulic conductivity values (k_A, k_B, and k_C) are defined based on the geological studies (Bayerisches Landesamt für Umwelt, 2017; Doppler et al., 2011), and, accordingly, three specific storage values (s_A, s_B, and s_C) and three specific yield values (γ_A, γ_B, and γ_C). These parameters were assumed to be homogeneous within each soil section (SA, SB and SC). Recharge into the saturated zone values ($Q_{i,j}^{(t)}$) are defined according to the deterministic estimations from the hydrological model made by Keilholz et al. (2015). Finally, the streams are parameterized considering two streambed conductance values for the canal (c_1 and c_2), three streambed conductance values for the river (r_1, r_2, and r_3), which are outlined according to observed differences in the morphology of the streams, and stream stage values ($\xi_{i,j}^{(t)}$) based on the previous estimations made by Merchán-Rivera et al. (2021). Groundwater field measurements were registered every six hours during the simulation period in four groundwater monitoring wells: Alzpitz, B1, B3, and B4 (Keilholz et al., 2015). These observations were used as the evidence for the Bayesian inference. Although we computed the hydraulic head values for the entire simulation period, we chose four simulation time steps to be representative of different phases of the event to present the results: before the event at stress period 86 (May 23, 2013), peak-flow at stress period 127 (June 02, 2013), recession phase at stress period 145 (June 07, 2013), and after the flood event at stress period 290 (July 13, 2013). We define the recession phase as the stage that immediately follows the peak-flow, whereas after the event refers to the phase where the declining period has ended. These separate periods were used along with the results and discussion to understand the temporal variation of the outcomes. Figure 5.1 includes details of the study, the model settings and the digital elevation model.

5.2.5.3 Scheme implementation

The hydraulic properties are summarized in Table 5.1, where $\mathcal{U}(a, b)$ denotes the prior belief distributed uniformly between a and b. Except for $Q_{i,j}^{(t)}$ and $\xi_{i,j}^{(t)}$, the uncertainty analysis considers the parameters as random variables that are simply sampled from a uniform distribution and used in the realizations of the scheme. The choice to set the prior beliefs to be uniform (i.e., non-informative) is a conservative assumption at costs of computational efficiency. In practice, this means that we need a larger sample size to obtain better estimates

of the posterior distribution during Bayesian inversion. More informative prior distributions would require a smaller sample size to reach a similar precision. Note that the sampling strategy in the elementary effect method should be modified if non-uniform distributions are considered (Feng et al., 2019).

Table 5.1. Distribution properties of the stochastic input variables

Parameter	Zone	Notation	Distribution	Units
Hydraulic conductivity	SA	k_A	$\mathcal{U}(1e^{-4}, 1e^{-1})$	m/s
	SB	k_B	$\mathcal{U}(1e^{-4}, 1e^{-1})$	m/s
	SC	k_C	$\mathcal{U}(1e^{-6}, 1e^{-3})$	m/s
Specific storage	SA	s_A	$\mathcal{U}(1e^{-7}, 1e^{-3})$	$1/s$
	SB	s_B	$\mathcal{U}(1e^{-7}, 1e^{-3})$	$1/s$
	SC	s_C	$\mathcal{U}(1e^{-7}, 1e^{-3})$	$1/s$
Specific yield	SA	γ_A	$\mathcal{U}(0.10, 0.40)$	–
	SB	γ_B	$\mathcal{U}(0.10, 0.40)$	–
	SC	γ_C	$\mathcal{U}(0.10, 0.40)$	–
Recharge multiplier	–	R	$\mathcal{U}(0.00, 2.00)$	–
Conductance of the canal	S1	c_1	$\mathcal{U}(1e^{-5}, 9e^{-1})$	m^2/s
	S2	c_2	$\mathcal{U}(1e^{-5}, 9e^{-1})$	m^2/s
Conductance of the river	S1	r_1	$\mathcal{U}(1e^{-7}, 9e^{-4})$	m^2/s
	S2	r_2	$\mathcal{U}(1e^{-7}, 9e^{-4})$	m^2/s
	S3	r_3	$\mathcal{U}(1e^{-7}, 9e^{-4})$	m^2/s
Stream stage variation	–	ψ	$\mathcal{U}(-0.145, 0.145)$	m

The recharge influx into the saturated zone $Q_{i,j}^{(t)}$ is spatially distributed over the domain and varies at every stress period t of the simulation. Keilholz et al. (2015) estimated deterministic values for recharge into the saturated zone $\tilde{Q}_{i,j}^{(t)}$ in a regional hydrologic model using MIKE SHE (DHI, 2013). In our research, the uncertainty in these recharge values is introduced as a single multiplier R for all the grid cells affected by recharge at all time steps, similarly to the approach employed by Mustafa et al. (2018). Hence, the random variable $R \sim \mathcal{U}(a, b)$ is used in combination with $\tilde{Q}_{i,j}^{(t)}$ to obtain the corrected spatial distributed recharge $Q_{i,j}^{(t)}$, such that

$$Q_{i,j}^{(t)} = \tilde{Q}_{i,j}^{(t)} \times R \ . \qquad \textit{Eq. 5.15}$$

Similarly, Keilholz et al. (2015) provided scatter stage information for the river and the canal. These scatter data were post-processed by Merchán-Rivera et al. (2021) to obtain the stream head $\tilde{\xi}_{i,j}^{(t)}$ at every cell that represents the river and the canal. Hence, the streams are represented as time-variant and spatially distributed inputs. The uncertainty in the stage is included by the error $\psi \sim \mathcal{U}(a, b)$, where the bounds a and b are approximated according to the works by Willems (2011) and Willems and Stricker (2012). This means that ψ increases or reduces the stream stage $\tilde{\xi}_{i,j}^{(t)}$, for all of the stress periods t at each cell i, j that represent the streams to obtain

$$\xi_{i,j}^{(t)} = \tilde{\xi}_{i,j}^{(t)} + \psi \ . \qquad \textit{Eq. 5.16}$$

The implementation of the elementary effects considers all parameters mentioned in Table 8.1 as input factors. Given that the values of p and m are primarily an experimental choice (Saltelli et al., 2004), we performed an extensive exploration of different factor levels and sampling size by constructing various experimental combinations using p = 4, 6, 8 and 10, and m = 10, 20 and 30. The elementary effects approach reduces the dimensionality of our problem and provide a list of influential factors that are later used in the Bayesian inversion with the DREAM algorithm. The posterior distributions are calculated from the last 50% of the samples generated with the DREAM algorithm from 10000 realization. We explore the posterior predictive distributions of the groundwater heads at every element of the domain and every stress period. To compute the threshold $\kappa_{i,j}$, we define $T_{i,j}$ with the digital elevation model (DEM) of the region (Bayerisches Landesamt für Umwelt, 2017) and the groundwater depth d to be equal to 0.5 and 1.5. Note that d values are arbitrarily selected, and they can simply be modified once the posterior predictive distributions are quantified. The DEM resolution is 5×5 m cell size. Finally, we define the threshold $\hat{\kappa}_{i,j}$ using the cellar depth records from the household survey run by Disse et al. (2015) in April 2014: $\hat{\kappa}_{H1}$ = 459.0 m a.s.l. (above sea level), $\hat{\kappa}_{H2}$ = 458.6 m a.s.l., $\hat{\kappa}_{H3}$ = 459.4 m a.s.l., $\hat{\kappa}_{H4}$ = 461.1 m a.s.l., $\hat{\kappa}_{H5}$ = 460.1 m a.s.l., $\hat{\kappa}_{H6}$ = 461.0 m a.s.l., $\hat{\kappa}_{H7}$ = 460.3 m a.s.l.

We employ the SALib Python library (Herman and Usher, 2017) to compute the elementary effect indices with the efficient sampling strategy introduced by Campolongo et al. (2007). The DREAM algorithm was implemented using the SPOTPY framework (Houska et al., 2015). The probability maps in the results were created by arranging the output data in matrix arrays using the Numpy library (Harris et al., 2020) and plotting them with the Matplotlib library (Hunter, 2007) in Python 3. The algorithm for implementing the exposed approach was written in Python 3, and the files are available in the research dataset (Merchán-Rivera, 2021).

5.3 Results and discussion

5.3.1 Sensitivity analysis

Based on the values of μ^*, we obtain a ranking of model sensitivity that can be easily interpreted (see Figure 5.2). A high absolute measure of central tendency μ^* denotes an input with a significant overall influence on the output. Hence, the most sensitive parameters are k_A, k_B, γ_A, R, c_2, and r_2. Also, there are spatial and temporal variabilities in the results of the elementary effects. The positions in the ranking change depending on the location and the phase of the event. We observe higher values of the elementary effects metrics at the peak-flow. Similarly, we can see more significant differences between the minimum and maximum values of μ^* at this phase. The spatial variation in the sensitivity of the recharge multiplier R occurs due to the heterogeneous distribution of the recharge into the saturated zone $\tilde{Q}_{i,j}^{(t)}$. The parameters that describe the streams (c_1, c_2, r_1, r_2, r_3, and ψ) gain relevance close to the streams at the monitoring wells Alzpitz and B3. The sensitivity of the canal conductance c_2 is also large at B1 and H1.

The second sensitivity measure that we obtain is the spread σ. A high value of σ indicates input factors with a non-linear effect in the model output, the existence of parameter interactions, or both. The ratio σ/μ^* is an indicator of model linearity (if $\sigma/\mu^* = 0$), or non-linearity (if $\sigma/\mu^* > 0$). Also, this indicator can occasionally give evidence of monotonic and non-monotonic model responses, when $0 < \sigma/\mu^* < 0.5$ and $\sigma/\mu^* > 0.5$, respectively (Garcia Sanchez et al., 2014). In Figure 5.3, we display all the outcomes of μ^* and σ from every combination of p and m and classify them based on the event phase in a scatter plot. Overall, the model behavior is subject of non-linearities, non-monotonicities, or interactions between model parameters. The results also show temporal variation in this behavior. While the functional relationships between the input factors and the outputs are highly non-linear, interactive, or non-monotonic during the peak and the recession phase, the relationships tend to reduce these qualities before and after the event. Non-monotonic responses can occur with

respect to the input factors associated to the hydraulic conductivity, particularly k_A and k_B. The effect of the parameter interactions can increase due to the increased influx from the high staged-river seen in the peak-flow and the recession phase, which would also influence the non-monotonicity from k_A and k_B. Notice that the non-linearity of the model responses is not affected directly by variations in the influx from the streams and the recharge but by the effect that these have on the hydraulic gradient magnitude. Five parameters can be considered non-influential factors: k_C, s_A, s_B, s_C, and γ_C. As expected, the specific storage values are negligible because we study an unconfined aquifer and their contribution to the storativity is orders of magnitude lower than the specific yield. In the case of k_C and γ_C, the low values of μ^* are determined by the spatial location of the soil type SC. Hence, these five parameters are fixed to reduce the problem dimensionality for the Bayesian inversion from 16 to 11 calibration parameters. Even if a further reduction of the parameter space could be assumed and be quite useful for the application of the Bayesian inversion, we want to retain the properties of the original model for the scope of the study at the cost of higher computational demand.

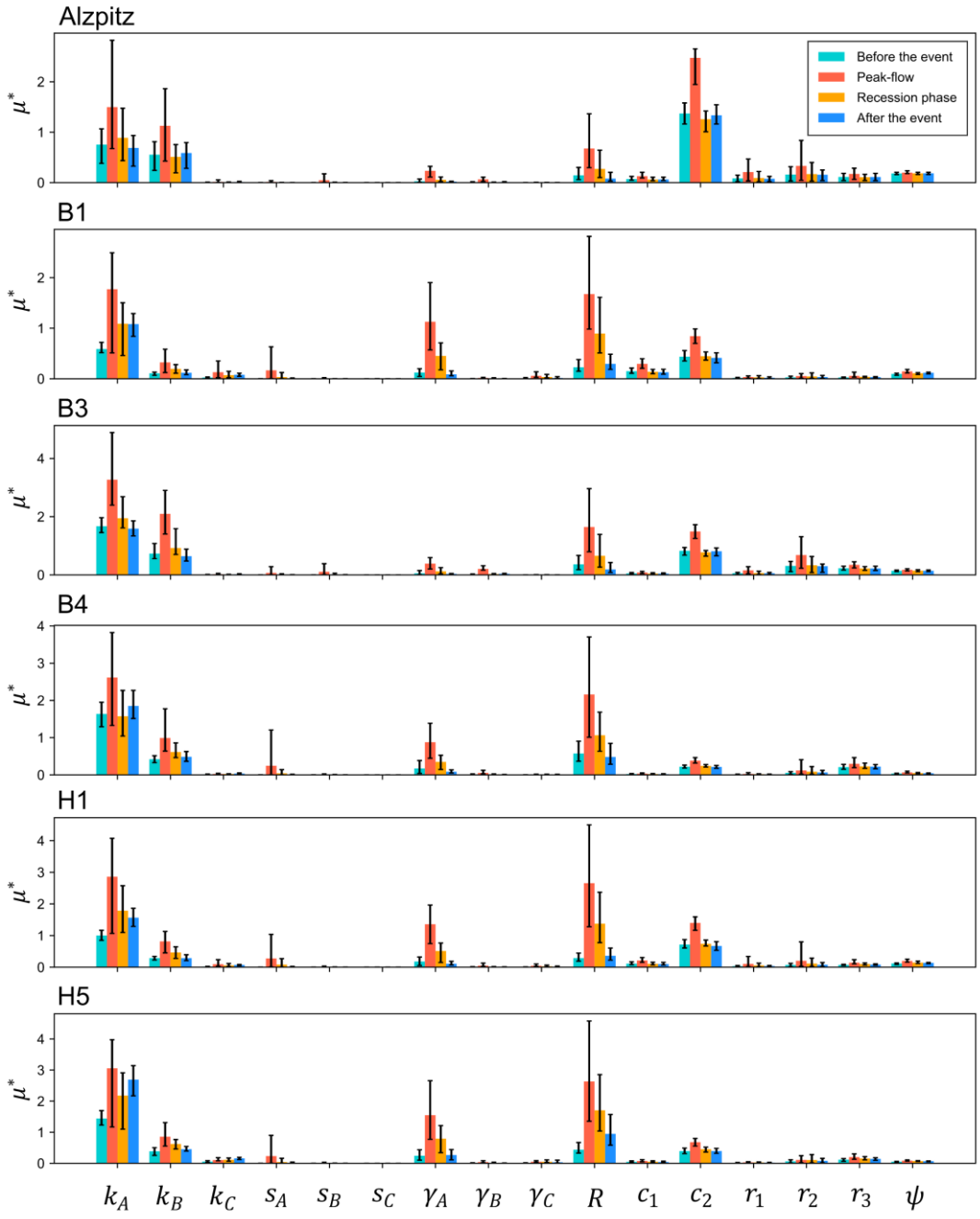

Figure 5.2. Elementary effects results per parameter at different location. The colored bars represent the mean value of μ^* at the different phases of the event. The upper end and lower end of the black whiskers show the maximum and minimum value of μ^*, respectively.

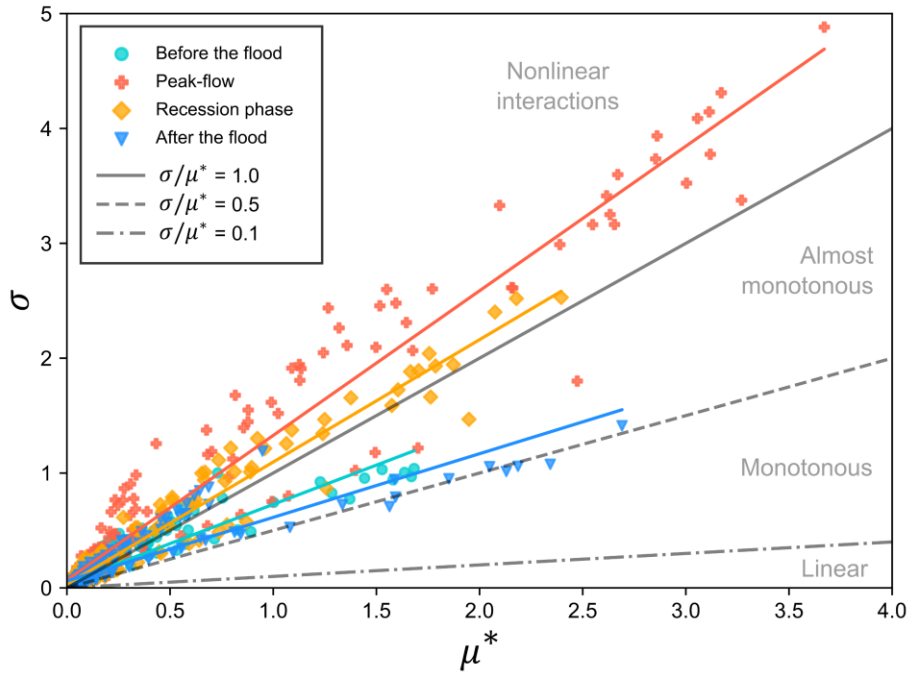

Figure 5.3. Covariance of μ^* and σ at different phases of the flood event. Colored lines show a simple linear regression to illustrate the responses at the different phases. Gray lines delimit the referential areas that describe nonlinear, almost monotonous, monotonous and linear interactions, according to the ratio σ/μ^*.

5.3.2 Bayesian inversion

In Figure 5.4, we can observe the prior and posterior discrete distributions of the sensitive parameters. These results show that the algorithm updated the distributions of the sensitive parameters, reducing their uncertainty. We also observe that most of the parameters tend to unimodality, except ψ, whose posterior distribution is only slightly updated in comparison to the prior distribution. This can be reasonably explained by the sensitivity analysis that shows low scores for this parameter. The statistical moments of the posterior distribution of the uncertain parameters can be found in Table 5.2. The expected values of the conductance from the river sections r_1 and r_2 range within the same order of magnitude. The latter suggests that the bed conductance of the river may be overparameterized, considering the location of the observation wells used for the inversion. Given these results and the outcomes of the sensitivity analysis, an additional reduction of the model dimensionality could be possible by grouping r_1 and r_2 in one parameter. We observe a high frequency of samples in the lower end of R that reduces the revised infiltration $Q_{i,j}^{(t)}$ used in the model evaluations. This implies that the deterministic values of the infiltration into the saturated zone extracted from the

regional model $\tilde{Q}_{i,j}^{(t)}$ do not represent accurate the system, whether by overestimating the inflow rates or the recharge extension. This remarks the importance of quantifying the uncertainty in the analysis of risk of these events. Still, note that R and ψ are random variables that aim to catch the uncertainty in model parameters that are fundamentally transient: recharge into the saturated zone $Q_{i,j}^{(t)}$ and river stage $\xi_{i,j}^{(t)}$. This means that a single random sample per evaluation may not exhaustively capture the temporal variability and the uncertainty of these parameters. Also, it is important to point out that the Bayesian approach relies in the information fed by the empirical evidence. Therefore, the location of the observation wells plays a fundamental role. Some parameters may not be adequately represented due to the location of the monitoring wells, such as R, c_1, r_1 and r_3.

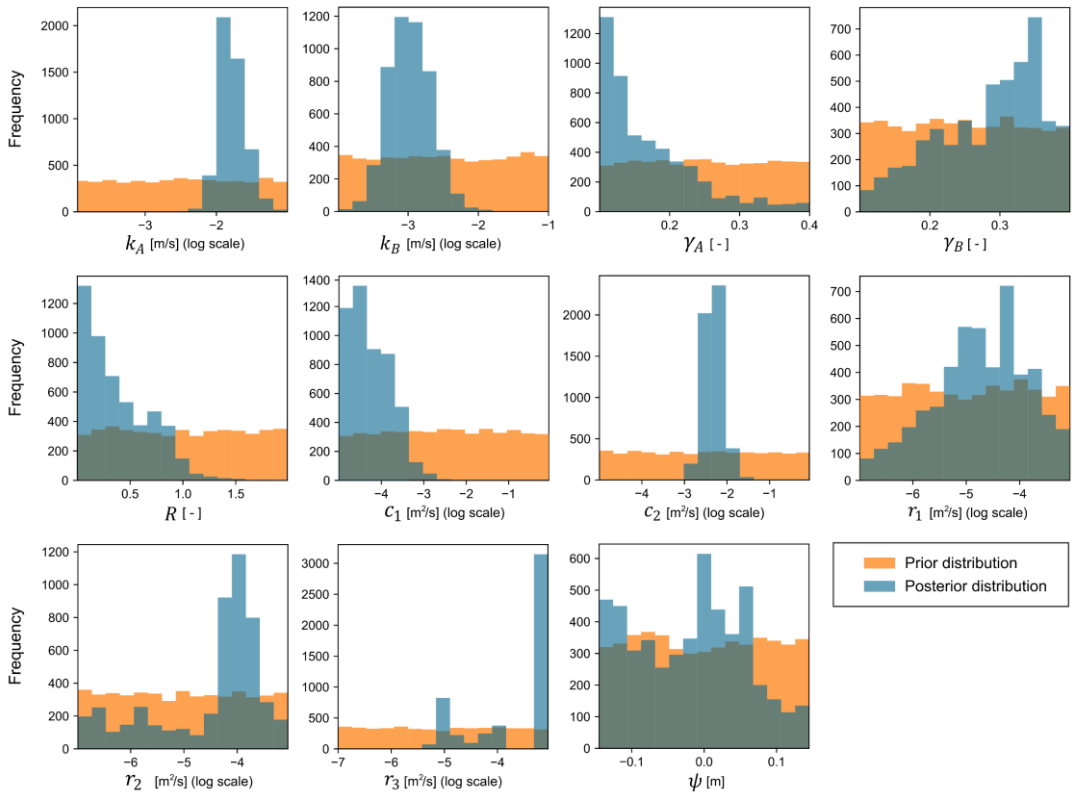

Figure 5.4. Prior and posterior discrete representation of the distributions for the classified sensitive parameters. The orange histogram shows the prior parameter distribution sampled from the Halton uniform distribution, while the blue histogram shows the posterior parameter distribution.

Table 5.2. Statistical moments of the posterior parameter distributions (mean μ_θ, the standard deviation σ_θ, the skewness γ_θ, and kurtosis β_θ), and best set of parameters

Parameter	Parameter units	μ_θ	σ_θ	γ_θ	β_θ	Best set
k_A	[m/s] (log scale)	-1.7742	0.3093	-1.1121	5.0517	-1.9021
k_B	[m/s] (log scale)	-2.8872	0.3952	0.4756	1.0179	-3.2105
γ_A	[-]	0.2111	0.0858	0.4965	-0.9822	0.1015
γ_B	[-]	0.2794	0.0783	-0.4364	-0.8639	0.1866
R	[-]	0.5662	0.4745	0.9019	0.0115	0.1304
c_1	[m^2/s] (log scale)	-3.9211	0.9285	1.6027	2.7368	-4.8203
c_2	[m^2/s] (log scale)	-2.3905	0.7497	-1.2957	3.8439	-2.3908
r_1	[m^2/s] (log scale)	-4.7159	1.0344	-0.3018	-0.8592	-5.1017
r_2	[m^2/s] (log scale)	-4.5951	1.0739	-0.747	-0.7445	-4.2346
r_3	[m^2/s] (log scale)	-4.005	1.0621	-0.898	-0.2509	-3.0910
ψ	[m]	-0.0225	0.0791	0.1594	-1.0402	-0.0924

The reduction of the model parametric uncertainty is evident after taking into consideration the observed data with the Bayesian approach (see Table 5.3 and Figure 5.5). In Figure 5.5, we can see the probability distribution of the groundwater heads considering the prior and posterior distribution of the sensitive parameters. A lower standard deviation σ_o in the hydraulic head distribution indicates that the values tend to be close to the central tendency metric μ_o (see Table 5.3). Figure 5.5 shows the approximation of the probability density function of the groundwater heads from the prior and the posterior predictive simulations at different locations and different phases of the event. The kernel density plot was calculated using Scott's Rule (Scott, 2010) over the finite output data of the groundwater heads located at the different monitoring wells. This plot is helpful to identify the position and relative amplitude of the density distributions and to recognize if the distribution is multimodal. The groundwater heads at Alzpitz, located immediately next to the river, display a bimodal distribution with the parameterization of the model using the prior distribution of the parameters. This distribution is later updated with the posterior to a unimodal distribution. The spread of the groundwater heads is evidence of significant uncertainty in the prior beliefs, which is driven by the interconnection with the river, especially during the peak-flow discharges. The interquartile range between the first and third quartile (Q3 – Q1 range) shows the variability around the median of 50% of the predictive values of the groundwater heads using the prior distribution of the parameters. We see that the Q3 – Q1 range is larger than one meter at Alzpitz and B3 for the model considering the prior distribution of the parameters.

Lastly, we can observe the skewness of the prior predictive distributions, which depict positive asymmetry about their mean. Figure 5.6 shows the final results of the predictive groundwater heads after applying the Bayesian inference. We use the mean and the interval $[\mu_o + \sigma_o, \mu_o - \sigma_o]$ of the predictive posterior distribution as a measure of the uncertainty. We observe that these metrics properly capture the observations, particularly in the wells Alzpitz and B3. At B4, the predictive uncertainty does not include the peak observations. Also, we observe disagreements in the responses at B1 that may occur due to the influence of the southern time-variant specified heads boundary conditions.

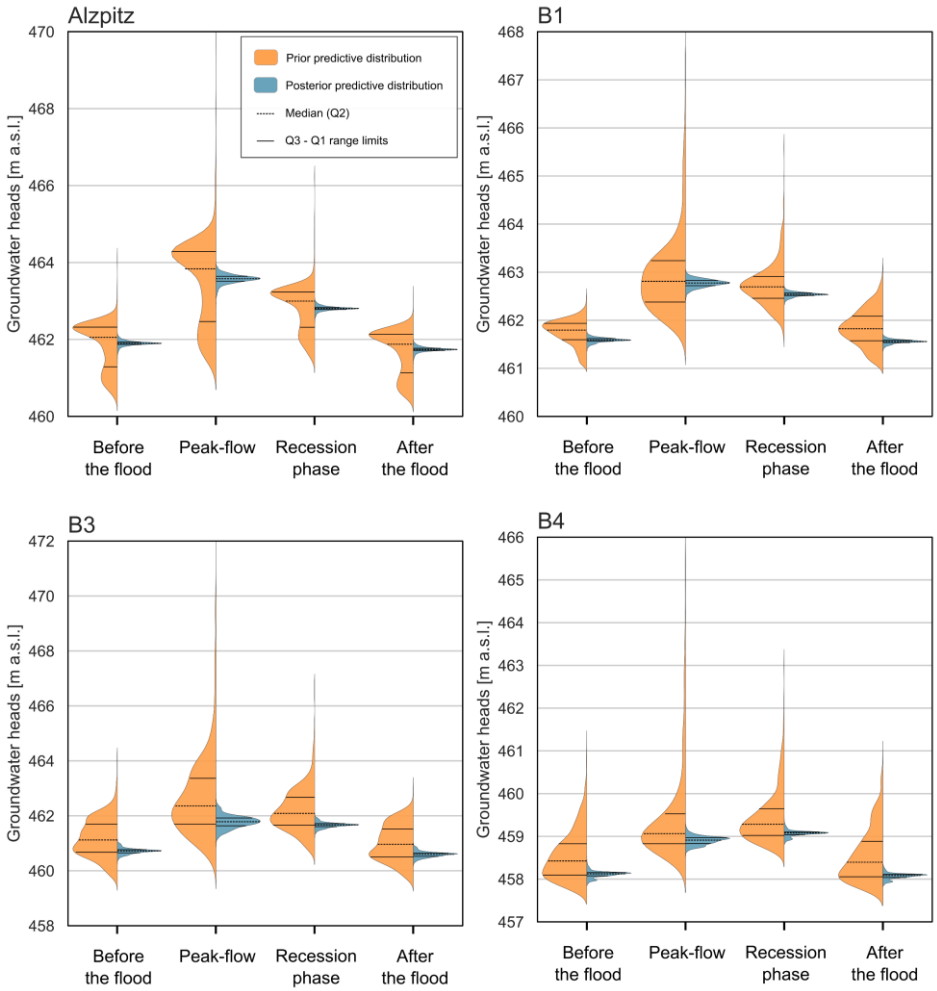

Figure 5.5. Violin plot of the probability density function of the groundwater heads from the prior (orange) and the posterior (blue) predictive distributions at observation wells and at different phases of the event. The second quartile (i.e., median) of the distribution is illustrated with the dashed line. First (Q1) and third quartiles (Q3) are represented by the continuous line. Probability distributions are scaled to obtain prior and posterior violins with the same width, so that the differences in their shapes are easily perceptible.

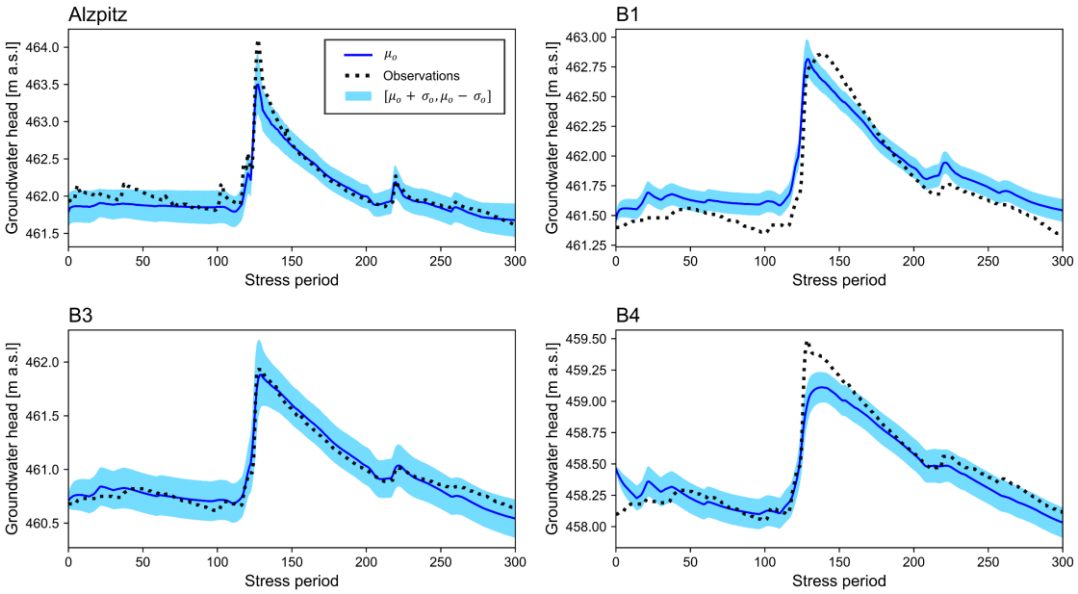

Figure 5.6. Predictive uncertainty for the groundwater flood event at different monitoring wells. the blue shade in the plots represents the interval $[\mu_o + \sigma_o, \mu_o - \sigma_o]$. The solid blue line indicates the mean of the posterior predictive distribution of the groundwater heads and the dotted line indicates the groundwater head observations.

Table 5.3. Statistical moments of the prior and posterior predictive uncertainty (mean μ_o and standard deviation σ_o) at the different monitoring wells during different phases of the event

Flood phase	**Dist.**	**Alzpitz**		**B1**		**B3**		**B4**	
		μ_o	σ_o	μ_o	σ_o	μ_o	σ_o	μ_o	σ_o
Before the flood	Prior	461.7874	1.1424	461.702	1.0063	461.1344	1.1659	458.4919	0.9965
	Posterior	461.8520	0.2225	461.5965	0.0923	460.7141	0.1851	458.1167	0.1211
Peak-flow	Prior	463.4296	1.5545	462.9069	1.3847	462.6298	1.8316	459.4000	1.4593
	Posterior	463.4992	0.3978	462.7843	0.1890	461.8404	0.3655	458.9123	0.1704
Recession phase	Prior	462.7484	1.1706	462.6818	1.1090	462.1369	1.2520	459.3888	1.0565
	Posterior	462.7654	0.2065	462.5491	0.0951	461.6666	0.1879	459.0749	0.1191
After the flood	Prior	461.6083	1.1259	461.7917	1.0442	460.9604	1.1409	458.4946	1.0216
	Posterior	461.6909	0.2146	461.5675	0.0938	460.5780	0.1749	458.0773	0.1225

5.3.3 Probability maps

The Bayesian approach allows us to study groundwater flood events considering the posterior distribution of the groundwater levels, which can be used for subsequent analysis, such as transport modeling, scenario modeling, or assembling more complex model structures. In our case, the posterior distributions at every cell of the domain can be used to create probability maps of susceptibility to groundwater flooding based on limit exceedances. We present two types of maps in this section. The first one is a distributed map based on the water depth levels in relation to the topographic level (Figure 5.7 and Figure 5.8). The second type is a graduated symbol map, where the size of the circles indicates the probability of exceedance given the depth of a specific house cellar (Figure 5.9).

Figure 5.7 and Figure 5.8 show the probability of having groundwater tables rising at the defined thresholds $\kappa_{i,j}(d = 1.5)$ and $\kappa_{i,j}(d = 0.5)$, respectively. The maps include the outcomes of simulations with the prior uncertainty (Figure 5.7a and Figure 5.8a) and the revised uncertainty from the Bayesian inversion (Figure 5.7b and Figure 5.8b). Areas with a low probability of exceedance are reduced in the maps built with the posterior distributions, thanks to the reduced variability in the sensitive parameters. Many zones are highly susceptible to groundwater flooding, even before and after the peak-flow. This agrees with reports of cellar inundations out of the peak-flow event and the high groundwater levels that can also be observed during non-flood seasons (Bayerisches Landesamt für Umwelt, 2020). The heavy precipitation at the end of May and the beginning of June 2013 (between stress period 115 and stress period 130) could have been the inundation catalyst, but the results show a high groundwater table at every phase of the event regardless of the heavy rainfall. Indeed, initial conditions, such as soil saturation before the event can influence recharge from rainfall. The underground infrastructure and properties can hence be exposed during longer periods to groundwater flooding and not only during specific hydrological events. The uncertainty in the soil saturation, parametrized using the recharge multiplier in this study, is essential because the occurrence, duration and severity of groundwater flooding will be determined by both the antecedent water table and groundwater recharge rate.

During the peak-flow and the recession phase, the probability of having groundwater depths above 1.5 m reaches maximum values. This shows the relatively slow decrease in the hydraulic head in the recession phase in comparison with fluvial floods. Groundwater flooding can last for an extended period, and infrastructure and property damage can be associated with long-lasting exposure. By comparing the outcomes from prior and posterior evaluations, we observe cells where the prior beliefs overestimate the exceedance probabilities while others underestimate them. In such cases, preconceptions based on one single forward simulation could be misleading. Maps over the basis of a distributed model help to avoid such biases and identify spatial responses that may be overlooked otherwise.

Also, creating the maps with a Bayesian approach increases the spatial confidence of the groundwater flooding susceptibility. We mainly assign this improvement to the updated posterior distributions of the hydraulic conductivity (k_A and k_B), which are very sensitive parameters and describe the ability of the material to transmit the fluid through the pore space within significant regions of the domain. Comparing Figure 5.7 and Figure 5.8, we can observe that the choice in the threshold value *d* is very important for the delineation of the areas affected by groundwater flooding. Hence, it should be carefully chosen according to site-specific problematics or different values of *d* should be investigated to have a clear picture of the possibly inundated areas.

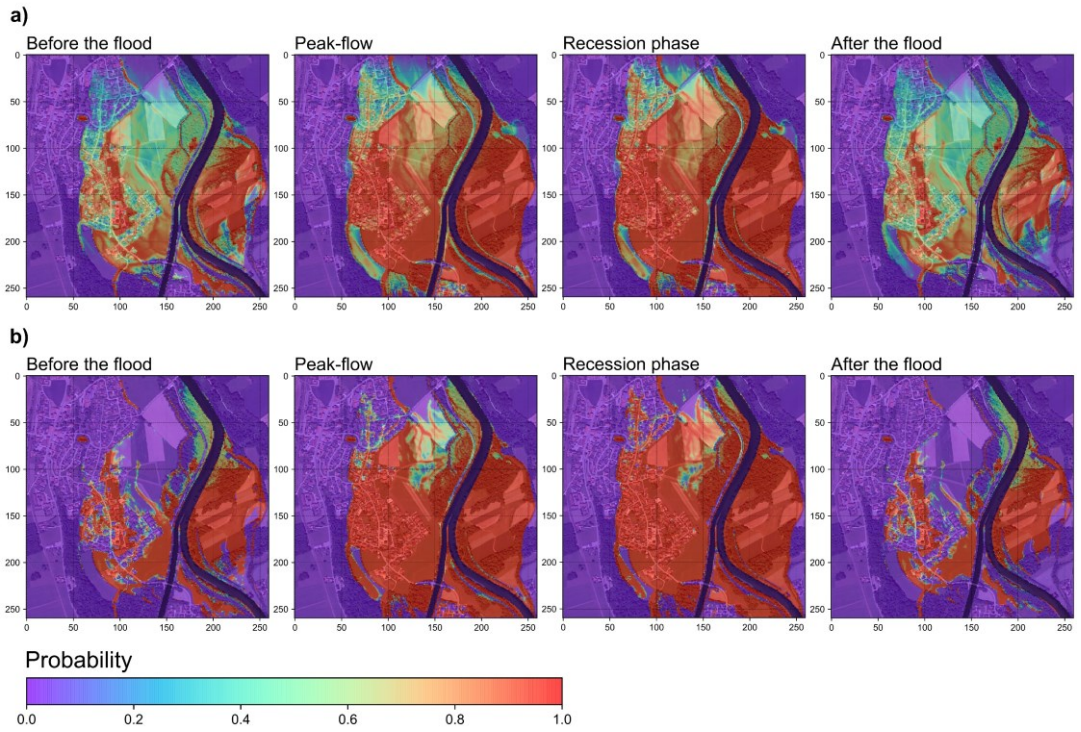

Figure 5.7. Probability maps of groundwater depth equal to or below 1.5 m at different phases of the event. Maps are created with a) prior predictive distribution and b) posterior predictive distribution.

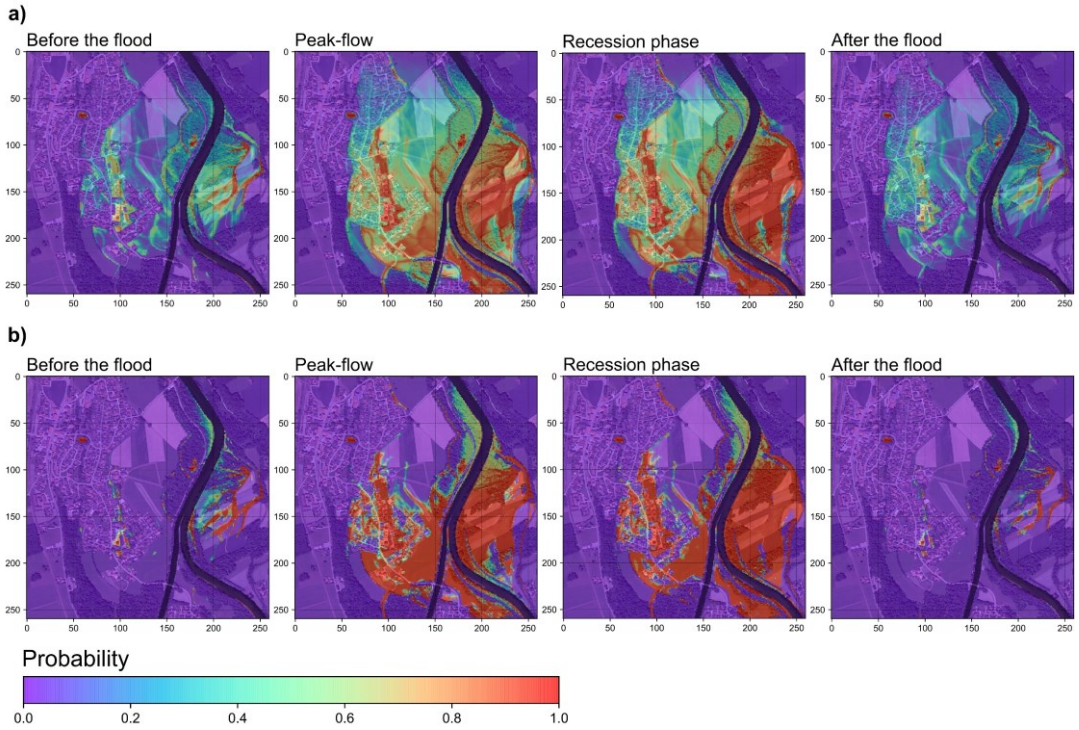

Figure 5.8. Probability maps of groundwater depth equal to or below 0.5 m at different phases of the event. Maps are created with a) prior predictive distribution and b) posterior predictive distribution.

Based on the household survey, we define the threshold $\tilde{\kappa}_{i,j}$ at different residential properties and the resulting maps can be observed in Figure 5.9. The properties selected in this analysis are far enough from the boundary conditions such that they are not influenced by the time-variant specified heads. We observe that the probability of reaching the cellar depth is unrelated to the distance to the river (see probabilities of building H2 and H3). Given the high groundwater table of the simulated period, it is very likely to reach the cellar depths at H1, H2, H3, and H6 even before and after the peak event. The probability of groundwater levels reaching the cellar is higher at the recession phase at H2, H5, H6, and H7. These results may imply a delayed propagation of the flood wave from the river into the aquifer.

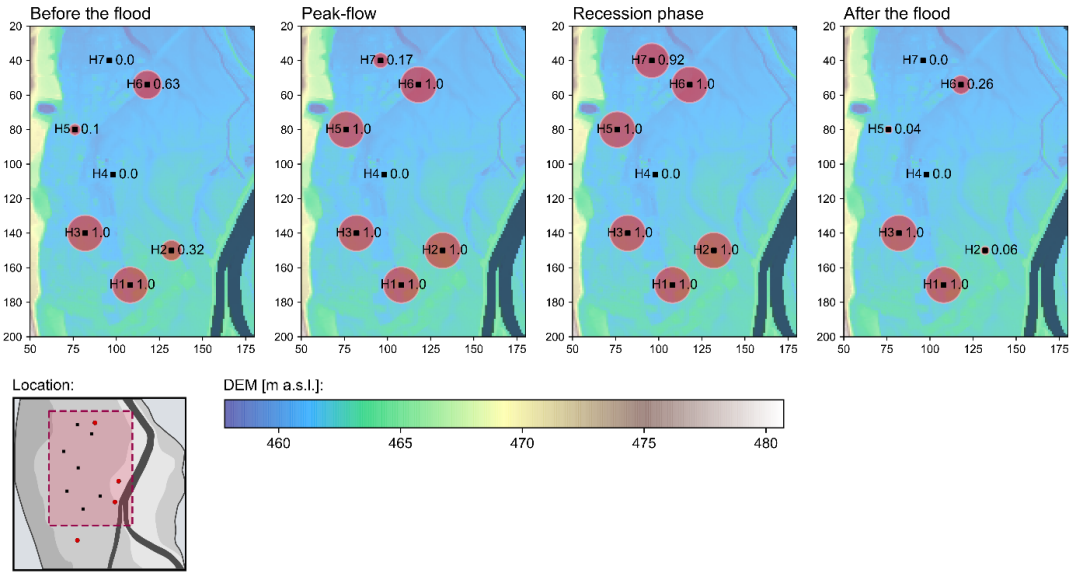

Figure 5.9. Probability of groundwater levels rising to or above the depths of the cellars. Graduated symbols (red circles) indicate the probability. The image displays a specific section of the model domain.

A drawback of the presented scheme is the memory requirement to store the element-wise data to construct the probability density functions. Still, in practice, it is possible to cluster the output data in relation to their spatial and temporal relevance and build maps of smaller regions. This means, once the zones and periods of major importance are identified, there is no need to keep in memory the simulation data that is out of the cluster. The presented results are obtained from a groundwater flow model that evaluates one actual event, which involves a relatively short timeframe of simulation, compared to mapping products that measure susceptibility to groundwater flooding from the description of the return period. However, the approach can be easily extended considering appropriate design parameters (e.g., changing the return period of the precipitation event, of the peak river discharge and/or of the volume of the event). This single event approach could be informative for industries, property managers, or insurance companies to evaluate the susceptibility to groundwater flooding of underground structures.

5.4 Conclusions

The broad implication of this research is the presentation of a Bayesian-based framework to create probability maps of susceptibility to groundwater flooding in order to incorporate the parameter uncertainties in the risk imagery. The scheme proposes to break down the uncertainty and sensitivity of one flood event into spatial and temporal terms and compute the statistics of interest at each domain element. The elementary effects method is used to reduce the problem dimensionality by quantifying the model sensitivity with a relatively low number of model evaluations. We use the DREAM algorithm as an MCMC-based technique to estimate the posterior distributions of the relevant uncertain parameters and reduce the uncertainty in the predicted groundwater heads. Finally, we propose to explore the posterior probability distribution of the groundwater heads to compute the exceedance probability based on the groundwater depths and cellar depths. Two types of maps are created to describe the susceptibility to groundwater flooding: a distributed map using the groundwater depth threshold, and a graduated symbol map given the depth of a specific house cellar.

The approach is illustrated with an application in a numerical model that describes the groundwater flood event in the Alz River valley in 2013. We are able to increase the spatial confidence of the results thanks to the reduction in the uncertainty during the inference process. By using a relatively large temporal scale, we are able to employ accurate temporal resolutions to detect the exposure to groundwater inundation at particular properties and areas. The framework can be applied over one flood event and this may be considered a promising aspect due to the reduced amount of data and the low computational demand. The posterior probabilities of the groundwater head and the exceedance evaluation help us distinguish highly exposed zones from those exposed only during peak-flow and the recession phase. This is relevant in practical applications because definitions of the susceptible zones can be easily constructed from a probabilistic perspective, and the accuracy of the simulations can be updated with new evidence data. In addition, these findings provide additional information about the incidence of groundwater flooding beyond the flood season. In this specific case study, the results indicate that infrastructure and property can be long-lastingly exposed to inundation hazards.

Finally, we stress the importance of opting for a Bayesian approach to understand groundwater flood events and create risk imagery. The temporal and spatial nature of groundwater flow confirms that the problem can be presented from a different perspective than the view of traditional flood events. Besides the exposure of the assets, groundwater flooding risk depends on temporal and spatial details from hydrological, climatic, and geomorphological elements. Ultimately, this level of detail makes flood mapping the crucial tool for flood risk management employed by a wide variety of partakers (such as planners,

developers, insurance companies, and property owners). But it is not possible to characterize the hydrogeological systems in such detail without being affected by uncertainty, and an explicit quantification is therefore required. Probability maps built over inverse methods can be relevant not only for incorporating the uncertainty and improving the reliability of the model but also for the accuracy of the message that is transmitted to different actors.

6 Polynomial chaos expansions for flow field dynamics

Abstract

Fluctuating stream stages and peak-flow events can significantly influence the interactions between streams and aquifers and modify the hydraulic gradient, the flux exchange and the subsurface flow paths. As a result, stagnation zones and reverse flow may appear in different parts of an aquifer and at different times. These features of the flow field play a relevant role in the transport, transformation, and residence time of solutes, pollutants, and nutrients in the subsurface. However, their identification using numerical models is complex not only because of highly non-linear dynamics, but also due to significant uncertainties in the model input data which propagate into the quantities of interest. In this work, we use an approach based on polynomial chaos expansions to map the probability of occurrence of stagnation zones and reverse flow during a flood event. We quantify the propagation of uncertainty into the groundwater flow field due to the applied river boundary conditions. Then, we evaluate the responses of the posterior probabilities in an element-wise fashion using a set of flow classification criteria and kernel density estimations. The proposed methodology is flexible because it employs a non-intrusive pseudo-spectral technique and, consequently, it can be applied straightforwardly in pre-existing models. The regions near the confluence of two streams in the studied area are prone to present transient stagnation and reverse flow.

Material from:
Merchán-Rivera, P., Wohlmuth, B., Chiogna, G., 2021. Identifying Stagnation Zones and Reverse Flow Caused by River-Aquifer Interaction: An Approach Based on Polynomial Chaos Expansions. Water Resources Research. https://doi.org/10.1029/2021WR029824

6.1 Introduction

There is a long-standing scientific awareness of the importance of the interactions between streams and aquifers (Brunner et al., 2017; Krause et al., 2014; Lewandowski et al., 2020, 2019; Magliozzi et al., 2018; Stanford and Ward, 1988; Winter, 1999, 1998). Many investigations describe the role of the dynamics of these interactions in the transport, degradation, and residence time of solutes and pollutants (Boano et al., 2014; Elliott and Brooks, 1997; Singh et al., 2020; Trauth and Fleckenstein, 2017), the transport of nutrients, the ecosystem metabolism and the biogeochemical transformations at the interface (Boano et al., 2014; Findlay, 1995; Jones and Holmes, 1996; Pinay et al., 2015), as well as the modulation of temperature (Arrigoni et al., 2008; Bhaskar et al., 2012; Gerecht et al., 2011; Marzadri et al., 2013). Mass and energy exchange are defined by the distribution of the hydraulic heads, the flow path directions, the canal bed conditions and the stream hydraulics (Lewandowski et al., 2019; Woessner, 2000). Thus, the stream-aquifer interaction is a function of space and time that may vary not only due to the geomorphologic and hydrogeologic controls, but also due to the occurrence, magnitude and distribution of hydrologic conditions (e.g., flood events) and anthropogenic impacts (e.g., hydropeaking). Numerous studies have also reported that rapid and fluctuating stages and peak-flow events can significantly affect the stream-aquifer interaction and modify the water flux, the residence times and the flow paths in the subsurface flow (Bernard-Jannin et al., 2016; Boano et al., 2013; Cardenas, 2008; Casas-Mulet et al., 2015; Malzone et al., 2016b; Singh et al., 2020; Trauth and Fleckenstein, 2017; Wu et al., 2018). Still, as recognized by Conant et al. (2019) and Krause et al. (2017, 2014), we need to develop new methods to describe the stream-aquifer dynamics in spatial and temporal terms to advance in the mechanistic understanding and predictability of these systems.

Irregular flow paths may affect fluid mixing and transport (Zhang et al., 2009) and consequently, reactive solute transport in geophysical flows (Chiogna et al., 2012; Sund et al., 2015). For instance, fluctuating head gradients change the rates of the groundwater flow and can create stagnation zones (Anderson and Munter, 1981; Cardenas, 2008; Tóth, 1963; Winter, 1976), regions associated with stagnation or equilibrium points (Jiang et al., 2011), where the groundwater velocity is zero (Bear, 1972). Non-trivial flow patterns can be observed near the stagnation points, which are relevant to the identification of the origin and fate of fluids and solutes (Bresciani et al., 2019). These points can allocate mixing and highly reactive regions, control the behavior of dissolution, dissipation, and reaction rates (Hidalgo et al., 2015; Hidalgo and Dentz, 2018; Jiang et al., 2014), and promote biogeochemical transformations (Krause et al., 2014; Pinay et al., 2015; Singh et al., 2020). Moreover, the location of stagnation points supports the description of the groundwater flow patterns in regimes that are driven by topographical and morphological configurations (Gomez and

Wilson, 2013; Jiang et al., 2011; Ren and Zhao, 2020; Wang et al., 2017). Additionally, transient stages in the stream-aquifer interactions can be relevant to the evaluation of multi-directional variations in the flow field. The rise of stream stages may reverse the dominant direction of the groundwater flow regime (Hunt et al., 2006) and affect the circulation of nutrients and solutes (Dudley-Southern and Binley, 2015). Additionally, the reversals in the hydraulic gradient can switch between losing and gaining stream conditions, and influence the infiltration depth of solutes and the reaction rates in the subsurface (Trauth and Fleckenstein, 2017).

Groundwater numerical models are frequently used to understand stream-aquifer interactions (Anderson et al., 2015; Peyrard et al., 2008). Major uncertainties may propagate into the model outcomes due to the error in the observed hydrological variables, the parameterization and structure of the model, as well as the conceptual assumptions and simplifications (Brunner et al., 2010; Di Baldassarre and Montanari, 2009; Götzinger and Bárdossy, 2008). In the field of hydrology, the propagation of the uncertainty has often been quantified by implementing Monte Carlo methods and related ensemble techniques (Beven and Binley, 1992; Kuczera and Mroczkowski, 1998; Vrugt et al., 2003). The main drawbacks of these approaches are typically the high number of simulations to cover the stochastic space of the uncertain parameters accordingly (Cools and Nuyens, 2016). Spectral expansion methods, such as generalized Polynomial Chaos (gPC), are suitable options to tackle these issues, particularly, to solve low-dimensional stochastic problems (Le Maitre and Knio, 2010; Smith, 2013). By using gPC expansions, we can represent different stochastic processes based on a suitable orthogonal polynomial basis (Rajabi, 2019; Xiu, 2009; Xiu and Karniadakis, 2002) and represent the full randomness of the system responses with expansion coefficients (Rajabi et al., 2015).

Previous investigations have properly implemented polynomial expansion methods to solve simplified analytical problems associated with hydrology, hydrogeology and hydraulics (Esfandiar et al., 2015; Francis et al., 2010; Gibson et al., 2014; Litvinenko et al., 2020; Maina and Guadagnini, 2018; Meng and Li, 2017; Oladyshkin et al., 2012; Rajabi, 2019; Sochala and Le Maître, 2013; Zhang and Lu, 2004). Yet, the application of polynomial expansion techniques in hydrological field studies have received less attention (Deman et al., 2016; Ghaith and Li, 2020; Laloy et al., 2013; Rajabi and Ataie-Ashtiani, 2016). In addition, evaluation of the polynomial expansions performance in groundwater applications is still an open matter (Rajabi, 2019), and its application for the quantification of the uncertainty caused by stream-aquifer interactions remains unexplored. In fact, the efficiency of spectral methods is problem-dependent (Le Gratiet et al., 2017). Therefore, to benefit from the application of these tools and to produce appropriate conclusions, we need to examine a large number of hydrological case studies.

This work aims to map the occurrence of complex flow processes caused by stream-aquifer interactions in terms of temporal dynamics and spatial patterns. By exploiting the strengths of gPC expansions, we want to distinguish reverse flow and stagnation hotspots and describe them in terms of probability of occurrence. We use gPC expansions to quantify the propagation of uncertainty in the groundwater flow field due to the uncertain river boundary conditions during a flood event. We define the evaluation criteria to classify flow types and explore the posterior probabilities in an element-wise fashion (i.e., cell-by-cell) of a distributed model using kernel density estimations. The approach that we propose aims to assess the randomness of the input uncertainty of parameters that are variable in time and hence are commonly unknown in the parameterization of stream-aquifer relations, such as the streambed conductance and the stream stages. These parameters are often used to fine-tune, recalibrate, and update the hydrogeologic models. Then, hydraulic conductivity, specific storage, specific yield and effective porosity are excluded from our set of stochastic parameters. Even if these aquifer properties are uncertain and can be evaluated using gPC theory, once a numerical model is developed, they are assumed as constant input parameters over time (Bachmat et al., 1978; Osman, 2013). On the other hand, variation of the streambed conductance as a function of time has been largely reported (Cui et al., 2020; Hatch et al., 2010; Hubbs, 2006; Stewardson et al., 2016), and the stream stage is, by definition, a fluctuating attribute of the streamflow (Reddy, 2005). Furthermore, by using pseudo-spectral expansions, the groundwater model does not require to be modified and can be treated as a black box in the computational procedure. Hence, this method can be applied to pre-existing models where the spatial and temporal implications of the stream-aquifer interactions play a relevant role.

6.2 Methods

6.2.1 Groundwater flow and river boundary conditions

Transient groundwater flow in a heterogeneous unconfined aquifer, when the coordinate system is oriented parallel to the major axes of anisotropy, can be expressed by a partial differential equation (Fetter, 1999):

$$\frac{\partial}{\partial x}\left(k_{xx}\frac{\partial h}{\partial x}\right)+\frac{\partial}{\partial y}\left(k_{yy}\frac{\partial h}{\partial y}\right)+\frac{\partial}{\partial z}\left(k_{zz}\frac{\partial h}{\partial z}\right)+W=S_s\frac{\partial h}{\partial t}\ , \qquad \textit{Eq. 6.1}$$

where h is the piezometric head [L], k_{xx}, k_{yy}, and k_{zz} represent the hydraulic conductivity along the x, y, and z coordinate axes [LT^{-1}], S_s is the specific storage [L^{-1}], and W is the volumetric flux per unit volume to represent the sources and sinks [T^{-1}]. For practical applications, Eq. 6.1 is often solved by numerical methods as a set of spatially discrete points in the center of a cell. So, the rate of change in storage within each cell is equal to the sum of flows into and out of the cell, as follows (Harbaugh, 2005):

$$\sum Q_i = S_s \frac{\Delta h}{\Delta t} \Delta V \quad , \qquad \textit{Eq. 6.2}$$

where Q_i is the i component of the flow rate into the cell that includes the source and sink terms [L^3T^{-1}], ΔV is the cell volume [L^3], and Δh [L] is the change in the groundwater head over a time interval Δt [T]. External sources or stressors (e.g., rivers, artificial waterways and lakes) can be represented as Q_i elements to predict head distributions at successive times for transient simulations. The interaction between surface water and groundwater is frequently conceptualized as a boundary condition for the head-dependent flux (Anderson et al., 2015; Brunner et al., 2010; Di Ciacca et al., 2019). Hence, the flux exchange between streams and aquifers, Q_e, is represented as follows:

$$Q_e = \begin{cases} c_r(h_r - b_r), & h_a \leq b_r \\ c_r(h_r - h_a), & h_a > b_r \end{cases} , \qquad \textit{Eq. 6.3}$$

where c_r is the streambed conductance [L^2T^{-1}], h_r is the water level or stream stage [L], b_r is the bottom of the streambed [L], and h_a represents the hydraulic head at the node in the cell underlying the stream reach [L]. The term c_r in the river package of MODFLOW-2005 is a resistance factor defined by the stream width w_r [L], the length of the conductance block l_r [L], the thickness of the streambed m_r [L], and the vertical hydraulic conductivity of the streambed material k_r [LT^{-1}] (Harbaugh, 2005):

$$c_r = \frac{k_r \, l_r \, w_r}{m_r} \ . \qquad \textit{Eq. 6.4}$$

Streambed conductance is a broadly applied approach in hydrogeologic modeling (Morel-Seytoux, 2019). Nonetheless, it is a very simplified conceptualization of the stream-aquifer interactions that assumes homogeneity and isotropy of the streambed hydraulic conductivity within the cell (Cardenas and Zlotnik, 2003; Ghysels et al., 2019, 2018). Furthermore, the river package is not able to represent flow in the unsaturated zone (Brunner et al., 2010; Ghysels et al., 2019). In our application, the unsaturated flow under the stream can be neglected due to the active hydraulic connection during the simulated period. On the other hand, major roles are played by c_r and h_r, and they are included in the uncertainty analysis accordingly. Overall, these parameters can show large spatial and temporal variability, and they are frequently uncertain, hardly accessible, or even unknown. In practice, c_r is a lumped parameter that cannot be easily measured in the field, that comprises various properties of the streambed (Cousquer et al., 2017; Mehl and Hill, 2010), and that is often estimated by calibration (Morel-Seytoux et al., 2017). The uncertainty in the estimation of h_r originates from the stream flow data (Di Baldassarre and Montanari, 2009) and the model structure (Georgakakos et al., 2004).

To define the velocity distribution, transient simulations can be represented as a series of discrete steady-state flow periods (Pollock, 2012). The stationary version of Eq. 6.1 can be rewritten in terms of the average linear groundwater velocity as:

$$\frac{\partial}{\partial x}(\eta v_x) + \frac{\partial}{\partial y}\left(\eta v_y\right) + \frac{\partial}{\partial z}(\eta v_z) = W \ , \qquad \textit{Eq. 6.5}$$

where v_x, v_y, and v_z represent the principal components of the averaged linear velocity [L/T], and η is the effective porosity [-]. Then, to obtain the averaged linear velocity component across one face of the cell, we can represent the volumetric flow rates across the finite-sized cell within a structured aligned grid in this fashion:

$$\frac{(\eta v_{x_2} - \eta v_{x_1})}{\Delta x} + \frac{(\eta v_{y_2} - \eta v_{y_1})}{\Delta y} + \frac{(\eta v_{z_2} - \eta v_{z_1})}{\Delta z} = \frac{Q_s}{\Delta x\, \Delta y\, \Delta z} \,. \qquad \textit{Eq. 6.6}$$

Eq. 6.6 is formed by Q_s as the internal sources or sinks within the cell, Δx, Δy, and Δz as the dimensions of the cell in the respective coordinate directions, and the components v_{x_1}, v_{x_2}, v_{y_1}, v_{y_2}, v_{z_1}, and v_{z_2} that represent the velocities perpendicular to the respective coordinate direction at the six faces of the cell. Eq. 6.6 can be solved using the values of the groundwater heads Δh at a given distance Δl [L] by substituting each of the flow terms by Darcy's law. For instance, Eq. 6.7 exemplifies the definition of the velocity perpendicular to the x-direction at one face (Pollock, 2012):

$$v_{x_1} = \frac{Q_{x_1}}{\eta \Delta \mathrm{y} \Delta z} = \frac{-k_{xx} \Delta h_{x_1}}{\eta \Delta l_{x_1}} \,. \qquad \textit{Eq. 6.7}$$

6.2.2 Polynomial chaos expansion and pseudo-spectral approach

Within the context of uncertainty quantification, generalized Polynomial Chaos theory (Xiu and Karniadakis, 2002) refers to the representation of random spaces by spectral expansions (Smith, 2013; Xiu, 2009). Following the generalized Cameron-Martin theorem (Cameron and Martin, 1947), we define a second-order random (finite variance) process (Smith, 2013) by a general polynomial approximation:

$$f(s,t;\Phi) = \sum_{i=0}^{\infty} \hat{c}_i(s,t) \Psi_i(\Phi) \,, \qquad \textit{Eq. 6.8}$$

where $f(s,t;\Phi)$ is the output function defined by both the deterministic spatio-temporal dependencies $\{s,t\}$, and the stochastic dependencies $\Phi = (\varphi_1, \dots, \varphi_d)$, $\hat{c}_i(s,t)$ are deterministic coefficients, and $\Psi_i(\Phi)$ are orthogonal polynomials that form the basis for the stochastic component of the solution. The random events Φ represent the stochasticity in the system due to uncertain parameters, source terms, initial or boundary conditions, etc. For the

case of this study, this is the uncertainty related to the parameterization of the river boundary conditions: c_r and h_r. In practice, the series in Eq. 6.8 must be truncated after *N* terms, to obtain a finite approximation:

$$f(s,t;\Phi) \approx \sum_{i=0}^{N} \hat{c}_i(s,t)\Psi_i(\Phi) \ . \qquad \textit{Eq. 6.9}$$

In Eq. 6.8 and Eq. 6.9, we observe that the polynomial approximation separates the deterministic and the stochastic components. The polynomial basis functions $\Psi_i(\Phi)$ must be properly specified according to the probability density function of the random variables (Xiu and Karniadakis, 2002). The basis construction of a single random variable $\psi_i(\varphi)$ will satisfy the orthogonality condition with respect to the density $\rho_\Phi(\varphi)$, such that:

$$\mathbb{E}\left[\psi_i(\Phi)\psi_j(\Phi)\right] = \int_\Gamma \psi_i(\varphi)\psi_j(\varphi)\rho_\Phi(\varphi)d\varphi = \langle\psi_i,\psi_j\rangle_\rho = \gamma_i\delta_{ij} \ , \qquad \textit{Eq. 6.10}$$

where $\langle\psi_i,\psi_j\rangle_\rho$ is the inner product of ψ_i and ψ_j on the interval Γ with the weighting function $\rho_\Phi(\varphi)$, $\gamma_i = \mathbb{E}\left[\psi_i^2(\Phi)\right] = \langle\psi_i\rangle^2$ is a normalization factor, and δ_{ij} denotes the Kronecker delta. As described later in section 6.2.5, to construct the orthogonal polynomials in this study, the uniform distributions of the river and canal conductance lead to the Legendre-chaos polynomials, while the Hermite-chaos polynomials correspond to normal distribution of the stream stages.

As stated by Smith (2013), the representation of random processes that are functions of d multiple independent random variables is analogous to the univariate case and the multidimensional basis can be constructed as tensor products of univariate polynomials. Since the underlying $\Psi_i(\Phi)$ in Eq. 6.9 are known and previously defined, we only need to compute $\hat{c}_i(s,t)$ to obtain the gPC expansion. In this work, we apply a non-intrusive expansion known as the pseudo-spectral approach (Xiu, 2007). We use this method because it applies a set of deterministic model resolutions using specific realizations of Φ to construct approximations (Le Maitre and Knio, 2010). Therefore, we can treat the solver as a black box in the computational procedure. This process requires numerical integration. In this work, we use an optimal Gaussian quadrature (Gautschi, 1968; Golub and Welsch, 1968) over a full tensor

product of integration order K to achieve order n polynomials. This specifies a set of gaussian quadrature nodes $q_k = (q_1, \dots, q_K)$ and weights $w_k = (w_1, \dots, w_K)$, following the method defined by Gautschi (1968). Then, the number of model evaluations P is equal to $(K+1)^d$. The calculation of $\hat{c}_i(s,t)$ then follows:

$$\hat{c}_i(s,t) = \langle f(s,t,\varphi), \psi_i(\varphi) \rangle_\rho \; = \; \int_\Gamma f(s,t,\varphi)\psi_i(\varphi)\rho_\Phi(\varphi)d\varphi \;\; , \qquad \textit{Eq. 6.11}$$

$$\hat{c}_i(s,t) \approx \sum_{k=0}^{K} f(s,t,q_k)\psi_i(q_k)\, w_k \;\; . \qquad \textit{Eq. 6.12}$$

The number of nodes K can be defined by $(n+d)!/n!\, d! - 1$ (Smith, 2013; Xiu, 2010) to represent the n interaction terms optimally, or by using experimental combinations such as the empirical rule $K = (d-1)N$, where $N = n+1$ (Sudret, 2008). Once the forward deterministic evaluations are run and $\hat{c}_i(s,t)$ are approximated, we can compute the polynomial expansions $f(s,t;\Phi)$. We can also straightforwardly obtain the first and second statistical moments by the following equations:

$$\mathbb{E}[f(s,t;\Phi)] = \mu_f = \; \hat{c}_0(s,t) \;\; , \qquad \textit{Eq. 6.13}$$

$$\mathbb{V}[f(s,t;\Phi)] = \sigma_f^2 = \; \sum_{k=1}^{K} \hat{c}_k^2(s,t) \;\; . \qquad \textit{Eq. 6.14}$$

6.2.3 Kernel density estimation

The statistics of the quantity of interest, μ_f (expected value) and σ_f (standard deviation), are point estimates because they represent a single value in the parameter space. However, for understanding the uncertainty and extending the analysis to the spatial and temporal variations, computing the underlying probability density function may be quite informative, and also practical to estimate the probability of occurrence of stagnation points and reverse flow. We apply a non-parametric estimation technique known as kernel density estimation (Silverman, 1998; Wand and Jones, 1995). This method calculates the density function by weighting the distances of the realizations from a point x. The kernel estimator $\hat{f}(x)$ is defined by:

$$\hat{f}(x) = \frac{1}{nb_\xi} \sum_{i=1}^{n} \xi\left(\frac{x - X_i}{b_\xi}\right). \qquad \textit{Eq. 6.15}$$

where X_i are independent data points drawn from the actual gPC expansions, b_ξ is the window width or bandwidth, ξ is the window function that determines the shape of the kernel, and n is the sample size. For this study, b_ξ is defined following Scott's Rule as $b_\xi \equiv 3.5\sigma n^{-1/3}$ (Scott, 2014), and κ is a Gaussian kernel defined as:

$$\kappa\left(x, b_\xi\right) \propto e^{-\frac{x^2}{2{b_\xi}^2}}. \qquad \textit{Eq. 6.16}$$

Once we define the quadrature degree K that is able to represent the randomness of the uncertain inputs at a low computational cost and with a small error in relation to the observed heads, we replicate the method in an element-wise operation to find $\hat{f}(x)$ and obtain the point estimates and posterior probability distributions for each cell of the domain.

6.2.4 Flow criteria classification

The posterior probability distributions can be evaluated according to a set of criteria that reflect the occurrence of particular flow types (i.e., stagnation points and flow reversal) at different phases of the event. The first criterion states the probability of finding stagnation cells, which are cells where the local magnitude of the flow field can be equal to zero. We can

explain this condition by defining the cumulative distribution function $\hat{F}_V(v)$ from the previous kernel estimator, as follows:

$$\hat{F}_V(v) = P(V \leq v) \quad , \qquad \textit{Eq. 6.17}$$

where the right-hand side is the probability that the magnitude of the flow field V takes on a value less than or equal to v. Then, the probability of finding stagnation cells can be written as:

$$P(V = 0) = \hat{F}_V(0) \quad . \qquad \textit{Eq. 6.18}$$

To identify the probability of occurrence of reverse flow, we need to define a flow field direction of reference with an angle $\bar{\theta}$. Based on this reference direction, we define a flow as reverse when the angle of the evaluated flow direction θ is within the interval $[\alpha, \beta]$, where:

$$\alpha = \bar{\theta} - 135° \ , \qquad \beta = \bar{\theta} + 135° \ . \qquad \textit{Eq. 6.19}$$

Figure 6.1 shows an example of these criteria for a hypothetical reference direction with an angle $\bar{\theta}$ = 135° (red arrow), which means that the flow runs from southeast to northwest. We assume a flow reversal when the angle θ varies between α = 0° and β = 270° (gray area), because the flow is no longer flowing to the north nor to the west. In practice, we need to find the angles of the reference directions for every cell in order to map the probability. Notice that the reference flow field direction can be adapted to the requirements of the study, the temporal span and discretization of interest, and the hydraulic responses of the system. For instance, in this study, we use the mean as measurement of central tendency to define $\bar{\theta}$:

$$\bar{\theta} = \frac{1}{n_s}\sum_{i=t_s}^{t_f} \mu_{\theta_i} \ , \qquad n_s = 1 + \left(t_f - t_s\right), \qquad \textit{Eq. 6.20}$$

with μ_{θ_i} representing the expected values of the flow field angle computed with the polynomial expansions, with t_s and t_f representing the first and last stress periods between two flood events or, in our study, the beginning of the simulation and the flood event, and with n_s denoting the number of stress periods between t_s and t_f. Finally, we can define the probability of finding reverse flow and express it in terms of a cumulative density function:

$$P(\alpha \leq \theta \leq \beta) = \begin{cases} \hat{F}_\theta(\alpha) - \hat{F}_\theta(\beta) \ , & \alpha > \beta \\ \hat{F}_\theta(\alpha) + (1 - \hat{F}_\theta(\beta)) \ , & \alpha < \beta \end{cases} . \qquad \textit{Eq. 6.21}$$

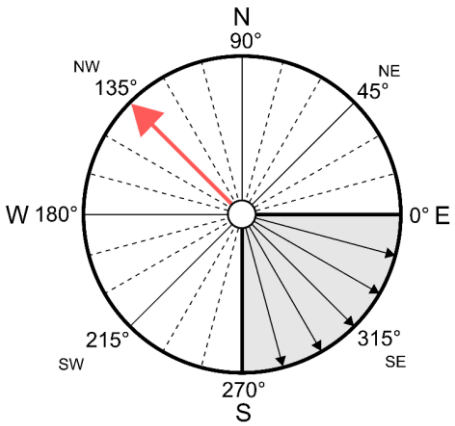

Figure 6.1. Reverse flow criteria representation: the red arrow represents the reference flow direction before a flood event, the gray area represents the interval within which the directions are considered reversal flows.

6.2.5 Case study and algorithm implementation

We applied the exposed approach to a real case model. The study area is in the Alz valley in Tacherting, Germany. Figure 6.2a shows the site location and the schematics of the numerical model. The Alz river flows from south to north along the valley. We can also observe an

artificial waterway, the Alz canal, that acts as a tributary of the river. The river and the canal are hydraulically connected to an unconsolidated shallow sedimentary aquifer (Keilholz et al., 2015; Merchán-Rivera et al., 2018). The bottom of the aquifer is located at 430 m a.s.l (above sea level) and it has an average depth of ~30 m (Doppler et al., 2011). As shown in Figure 6.2b, the region was affected by a flood event due to heavy rainfall events at the beginning of June 2013.

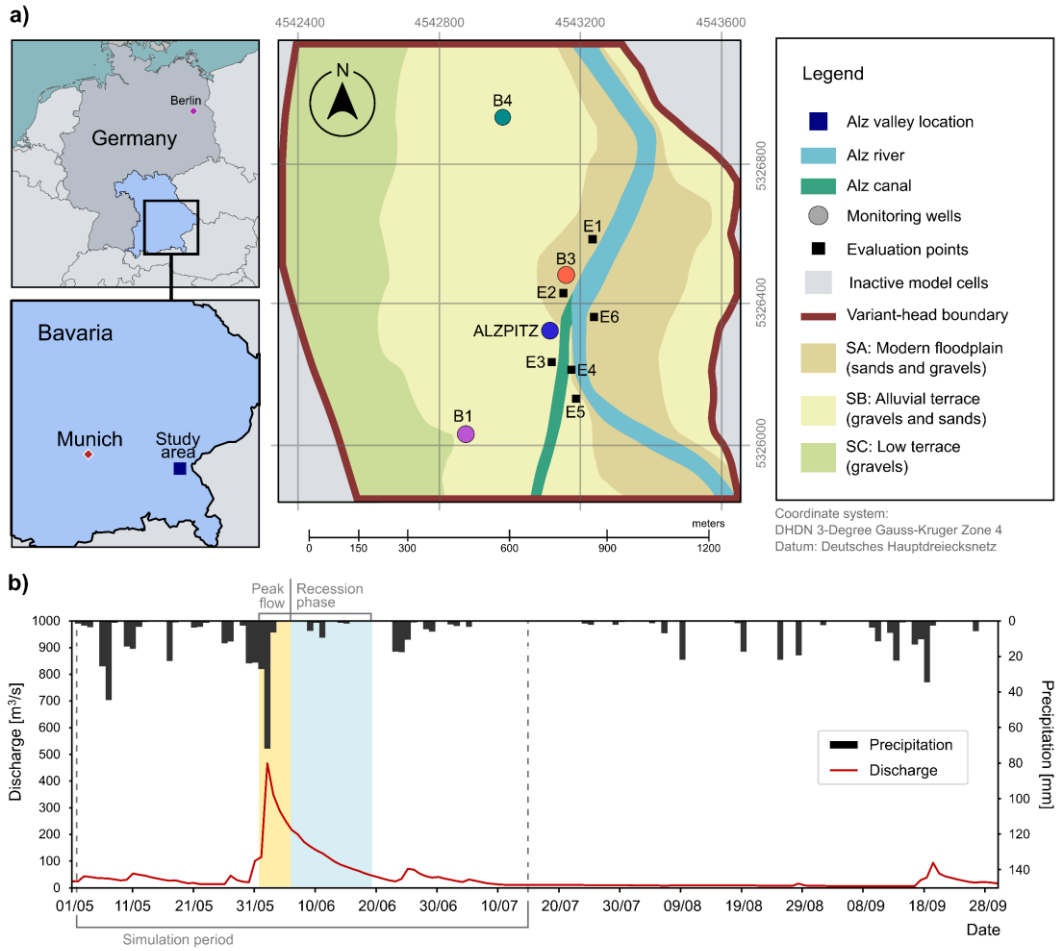

Figure 6.2. Flood event in 2013 in the Alz valley description: a) study area location and numerical model settings, and b) measured discharge in the river Alz and precipitation rate.

To describe the interaction between the streams and the aquifer, we built a groundwater numerical model using MODFLOW-2005 (Harbaugh, 2005). This model is based on the model presented in Merchán-Rivera et al. (2018) and the data collected in Keilholz et al. (2015). The spatial domain of the model is subdivided into a finite-difference grid formed by one layer (vertical representation), 260 rows, and 260 columns (horizontal representation).

The simulation period covers 75 days from 02-May-2013 00:00:00 to 15-Jul-2013 18:00:00, and it is discretized in 300 stress periods of six hours intervals. The number of stress periods used to define n_s is equal to 100 (from 02-May-2013 to 26-May-2013). The aquifer properties of the model were defined according to the underlying geological features presented in previous studies (Bayerisches Landesamt für Umwelt, 2017; Doppler et al., 2011). These studies identified three main soil types in the area: a younger floodplain underneath the Alz river formed by gravel and sand (SA), an alluvial terrace formed by gravel and sand (SB), and a low terrace mainly formed by gravel (SC) (Figure 6.2a). The soil properties allow a very dynamic behavior of the groundwater flow due to the high permeability of the porous media, the good hydraulic connection with the adjacent streams, and the relatively high rainfall recharge. The hydraulic conductivity, the specific storage, the specific yield of the three soil types and the effective porosity are not considered calibration parameters in this study, since we are using a model that has already been calibrated, and we do not consider these parameters as time dependent. The groundwater responses are field measurements that were registered every six hours in four groundwater monitoring wells: Alzpitz, B1, B3, and B4 (Keilholz et al., 2015). The hydraulic conductivity, specific storage, specific yield and effective porosity for each soil zone were calibrated in previous studies (Keilholz et al., 2015; Merchán-Rivera et al., 2018) and are based on the soil properties (Bayerisches Landesamt für Umwelt, 2017; Doppler et al., 2011). Table 6.1a summarizes the parameterization of the numerical model.

Three boundary conditions were imposed in the model. Firstly, time-variant specified-heads (CHD) were used to simulate the variation in the water table at the borders of the domain. By applying this option, transient heads were adjusted at every stress period. Secondly, we included recharge into the saturated zone to simulate the distributed flux from the top of the domain due to infiltration. Thirdly, we used the river package (Harbaugh, 2005), the streambed conductance and hydraulic head in the stream to simulate the interaction between surface water and the aquifer. A regional hydrologic model built in MIKE SHE (DHI, 2013) by Keilholz et al. (2015) was used to obtain the scatter stage information for the river and the canal, the recharge into the saturated zone, and the groundwater heads to define the time-variant specified-heads, which change in time and space.

The uncertainty in the river boundary conditions is introduced by the experimental error in the stream stage ε and the streambed conductance c_r, which are assumed to be random variables. The uncertainty related to stream discharges of the region has been previously quantified by Willems (2011) and Willems and Stricker (2012). These works extensively study the uncertainty in the physical measurements of the rivers of the region and describe a normal distribution for the uncertainty in the discharges and the head measurements of the river Alz. This choice considers that the normal distribution is the best limiting distribution for a parameter that is defined from a finite set of physical measurements (Fornasini, 2008). Based on these settings, we then computed the rating curve and the corresponding propagation

of the uncertainty in the stream stage. The spectral expansions introduce the stochasticity of this parameter by using the quadrature node values as a noise value ε. This means that ε increases or reduces the stream stage h_r, for all of the stress periods of the model at each cell that represent the streams. Hence, the stream stages $\hat{h}_r$ used in the deterministic evaluations are defined using a random variable $\varepsilon \sim \mathcal{N}(\mu_\varepsilon, \sigma_\varepsilon)$ to represent the stage error, where $\mu_\varepsilon = 0$, as follows:

$$\hat{h}_r = h_r + \varepsilon \quad . \qquad \textit{Eq. 6.22}$$

For the definition of prior parameter distributions of the conductance, we consider physically suitable ranges according to the streambed material. In addition, given the lack of prior information related to the conductance properties of the streambed, we assume uniform density distributions to maximize the entropy for both the canal and the river conductance $\mathcal{U}(a, b)$ (Cousquer et al., 2017; Zeng et al., 2016). Table 6.1b includes the actual values that were applied for the prior distributions.

Table 6.1. Model parameters: a) deterministic hydraulic parameters and b) stochastic stream parameters.

Model parameters	**Value**	**Unit**
a) Deterministic parameters		
Hydraulic conductivity SA	7.0131e^{-03}	m/s
Hydraulic conductivity SB	1.0617e^{-03}	m/s
Hydraulic conductivity SC	1.3068e^{-04}	m/s
Specific storage SA	2.2475e^{-05}	$1/m$
Specific storage SB	1.9938e^{-06}	$1/m$
Specific storage SC	2.8263e^{-05}	$1/m$
Specific yield SA	1.6561e^{-01}	$-$
Specific yield SB	1.6057e^{-01}	$-$
Specific yield SC	2.0543e^{-01}	$-$
Effective porosity	0.3500	$-$
b) Stochastic parameters		
Stream stage error	Normal ~ $\mathcal{N}(0, 0.145)$	m
Conductance of the river	Uniform ~ $\mathcal{U}(1e^{-7}, 9e^{-4})$	m^2/s
Conductance of the canal	Uniform ~ $\mathcal{U}(1e^{-5}, 9e^{-1})$	m^2/s

The magnitude and direction of the flow fields were calculated at the center of the cell by computing the flow face-to-face from the MODFLOW outputs and applying the same semianalytical algorithm described in a previous section and defined by Pollock (2012). We implemented the polynomial expansions, the non-intrusive pseudo-spectral projection, and the kernel density estimation using the Chaospy library (Feinberg, 2019; Feinberg and Langtangen, 2015) and the SciPy library (Virtanen et al., 2020).

The simulated groundwater heads were evaluated in relation to the set of observed values. Also, we validated the results obtained from the gPC method by comparing the simulated groundwater heads with the results from the application of a quasi-Monte Carlo method (qMC) with $S = 1000$ samples. The sampling points for the qMC were generated using Halton sequences (Halton, 1964) as a low-discrepancy arrangement to reduce the variance in the samples and considering that the convergence rate of quasi-random sequences is $\mathcal{O}(\ln N^d/N)$ (Smith, 2013). Further explanations of how the collocation of the uncertain values differs between the methods are provided in Annex A of the Supplementary Material for illustrative purposes.

6.3 Results and Discussion

To present some of the results clearly, we extracted them at specific time steps to understand the responses of the system at the following time steps: before the event at stress period 86 (23-May-2013), peak-flow at stress period 127 (02-Jun-2013), recession phase at stress period 145 (07-Jun-2013) and after the flood event at stress period 290 (13-Jul-2013).

We performed various tests to define K and n, which included the application of the empirical rule presented by Sudret (Sudret, 2008), the full factorial design (Smith, 2013; Xiu, 2010), and a series of experimental combinations. We calculated the mean absolute error [L] of the expected values of the groundwater head [L] from the gPC expansions and the qMC sampling [L] in relation to the observed values at the monitoring wells. The results from these evaluations are displayed in Table 6.2. As mentioned by Debuscherre (2017), in practical applications of the polynomial expansions, the selection of the order of representation of the expansions is an experimental choice that depends on the problem. We observed that low quadrature degrees were able to capture the dependence between the solution and the stochastic spaces. Indeed, the convergence of the results does not significantly improve by using $K > 4$. Consequently, we applied $K = 4$ and $n = 4$ to proceed with the quantification of uncertainty and the creation of probability maps. In addition, to validate this choice against the qMC results, we performed a comparison of the spatial distribution of the statistical

moments of the hydraulic heads at different phases of the flood event that can be found in the Annex B of the Supplementary Material.

Table 6.2. Mean absolute error (in meters) of the expected values at the monitoring wells using different values of quadrature degree and qMC validation with 1000 samples.

Method	K	n	P	Monitoring well				Average
				Alzpitz	B1	B3	B4	
gPC	2	2	27	0.0971	0.1999	0.1836	0.0952	0.1440
	3	1	64	0.1262	0.1876	0.1590	0.0919	0.1412
	3	3	64	0.1262	0.1876	0.1590	0.0919	0.1412
	4	1	125	0.1165	0.1916	0.1663	0.0926	0.1417
	4	2	125	0.1165	0.1916	0.1663	0.0926	0.1417
	4	4	125	0.1165	0.1916	0.1663	0.0926	0.1417
	5	2	216	0.1187	0.1905	0.1649	0.0925	0.1416
	5	3	216	0.1187	0.1905	0.1649	0.0925	0.1416
	5	5	216	0.1187	0.1905	0.1649	0.0925	0.1416
	6	2	343	0.1184	0.1907	0.1650	0.0925	0.1417
	6	3	343	0.1184	0.1907	0.1650	0.0925	0.1417
	8	3	729	0.1184	0.1907	0.1650	0.0925	0.1417
	9	2	1000	0.1184	0.1907	0.1650	0.0925	0.1416
	10	4	1331	0.1184	0.1907	0.1650	0.0925	0.1417
	12	5	2197	0.1184	0.1907	0.1650	0.0925	0.1417
qMC	-	-	1000	0.1205	0.1896	0.1628	0.0922	0.1413

Figure 6.3 includes the observed groundwater heads and the statistical moments that we obtained using the gPC method along the whole simulation period. The expected value and the standard deviation are represented by μ_h and σ_h, respectively. Notice that the colored shade in the plots represents the interval $[\mu_h + \sigma_h, \mu_h - \sigma_h]$. Overall, the model responses are more accurate in the monitoring wells close to the streams. The expected values at Alzpitz, the closest monitoring well to the streams, represent the observed values properly and mimic the responses of the aquifer during the flood event. The Alzpitz monitoring well is placed in the riverbank and the discrepancies observed between modeled and measured data may be a consequence of the inability of the model to replicate the propagation of the overbank flow on the flood plain. This would lead to the underestimation of the exchange flow at the peak

of the event. Similarly, the responses at B3 are well characterized, even though there is a bias in relation to the expected value of the heads. Regarding the uncertainty bounds, we see that the prediction intervals of one standard deviation cover the ranges of the observed values in the monitoring wells located immediately close to the streams. On the other hand, the results at B1 and B4 are less accurate than the results at Alzpitz and B3 and do not properly match the values of the observations. We attribute these outcomes to inaccuracies in the time-variant specified-head boundary conditions that mainly control the groundwater flow at these points and were extracted from the pre-existing regional model (Keilholz et al., 2015). In our research, we primarily relied on the evaluation of Alzpitz and B3, because these are in the vicinity of the streams and the main drivers are the boundary conditions imposed in the canal and the river.

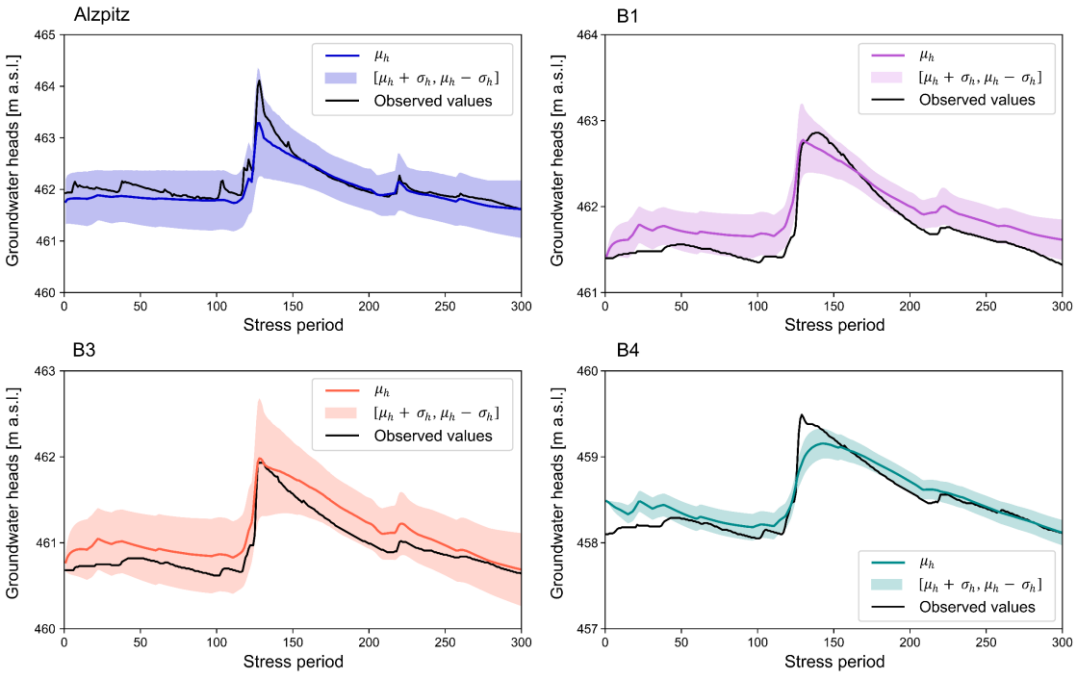

Figure 6.3. Simulated groundwater heads (colored line), observed values of the groundwater head at the monitoring wells (black line) and uncertainty bounds of the groundwater head (colored shade).

The uncertainty at the peak-flow of the flood event is higher than the uncertainty before the event and at the recession phase (see Table 6.3). Therefore, despite the fact that the uncertainty in the stream stage has the same statistical distribution over time, the highest uncertainties are observed during the peak-flow event. The deviation for the stage uncertainty was defined based on the uncertainties calculated by Willems (2011) for high discharge conditions, but

not for extreme event conditions. Notice that the uncertainty in discharge and head observation during exceptional flow conditions (e.g. during flood events) can be higher than the uncertainty under ordinary flow conditions (Di Baldassarre and Montanari, 2009).

Table 6.3. Predictive uncertainty represented by the standard deviation results (in meters) at different phases of the flood event computed at the monitoring wells.

Monitoring well	Before flood Stress period: 86	Peak-flow Stress period: 127	Recession phase Stress period: 145	After flood Stress period: 290
Alzpitz	0.5744	1.0737	0.5765	0.5326
B1	0.2510	0.4489	0.2548	0.2225
B3	0.4254	0.6987	0.4580	0.4032
B4	0.1522	0.1796	0.1697	0.1420

The propagation of uncertainty in the groundwater flow field was also quantified and the results were extracted at six different points (from E1 to E6), which are shown in Figure 6.2a. Since the magnitude and direction of the flow fields respond to the hydraulic gradients, the different evaluation points show the behavior of the subsurface system depending on the river and the canal behavior. The high stages in the streams increase the steepness of the gradients and raise the expected value of the velocity μ_v in the vicinity of the streams (see Figure 6.4). This effect and the large hydraulic conductivity of the gravel and sand in the alluvial plain allow a rapid increase of the magnitude of the flow field. Therefore, it is possible to see the highest average velocities at the peak-flow in all six monitoring points. During the recession phase of the flood, the velocity not only decreases but the uncertainty, which is represented by the standard deviation σ_v, also drops because of the reduction in the head difference between streams and aquifer at this phase. The highest velocities are registered at E3 due to the hydraulic gradients and the hydraulic conductivity of the alluvial terrace.

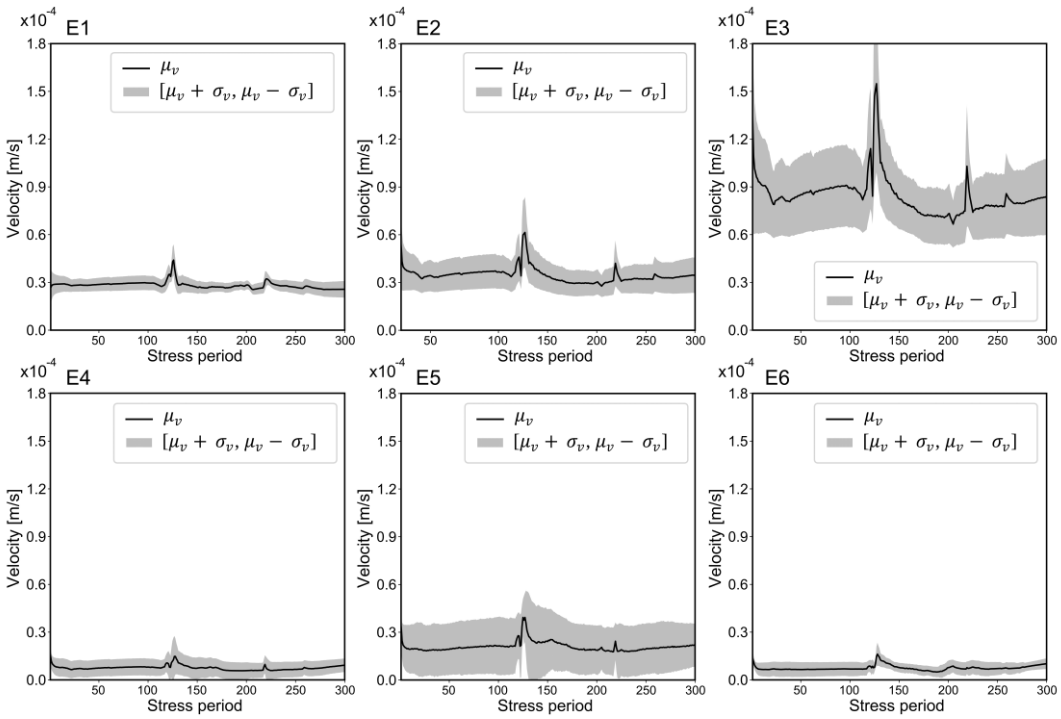

Figure 6.4. Simulated expected value of the flow field magnitude (black line) and uncertainty bounds of the flow field (gray shade).

As observed in E4 and E5, the velocity and the uncertainty south of the joining streams vary highly at short distances (~40 m between E4 and E5). In this region, the intensity of the signals is controlled by the conductance and the stage of both the canal and the river. The response at E4 may be a consequence of the dominance of the signal coming from the stream stage. Conversely, at E5, rather than one hydraulic pulse, more signals may affect the head variability and the propagated uncertainty in a similar magnitude due to the relative distance of both of the streams and their interaction with the regular groundwater flow regime. As observed, the standard deviations at E3 and E5 are higher than the standard deviation at the other evaluation points.

As seen in Figure 6.4, the results give evidence of a complex dynamic of the groundwater flow in the region where the streams converge. A limitation of our study is certainly the lack of field information from south of the convergence of the streams. This emphasizes the need and significance of quantifying the uncertainty due to surface water and groundwater interaction. To see the behavior south of the junction of the streams in detail, we extracted the

results of the flow fields to display the velocity vectors in Figure 6.5. Figure 6.5a includes the expected value of the flow fields at the different phases of the flood event, and Figure 6.5b shows the spatial distribution of the standard deviation of the velocity. Notice that Figure 6.5a and Figure 6.5b display the results in a logarithmic scale to facilitate the examination. With the same purpose, the vector arrows in Figure 6.5a only show the direction of the vector and were upscaled applying an interpolation that queries the nearest cell values.

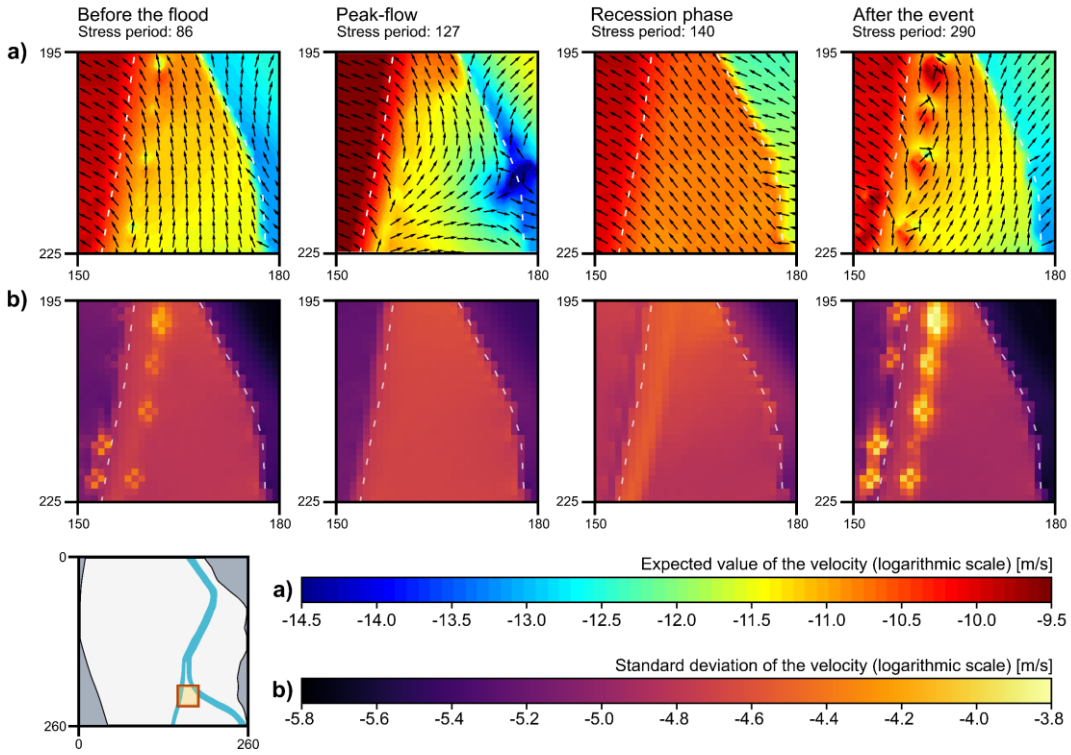

Figure 6.5. Statistics of the flow field at the river and canal confluence: a) expected value of the velocity (colored cells) and expected value of the direction (black arrows), and b) standard deviation of the velocity (colored cells). The river and canal locations are referenced by the white dashed line.

During the peak-flow, we observed major variations in the magnitude and direction of the flow field. The eastern side of the river shows slow flow due to the convergence of fluxes, while the flow velocity below the canal reaches its maximum. In the recession phase, we can observe a dominant orientation of the flow from southeast to northwest. The magnitude and direction almost recover to the initial state after the flood. In Figure 6.5b, we observe major uncertainties before and after the event. This may occur because there is not a single signal that independently controls the flow field in the selected domain during this period. Therefore,

small changes in the values of the stream parameters may imply significant modifications of the magnitude of the flow field at the meter-scale. Lower values of the standard deviation are found below the streams and also the recession phase is the least uncertain.

The probability density functions of the directions were obtained from the kernel density estimation. In Figure 6.6, we represent the probability density function of the flow field direction within a two-dimensional polar coordinate system labeled in degrees. In this reference system, the direction is defined by the angular coordinate in degrees, and the frequency is represented by the radial coordinate [-] as the distance from the origin. We observed variations in the direction of the flow field at every stage of the flood event. The significance of these variations depends on the spatial location and the underlying geomorphological and hydrological features. The evaluation points located west of the streams (E1, E2, and E3) present small changes in the expected value of the direction. However, the uncertainty is higher at E1 than at E2 and E3. South of the confluence of the streams, the orientations fluctuate considerably. As mentioned above, the flow fields depend on two diverse hydraulic pulses from different sources. One is the river, where the wave propagates without any immediate anthropogenic intervention. The second one is the canal, where the discharge is modulated by the upstream infrastructure. The E4, E5, and E6 evaluation points show major changes in the mean direction at every stage of the flood event. Similarly, the values of the standard deviation are higher, and the uncertainty varies highly at every stage of the event. The highest values of standard deviation of the direction can be observed at the peak of the event, particularly at E1, E4, E5, and E6. At the E5 evaluation point, we observe the most critical change in the orientation of the flow fields. Before the flood, we can observe the usual groundwater flow regime from southeast to northwest. At the peak of the flood event, the expected direction points towards the southeast. Afterward, during the recession of the flood, the flow follows the general reach regime in direction to the northeast. Observing E4 and E5 in Figure 6.6, and given the morphological conditions of the streams, we may expect to find reverse flow. However, we can also observe that, although the evaluation points are relatively close, the standard deviation and the mean of the direction can change considerably in short distances. This behavior is similar to the one observed in the velocity calculations. These substantial distinctions underline the need to define the effects of the uncertainties due to river boundary conditions in terms of space and time, particularly considering the limited field observations in this zone.

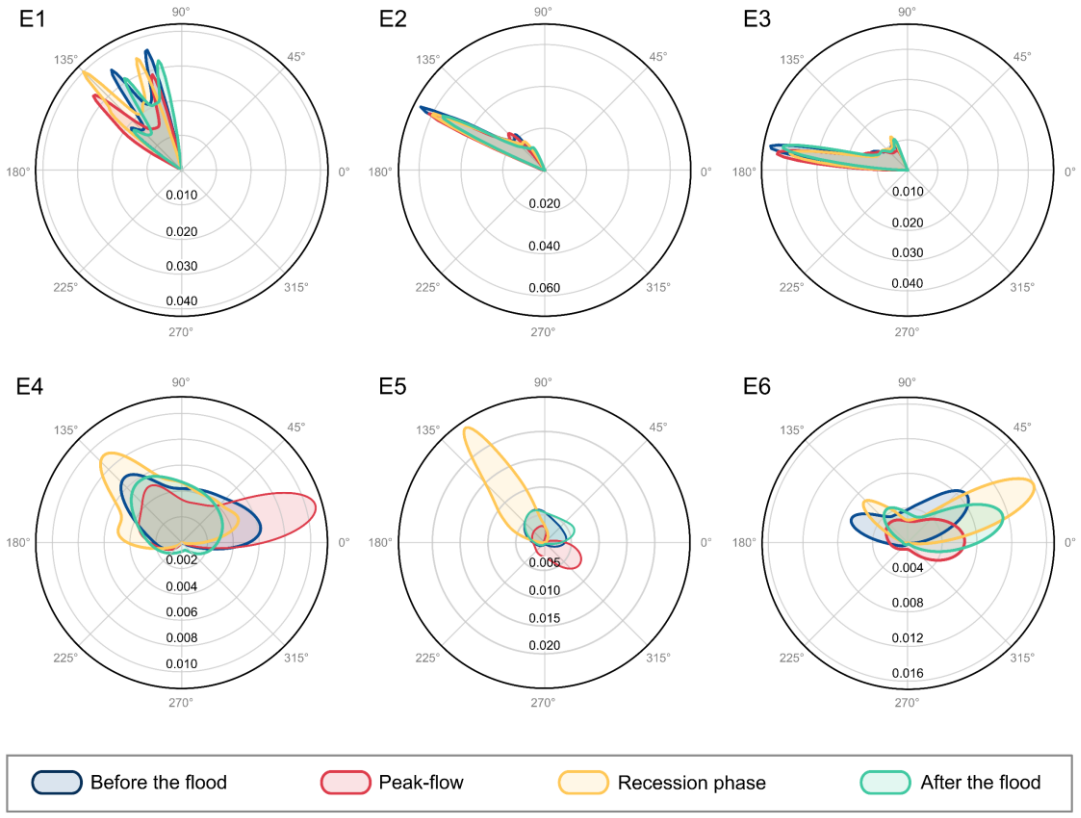

Figure 6.6. Propagation of uncertainty in the flow field direction. The probability density function of the flow field direction is represented within a two-dimensional polar coordinate system labeled in degrees.

The probability maps of the stagnation zones are presented in Figure 6.7a. We can distinguish different spots in space and time with higher sensitivity to the uncertainty in the river boundary conditions. In this case, we observe the probability of finding points where the local velocity is zero. Before and after the flood, we can observe black dots along the canal that show a relatively high probability of occurrence of stagnation points (~25%). This occurs in the places where different signals from the canal, the river and the aquifer meet. Also, at the junction of the canal and the river, it is possible to observe a stable stagnation region with a probability of occurrence from 10 to 15% for all the phases of the flood. This can occur due to the immediate counterflow that depends on the pressure heads of the streams that could produce the cancellation of the hydraulic pulses. The occurrence of stagnation zones decreases

highly during the peak-flow event because of the high hydraulic gradients, which increase the groundwater flow velocities. Nevertheless, at the peak-flow event, one can observe a fringe of a probable stagnation zone along the eastern border of the canal.

The second flow feature that we analyzed is the occurrence of reverse flows. We can observe the extracted results in Figure 6.7b. The probability of finding reverse flows in the domain dramatically increases during the peak-flow event, reaching a value of ~75%. One of the reasons for this is the high streambed conductance in the canal, which allows the exchange of flow during maximum discharge. At this phase, we have the highest hydraulic heads of the stage in the canal, which changes the regular hydraulic gradient and produces flows against the regional flow at the meter-scale. During the recession phase, the probability of finding reverse flows drops considerably. At this phase, the flood event starts a contraction defined by an extensive drop of the hydraulic gradients. It is also interesting to observe a spot of constantly high reverse probability allocated east of the junction of the streams. We attribute the high probabilities in this spot to the encounter of the discharges from the river and canal that increases the hydraulic pressure in the aquifer after the confluence of the two water bodies. The mean direction at this zone can be highly affected by the input uncertainty of stream stage and the conductance. Variations in these inputs can change the ordinary south-north flow to a lateral east-west flow due to the degree of flow exchange and can even affect the losing and gaining stream conditions. Regions near the confluence of the streams are prone to the presence of both stagnation points and reverse flow at different phases of the flood event. This area is very dynamic due to the interaction of the streams and the aquifer. Despite the apparent spatial correlation, there is a temporal difference in the responses. At peak-flow, the probability of stagnation zones increases and the probability of reverse flow decreases. In terms of fluid mixing, transport of solutes and temperature fluxes, these zones may play a meaningful role and may be highly affected by the uncertainties in the river boundary conditions. In our opinion, this is evidence of the importance of quantifying the uncertainty in the river boundary conditions and properly representing stream-aquifer interactions in numerical models.

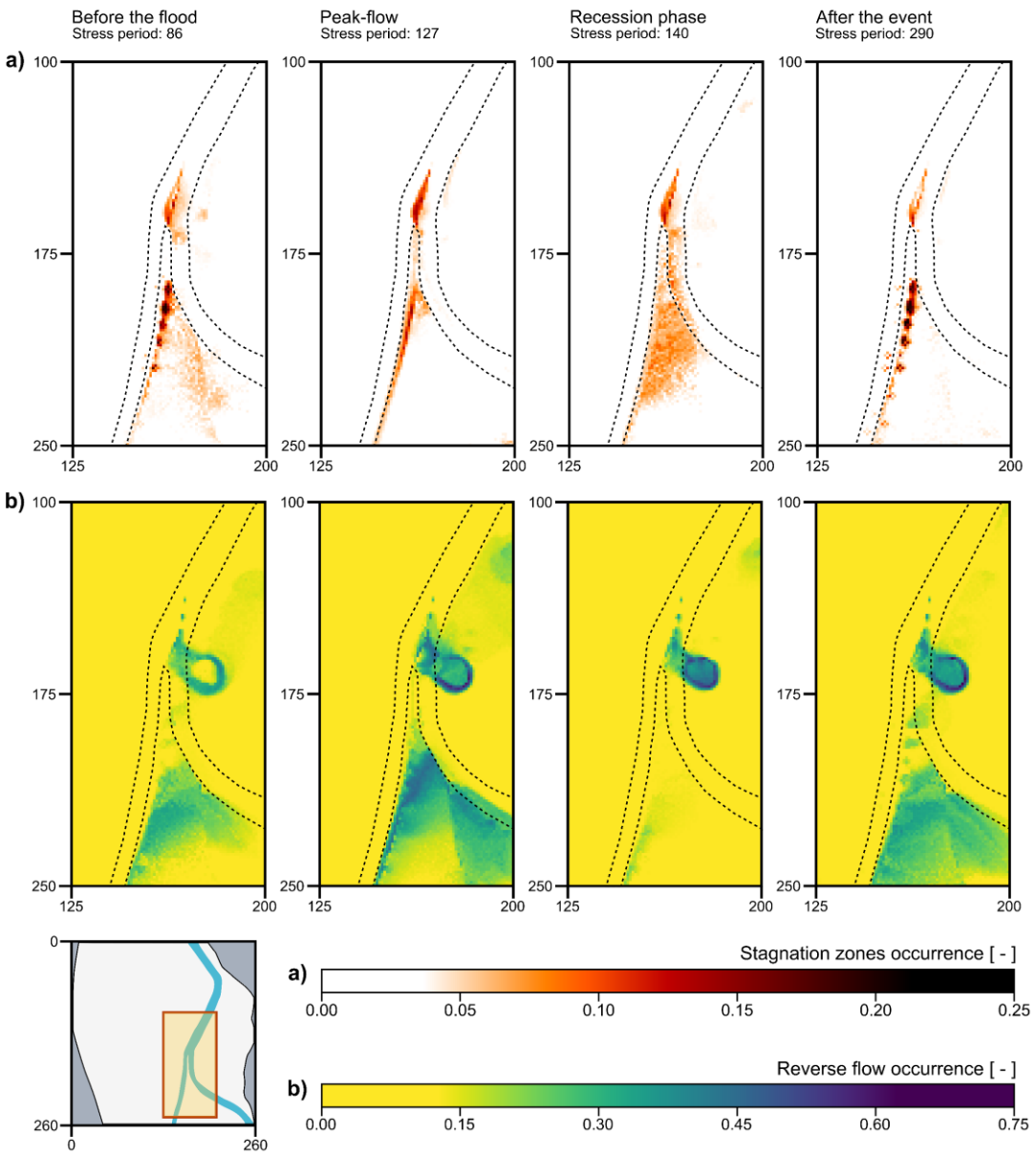

Figure 6.7. Probability of occurrence of flow features: a) stagnation zones at different phases of the flood event, and b) reverse flow at different phases of the flood event. The river and canal locations are referenced by the black dotted line.

6.4 Conclusions

In this study, we computed the probability of occurrence of stagnation zones and reverse flow in a numerical model based on the prior uncertainty of the river boundary conditions. The framework consists of the application of gPC expansions solved by a pseudo-spectral approach to obtain point estimates of the statistical information. We subsequently used kernel density estimations to take advantage of the information stored in the probability density functions of the quantities of interest. Finally, the flow fields were assessed according to a series of criteria that allowed us to identify hotspots of stagnation zones and reverse flow. A key feature of this work is the use of these techniques at every single cell of a distributed groundwater model. This allows us to explicitly map the flow field magnitude and direction in terms of statistical moments and the probability of occurrence in terms of spatial distribution and temporal variation.

This approach does not require further work for setting up pre-existing models, because the pseudo-spectral approach is a non-intrusive technique, and the solutions are achieved using a relatively low number of model evaluations (125 evaluations in this study). This means that a model can be treated as a black-box solver to calculate the expansion coefficients. This is quite practical considering that groundwater models that include river boundary conditions are often calibrated by tweaking the streambed conductance, which is a model parameter that can vary over time. Additionally, hydrogeological models are usually updated by adding time-variant processes, such as streamflow information and stream stages, for forecasting purposes. At the same time, we find this framework beneficial due to the flexibility to choose the precision and the computational cost. Due to the smooth dependence between the solution and the random spaces, a low quadrature degree may be sufficient to get accurate responses and other quantities of interest can be computed at a low marginal cost. Considering that the deterministic calculation at every element of a distributed model is usually the expensive part of the groundwater numerical simulations, an affordable approach is convenient for constructing spatial maps.

We validate the generalized polynomial chaos expansion as a method for quantifying the uncertainty in a real case study with a model that simulates flood events on surface water-groundwater interaction. The highest posterior uncertainties are found at the peak-flow phase, while the lowest uncertainties are observed at the recession phase of the flood. This occurs despite the fact that we used the same stream stage prior distribution over the whole simulation time to compute the expansion coefficients. The outcomes of this work give evidence of the complex hydrodynamic features occurring during the flood event due to the convergence of separate surface streams and their exchange flow with the aquifer. In consequence, there is significant uncertainty in the flow dynamics at the river boundaries that should be properly

quantified. This is reflected in the probability of finding stagnation and reverse flow at the meter and reach scale, despite the groundwater regime flowing predominantly along-valley. We can observe that the regions near the confluence of the streams are very dynamic and prone to exhibit stagnation zones and reverse flow. However, the probabilities of occurrence clearly vary at different phases of the flood event. At the peak-flow, the probability of occurrence of stagnation zones increases, while the probability of occurrence of reverse flow decreases. The major effects on the water flux and the flow paths are transitory and relative to the spatial location and the hydrogeological conditions of the stream-aquifer system. Although the methodology was applied to one specific case study, it can be more broadly stated that flow reversal and stagnation points can appear at the river confluence, where streams and highly permeable aquifers are well connected.

6.5 Annexes

6.5.1 Annex A: Collocation Method

Figure 6.8 illustrates how the collocation of the uncertain values differs between the gPC and the qMC methods. Figure 6.8a shows the abscissas of the quadrature nodes that define the three stochastic parameters in the full tensor grid of the gPC expansions when K = 4, while Figure 6.8b shows an equivalent number of sampled points (i.e. 125 samples) from the Halton sequences for the qMC method.

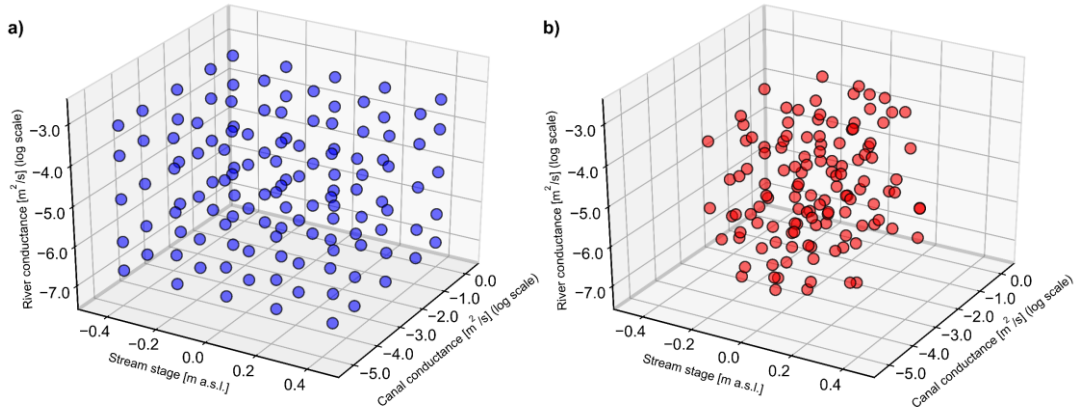

Figure 6.8. Evaluated parameter values using a) quadrature nodes for gPC expansions, and b) samples from Halton sequences for qMC simulations.

6.5.2 Annex B: Comparison between gPC and qMC methods

To evaluate the choice of the number of quadrature nodes that is used for generating the probability maps, we performed a comparison of the expected values and standard deviations of the hydraulic heads from the gPC approach using K = 4 and n = 4, and the qMC method with 500 samples. The responses of the methods at different phases of the flood event are evaluated through the difference in the expected value of the groundwater heads $D_{i,j}$ [L] (Eq. 6.23) and the relative difference of the standard deviation of the groundwater heads $R_{i,j}$ [-] (Eq. 6.24):

$$D_{i,j} = (\mu_{gPC})_{i,j} - (\mu_{qMC})_{i,j} \quad , \qquad \textit{Eq. 6.23}$$

$$R_{i,j} = \frac{(\sigma_{gPC})_{i,j} - (\sigma_{qMC})_{i,j}}{(\sigma_{qMC})_{i,j}} \quad . \qquad \textit{Eq. 6.24}$$

In Eq. 6.23, μ_{gPC} and μ_{qMC} are the simulated means of the groundwater heads [L] at the cell i, j from the gPC and the qMC approaches, respectively. In Eq. 6.24, σ_{gPC} and σ_{qMC} are the standard deviation values [L] at the cell i, j. The results of the validation are shown in Figure 6.9a and Figure 6.9b. Figure 6.9c shows the first and second statistical moments of the groundwater heads [L] from the gPC and qMC approaches along the whole simulation time at the monitoring wells. It also includes the interval $[\mu_{gPC} + \sigma_{gPC}, \mu_{gPC} - \sigma_{gPC}]$ for the gPC method and the interval $[\mu_{qMC} + \sigma_{qMC}, \mu_{qMC} - \sigma_{qMC}]$ for the qMC approach. Overall, we observe that both methods produce equivalent statistical moments for the groundwater heads. Due to this rapid convergence of the polynomial expansions, the use of a low number of deterministic model evaluations with the gPC approach does not imply major drawbacks. The highest difference in both the expected values and the standard deviations are found during the peak-flow event. The maximum difference in the expected head value is ~1.5 cm while the maximum relative difference in the standard deviation of the head distribution is ~1.5%.

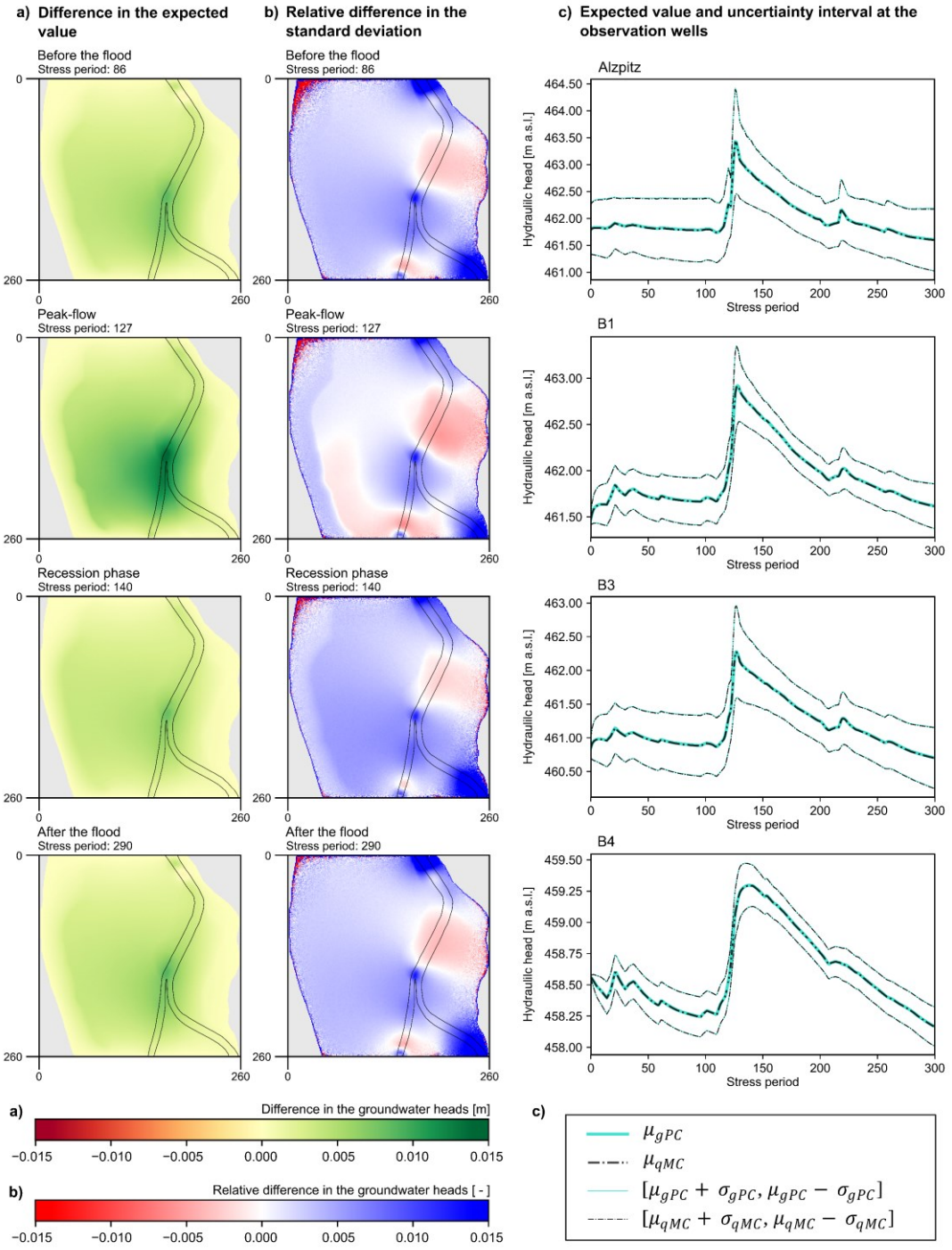

Figure 6.9. Comparison between gPC and qMC methods: a) difference of hydraulic head expected values at different stages of the flood event, and b) relative difference of the hydraulic head standard deviation at different stages of the flood event, and c) expected value and uncertainty intervals along the simulation period at the observation points.

7 Hydropeaking waves and flow topology

Abstract

Topological flow properties are proxies for mixing processes in aquifers and allow us to better understand the mechanisms controlling transport of solutes in the subsurface. However, topological descriptors, such as the Okubo-Weiss metric, are affected by the uncertainty in the solution of the flow problem. While the uncertainty related to the heterogeneous properties of the aquifer has been widely investigated in the past, less attention has been given to the one related to highly transient boundary conditions. We study the effect of different transient boundary conditions associated with hydropeaking events (i.e., artificial river stage fluctuations due to hydropower production) on groundwater flow and the Okubo-Weiss metric. We define deterministic and stochastic modeling scenarios applying four typical settings to describe river stage fluctuations during hydropeaking events: a triangular wave, a sine wave, a complex wave that results of the superposition of two sine waves, and a trapezoidal wave. We use polynomial chaos expansions to quantify the spatiotemporal uncertainty that propagates into the hydraulic head in the aquifer and the Okubo-Weiss. The wave-shaped highly transient boundary conditions influence not only the magnitude of the deformation and rotational forces of the flow field but also the temporal dynamics of dominance between local strain and rotation properties. Larger uncertainties are found in the scenario where the trapezoidal wave was imposed due to sharp fluctuation in the stage. The statistical moments that describe the propagation of the uncertainty highly vary depending on the applied boundary condition.

Material from:

Merchán-Rivera, P., Basilio Hazas, M., Marcolini, G., Chiogna, G., 2022 (submitted). Propagation of Hydropeaking Waves in Heterogeneous Aquifers: Effects on Flow Topology and Uncertainty Quantification. International Journal on Geomathematics

7.1 Introduction

Mixing plays a critical role in describing solute transport in aquifers (de Anna et al., 2014b; Rolle and Le Borgne, 2019). Understanding mixing-limited reactions in the subsurface is particularly relevant to recognize biogeochemical transformations (Boisson et al., 2013; Kang et al., 2019; Pinay et al., 2015), operate and design engineering remediation techniques (Cho et al., 2019; Mays and Neupauer, 2012; McCarty and Criddle, 2012; Neupauer et al., 2014), and understand hyporheic processes (Boano et al., 2014). A variety of methods have been developed to understand the transport dynamics in the subsurface and the effect that heterogeneous hydraulic properties have on spreading, dilution, and reactive mixing, (Valocchi et al., 2019). However, transport simulations are often computationally expensive and the quantification of uncertainties may result in a very time-consuming exercise (Lykkegaard et al., 2021; Smith, 2013). The relation between topological flow properties and mixing processes in aquifers (Bresciani et al., 2019; de Barros et al., 2012) and porous media (de Anna et al., 2014a; Engdahl et al., 2014; Wright et al., 2017) provides an interesting alternative to the solution of the transport problem. One advantage of investigating such relations is that the calculation of topological features of the flow field requires only the solution of the flow problem, which is much cheaper from the computational point of view than the solution of the flow and transport equations.

A topological quantity known as the Okubo-Weiss metric (Okubo, 1970; Weiss, 1991) was shown to be a good proxy for mixing potential (de Barros et al., 2012; Wright et al., 2017). This metric is commonly used in geophysics to identify filament from vortex structures (Casella et al., 2011; Roullet and Klein, 2010) and characterize them in terms of dominant forces of the flow field, such as vorticity, shear strain, and normal strain (de Barros et al., 2012; Wallace et al., 2021). Still, the quantification of such topological descriptors of the flow field is affected by the uncertainty that is caused by the heterogeneous nature of the aquifer (Geng et al., 2020; Valocchi et al., 2019). Significant efforts have been made to quantify the uncertainty affecting the predictions of solute concentration values caused by the generally unknown hydraulic conductivity field (Moslehi and de Barros, 2017; Nowak et al., 2010). However, in this work, we assume the hydraulic conductivity field as properly characterized and well known in order to focus on a different source of uncertainty, which did not receive comparable attention in the literature, i.e., highly transient boundary conditions.

In fact, transient boundary conditions can also be uncertain and affect the estimation of the topological properties of the flow field and, consequently, the understanding of mixing and transport processes in aquifers (Hester et al., 2021; Ziliotto et al., 2021). This is particularly the case of the aquifer area close to surface water bodies (Dudley-Southern and Binley, 2015; Merchán-Rivera et al., 2021; Santizo et al., 2020; Singh et al., 2020). In this work, we focus

on a river reach that is affected by hydropeaking, i.e., sudden changes in the hydraulic head of the river caused by the operation of hydropower plants. Such fluctuations display some typical periodicity (Pérez Ciria et al., 2020) and modify the natural hydrological behavior and hydraulic conditions of the streams (Hauer et al., 2017; Meile et al., 2011), which can impact the hyporheic zone (Sawyer et al., 2009; Singh et al., 2019) and propagate to the groundwater (Francis et al., 2010; Song et al., 2020). Moreover, since hydropeaking may depend on hydrological conditions (Li and Pasternack, 2021) and the dynamic behavior of the energy market (Chiogna et al., 2018; Pérez Ciria et al., 2019; Wagner et al., 2015), the stream head fluctuations entail uncertainty related to the peak amplitude and the temporal occurrence of the event.

The question that we aim at answering in this work is to what extent the shape and the uncertainty of hydropeaking waves affect the topology of the groundwater flow field quantified through the Okubo-Weiss parameter. To achieve our aim, we define one single realization of a two-dimensional heterogeneous aquifer and build modeling scenarios based on four typical settings for the stream fluctuations of the boundary conditions: a triangular wave, a sine wave, a complex wave (realized as the superposition of two sine waves), and a trapezoidal wave (Ferencz et al., 2019; Li and Pasternack, 2021; Sawyer et al., 2009). Moreover, we apply polynomial chaos expansion (Xiu and Karniadakis, 2002) to quantify the uncertainty due to the oscillatory boundaries and quantify the mean and standard deviation of the temporal and spatial values of the Okubo-Weiss metric.

The paper is structured as follows. Section 2 presents the synthetic case study, the deterministic and stochastic modeling scenarios, the polynomial chaos expansion method, and the topological metric that we use to describe the flow field. In Section 3, we present and discuss the results and findings related to the groundwater flow and the Okubo-Weiss metric and the quantification of the spatiotemporal uncertainty. We conclude this work in Section 4 by restating major findings and discussing the environmental implications of our results.

7.2 Methods

7.2.1 Groundwater flow equation

The governing equation of the two-dimensional transient groundwater flow in a heterogeneous, isotropic, and unconfined aquifer can be written as

$$\frac{\partial}{\partial x}\left(K_x h \frac{\partial h}{\partial x}\right) + \frac{\partial}{\partial y}\left(K_y h \frac{\partial h}{\partial y}\right) = s_y \frac{\partial h}{\partial t} \pm Q \,, \qquad \textit{Eq. 7.1}$$

where h is the hydraulic head [L], K_x and K_y are values of the hydraulic conductivity along the x and y coordinate axis [LT^{-1}], s_y is the specific yield of the porous medium [-], and Q describes the volumetric flux from source and sink terms [LT^{-1}] (Anderson et al., 2015; Bear, 1979). The initial conditions and Dirichlet boundary conditions can be denoted as

$$h(x, y, 0) = h_0(x, y), \qquad x, y \in \Lambda, \qquad \textit{Eq. 7.2}$$

$$h(x, y, t) = h_1(x, y, t), \qquad x, y \in \partial\Lambda, \qquad \textit{Eq. 7.3}$$

respectively, where $h_0(x, y)$ is the initial hydraulic head [L] in the domain in the flow region Λ; $h_1(x, y, t)$ is the known hydraulic head value of the boundary head [L], and $\partial\Lambda$ denotes the boundary region (Bear and Cheng, 2010; Cheng and Cheng, 2005).

7.2.2 Model description

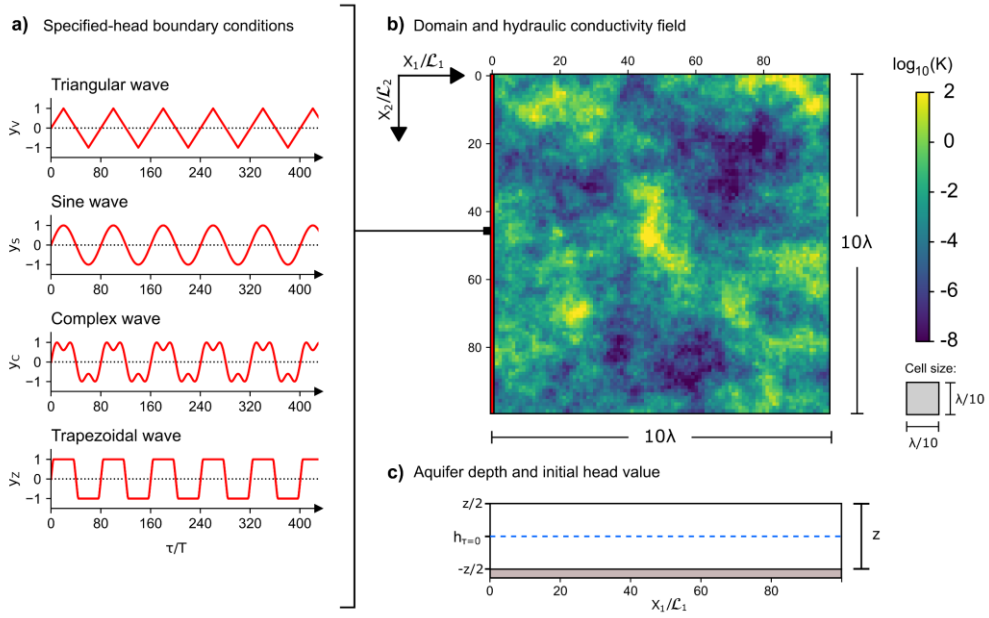

Figure 7.1. Model description: a) wave-shaped time-variant specified head boundary conditions, b) spatial domain and hydraulic conductivity field, and c) aquifer depth and initial groundwater head conditions

In our system, we consider a two-dimensional unconfined aquifer with lognormal heterogeneous isotropic hydraulic conductivity field $g(x) = \ln[K(x)]$ defined by the geometric mean $\mu_g = 1 \times 10^{-3}$ m/s, the geometric standard deviation $\sigma_g = 1.5$ m/s and the correlation length $\lambda = 10$ m, equivalent to porous medium formed by sands and gravels (Coduto, 1999). The area of the squared domain is $\mathcal{L}_1 \times \mathcal{L}_2 = 10\lambda \times 10\lambda$ with cell size $0.1\lambda \times 0.1\lambda$ (see Figure 7.1b). The distance between the ground surface and the bottom of the aquifer is $z = d(-z/2, z/2)$, the reference datum is the middle point $z_0 = 0$. The initial groundwater level conditions h_0 are set to a uniform water level in the domain, which matches the reference datum, so that $h_0 = z_0$ (see Figure 7.1c) and any simulation output h represents the relative movement of the groundwater head with respect to z_0. The time discretization of the simulation is τ/T, where T represents the simulation time length, and it is related to the wave frequency f such that $f = 1/(80\tau)$.

The discontinuous release of water from hydropeaking events tends to follow a periodicity. Hence, the stage fluctuation in the stream can be described by a periodic function $y(t + F) = y(t)$, where $F = 1/f$ is a nonzero value defined as the period [T]. We introduce the periodic

waves as specified-head boundary conditions, i.e., Dirichlet boundary conditions (Bear and Cheng, 2010), by fixing head values at the left border of the domain. The wave-shaped time series of heads represent the stream stage and the values at the boundary are time-dependent and updated as the simulation progresses. This setup assumes that the stage changes for the entire river reach considered simultaneously (i.e., no hydraulic model is used to describe the wave propagation along the reach) and strong connectivity between surface water and groundwater. These assumptions are consistent, for example, with the study of Sawyer (2009) focusing on the Colorado River in Texas. The top, bottom and right boundaries are defined as no-flow boundaries. We define the following periodic functions (see Figure 7.1a) to represent the effect of the hydropeaking on the left boundary conditions:

- Triangular wave:

$$y_V(t) = 4Af\left|\left\{\left(t-\frac{1}{4f}\right) \bmod \left(\frac{1}{f}\right)\right\}-\frac{1}{2f}\right| - A\,, \qquad \textit{Eq. 7.4}$$

- Sine wave:

$$y_S(t) = A\sin(2\pi f(t-p))\,, \qquad \textit{Eq. 7.5}$$

- Complex wave:

$$\begin{aligned} y_C(t) &= y_S^{\alpha}(t) + y_S^{\beta}(t) \\ &= A_\alpha \sin(2\pi f_\alpha(t-p_\alpha)) + A_\beta \sin\left(2\pi f_\beta(t-p_\beta)\right), \end{aligned} \qquad \textit{Eq. 7.6}$$

- Trapezoidal wave:

$$y_Z(t) \coloneqq \begin{cases} -A, & \text{if } y_V^*(t) < A; \\ A, & \text{if } y_V^*(t) > A; \\ y_V^*(t), & \text{otherwise,} \end{cases} \qquad \textit{Eq. 7.7}$$

$$y_V^*(t) = 4b_Z Af\left|\left\{\left(t-\frac{1}{4f}\right) \bmod \left(\frac{1}{f}\right)\right\}-\frac{1}{2f}\right| - b_Z A\,. \qquad \textit{Eq. 7.8}$$

Then, $y_V(t)$, $y_S(t)$, $y_C(t)$ and $y_Z(t)$ represent the time-variant specified-head boundaries for the triangular, sine, complex and trapezoidal wave scenario, respectively, t is the evaluation time step, A is the amplitude of the wave, p is the phase shift and f is the frequency. We shaped the trapezoidal wave using the stepwise function $y_Z(t)$ to remove the values that exceed the minimum and maximum limits defined by A, which depends on the outcomes of a triangular function $y_V^*(t)$. A coefficient b_Z is introduced to this triangular function to extend the amplitude A, which will determine the interval between minimum and maximum stage to be equal to $4/b_Z$ given the slope of the trapezoid legs with base angles $\theta = \arctan(4b_ZAf)$. The complex waveform is the result of combining two different sine waves ($y_S^\alpha(t)$ and $y_S^\beta(t)$) shaped by two different amplitudes (A_α and A_β), two phase shifts (p_α and p_β) and two frequencies (f_α and f_β).

7.2.2.1 Deterministic problem

As starting point, we want to observe the responses of the aquifer and the flow field topology assuming that all model inputs are known. Hence, there are four deterministic scenarios of one single deterministic transient flow problem, each applying one of the wave-shaped boundary conditions. The complex wave is defined by $A_\beta = 2A_\alpha/5$, $p_\beta = 3p_\alpha$ and $f_\beta = 3f_\alpha$ to satisfy symmetry relations between the periodic waves to match maximum (i.e., wave crest), minimum (i.e., wave through), temporal axis interceptions, and lag between two events. The trapezoidal wave is shaped considering $b_Z = 6$, so that the interval between minimum and maximum is equivalent to $1/12f$.

The spatial and temporal distribution of the groundwater heads and the Okubo-Weiss are analyzed with two-dimensional arrays. We are also interested in the variability of the groundwater head and the Okubo-Weiss metric at a certain distance $x_1/\mathcal{L}_1$ from the transient boundary conditions. Hence, we compute the variance in time at each discrete cell, and then the arithmetic mean of the variance relative to the distance $x_1/\mathcal{L}_1$. For simplicity we call $c_t^{i,j}$ the output of interest (i.e., groundwater heads or Okubo-Weiss metric) at a discrete cell with row i, and column j, at the time t, and follow

$$\sigma_{i,j}^2 = \frac{1}{T}\sum_{t=1}^{T}\left(c_t^{i,j} - \mu_c^{i,j}\right)^2, \qquad \mu_c^{i,j} = \frac{1}{T}\sum_{t=1}^{T} c_t^{i,j}, \qquad \textit{Eq. 7.9}$$

where $\mu_c^{i,j}$ is the mean of the output of interest at a discrete cell $\{i, j\}$ along all the evaluation time T. Then, the arithmetic mean of the variances at the distance $x_1/\mathcal{L}_1$ can be computed along column $j \approx x_1/\mathcal{L}_1$, such that,

$$\bar{\sigma}_j^2 = \frac{1}{n_i}\sum_{i=1}^{n_i} \sigma_{i,j}^2 \,, \qquad \textit{Eq. 7.10}$$

being n_i the number of the discrete rows.

7.2.2.2 Stochastic problem

We consider the amplitude A and phase p as uncertain parameters and we assume them as mutually independent random variables. On one hand, A represents the maximum water level in the stream, which fluctuates due to the variable discharges from the power plant, which in turn depends on market and seasonal conditions. The uncertainty is defined from a minimum and maximum stage fluctuation that follows a uniform distribution $A \sim \mathcal{U}(a_A, b_A)$, where $a_A = 0.9$ and $b_A = 1.1$. On the other hand, p represents the shift in the stage signal. This random variable then introduces the temporal uncertainty due to changes in the gate management, turbine control and discharge duration. The random variable p is uniformly distributed, such that $p \sim \mathcal{U}(a_p, b_p)$. The parameters a_p and b_p describe the phase difference and relates the offset with f using a factor o_p, so that $a_p = -1/(o_p f)$ and $b_p = 1/(o_p f)$. This arrangement simplifies the application at multiple hydropeaking scale events (e.g., sub-daily, daily, and weekly) because any shift in the phase is a ratio of the periodicity. In our problem setup, we set $o_p = 8$, which is equivalent to a phase difference of $1/8f$.

In the case of the complex wave, the problem increases to 4 stochastic dimensions given that it is formed by the superposition of two sine waves $y_S^{\alpha}(t)$ and $y_S^{\beta}(t)$. Like in the deterministic problem, we keep the proportional relations between the two waves $y_S^{\alpha}(t)$ and $y_S^{\beta}(t)$ that form the complex wave and the random variables that are assumed mutually independent. Hence, two random variables $A_\alpha \sim \mathcal{U}(a_A^{\alpha}, b_A^{\alpha})$ and $A_\beta \sim \mathcal{U}(a_A^{\beta}, b_A^{\beta})$ represent the amplitudes, where $a_A^{\alpha} = a_A$, $b_A^{\alpha} = b_A$, $a_A^{\beta} = 2a_A^{\alpha}/5$ and $b_A^{\beta} = 2b_A^{\alpha}/5$. Also, two random variables $p_\alpha \sim \mathcal{U}(a_p^{\alpha}, b_p^{\alpha})$ and $p_\beta \sim \mathcal{U}(a_p^{\beta}, b_p^{\beta})$ represent the phase differences, where $a_p^{\alpha} = a_p$, $b_p^{\alpha} = b_p$, $a_p^{\beta} = a_p^{\alpha}/3$ and $b_p^{\beta} = b_p^{\alpha}/3$.

In this work, we represent the dynamic system of the groundwater heads and flow topology as stochastic processes with uncertain boundary conditions using generalized polynomial chaos expansions. The statistical moments computed with the expansions and explained in the following section are also analyzed computing their arithmetic mean, analogous to Eq. 7.10. A summary of the specific parameters used in the deterministic and stochastic scenarios can be found in Table 7.1.

Table 7.1. Parameters used in the construction of the transient boundary conditions: a) deterministic scenarios, and b) stochastic scenarios.

Scenario	**Triangular wave**	**Sine wave**	**Complex wave**	**Trapezoidal wave**
a) Deterministic				
Amplitude	$A = 1$	$A = 1$	$A_\alpha = 1, \quad A_\beta = \frac{2A_\alpha}{5}$	$A = 1$
Phase	$p = 0$	$p = 0$	$p_\alpha = 0, \quad p_\beta = 3p_\alpha$	$p = 0$
Frequency	$f = \frac{1}{80}$	$f = \frac{1}{80}$	$f_\alpha = \frac{1}{80}, \quad f_\beta = 3f_\alpha$	$f = \frac{1}{80}$
Trapezoid shape coefficient	–	–	–	$b_Z = 6$
b) Stochastic				
Amplitude	$A \sim \mathcal{U}(0.9,1.1)$	$A \sim \mathcal{U}(0.9,1.1)$	$A_\alpha \sim \mathcal{U}(0.9,1.1)$, $A_\beta \sim \mathcal{U}\left(\frac{2(0.9)}{5}, \frac{2(1.1)}{5}\right)$	$A \sim \mathcal{U}(0.9,1.1)$
Phase	$p \sim \mathcal{U}\left(-\frac{1}{8f}, \frac{1}{8f}\right)$	$p \sim \mathcal{U}\left(-\frac{1}{o_p f}, \frac{1}{o_p f}\right)$	$p_\alpha \sim \mathcal{U}\left(-\frac{1}{o_p f_\alpha}, \frac{1}{o_p f_\alpha}\right)$, $p_\beta \sim \mathcal{U}\left(-\frac{1}{3o_p f_\beta}, \frac{1}{3o_p f_\beta}\right)$	$p \sim \mathcal{U}\left(-\frac{1}{o_p f}, \frac{1}{o_p f}\right)$
Frequency	$f = \frac{1}{80}$	$f = \frac{1}{80}$	$f_\alpha = \frac{1}{80}, \quad f_\beta = 3f_\alpha$	$f = \frac{1}{80}$
Trapezoid shape coefficient	–	–	–	$b_Z = 6$
Phase coefficient	$o_p = 8$	$o_p = 8$	$o_p = 8$	$o_p = 8$

7.2.3 Polynomial chaos expansion

7.2.3.1 Stochastic formulation

Let $(\Omega, \mathcal{F}, P)$ be a probability space, where Ω is a sample space, $\mathcal{F}$ is a σ-algebra on Ω, and P is a probability measure on Ω. Consider a function $u(t, x, \mathbf{\Phi})$ on the probability space $(\Omega, \mathcal{F}, P)$, where $\mathbf{\Phi} = [\Phi_1, \dots, \Phi_d]: \Omega \to \mathbb{R}$ is a random vector with a finite set of d mutually independent random variables with marginal probability density functions $\{\rho_{\Phi_i}(\varphi_i), i = 1, \dots, d\}$, and $\{t, x\}$ represent the deterministic temporal and spatial dependencies with a finite temporal horizon $t \in [0, T]$ within the spatial domain $\mathcal{D} \subset \mathbb{R}^2$ formed by fixed grid points $x = (x_1, x_2)$. Since each parameter $\Phi_i(\omega): \Omega \to \mathbb{R}$ is associated to a density $\rho_{\Phi_i}(\varphi_i)$ and $\omega \in \Omega$ is a realization in the underlying probability space, we reformulate the problem in the image probability space $(\Gamma, \mathcal{B}(\Gamma), \rho_{\mathbf{\Phi}}(\varphi) d\varphi)$, where $\Gamma = \prod_{i=1}^{d} \Phi_i(\Omega)$ is the sample space for the range of Φ_i, $\mathcal{B}(\Gamma)$ is the Borel σ-algebra on Γ, and $\rho_{\mathbf{\Phi}}(\varphi)$ is the joint density associated with $\mathbf{\Phi}$, described by

$$\rho_{\mathbf{\Phi}}(\varphi) = \prod_{i=1}^{d} \rho_{\Phi_i}(\varphi_i) \,. \qquad \textit{Eq. 7.11}$$

The output function is then a random process $u(t, x, \mathbf{\Phi}): [0, T] \times \mathcal{D} \times \Gamma \to \mathbb{R}$ with a finite variance. Following the generalized Cameron-Martin theorem (Cameron and Martin, 1947), we can represent it as an infinite series expansion of polynomials, which can be truncated to order K, such that

$$\begin{aligned} u(t, x, \mathbf{\Phi}) &= \sum_{\boldsymbol{\kappa}=0}^{\infty} \hat{u}_{\boldsymbol{\kappa}}(t, x) \mathbf{\Psi}_{\boldsymbol{\kappa}}(\mathbf{\Phi}) \\ &\approx \sum_{\boldsymbol{\kappa}=0}^{K} \hat{u}_{\boldsymbol{\kappa}}(t, x) \mathbf{\Psi}_{\boldsymbol{\kappa}}(\mathbf{\Phi}) \,, \end{aligned} \qquad \textit{Eq. 7.12}$$

where $\hat{u}_{\boldsymbol{\kappa}}(t, x)$ are deterministic expansion coefficients, $\mathbf{\Psi}_{\boldsymbol{\kappa}}(\mathbf{\Phi})$ represent the multivariate orthogonal polynomial basis function, and $\boldsymbol{\kappa} = \{\kappa_1, \dots, \kappa_d\} \in \mathbb{N}_0^d$ is a multi-index of non-negative integers of size d to identify the degree of the polynomials for the input variable Φ_i. To achieve n order of polynomials, K can be optimally defined by $[(n + d)!/n!\, d!] -$

1 (Smith, 2013; Xiu, 2010), or by using experimental designs, such as the empirical rule $K = (d-1) \times (n+1)$ (Sudret, 2008), to reduce the computational demand of the experiment. In this research, we define $K = 9$ and $n = 3$ for the triangular, sine and trapezoidal stochastic scenarios. The expansions in the complex scenario are calculated considering $K = 9$ and $n = 2$.

The orthogonal basis $\mathbf{\Psi_\kappa}$ must be accordingly specified to $\rho_{\Phi_i}(\varphi_i)$ (Xiu and Karniadakis, 2002). In this work, the uncertain input parameters associated to the boundary conditions $\mathbf{\Phi}$ are considered random variables uniformly distributed in the interval $[a, b]$, denoted by $\Phi_i \sim \mathcal{U}(a, b)$. An appropriate basis is formed by the family of Legendre polynomials, which are an orthogonal basis with respect to the weight function $\rho_{\Phi_i}(\varphi_i) = 1/2$ for all normalized $\varphi_i \in [-1,1]$. Given the assumption that the random variables are mutually independent, the multivariate Legendre polynomial basis function $\mathbf{\Psi_\kappa}(\mathbf{\Phi})$ can be defined as the tensor product of the associated univariate orthogonal polynomials ψ_{κ_i}, such that

$$\mathbf{\Psi_\kappa}(\mathbf{\Phi}) = \prod_{i=1}^{d} \psi_{\kappa_i}(\varphi_i)\,, \qquad \textit{Eq. 7.13}$$

which satisfies orthonormality conditions given that

$$\begin{aligned} \mathbb{E}\left[\psi_{\kappa_i}, \psi_{\tau_i}\right] &= \int_\Gamma \psi_{\kappa_i}(\varphi_i)\psi_{\tau_i}(\varphi_i)\rho_{\Phi_i}(\varphi_i)d\varphi_i \\ &= \langle \psi_{\kappa_i}, \psi_{\tau_i} \rangle_\rho \\ &= \delta_{\kappa_i\tau_i}\,, \end{aligned} \qquad \textit{Eq. 7.14}$$

where $\langle \cdot, \cdot \rangle$ denotes the inner product of the sequence of two polynomials $\{\psi_{\kappa_i}, \psi_{\tau_i}\}$ of degree κ_i and τ_i in the i th variable, $\delta_{\kappa_i\tau_i}$ represents the Kronecker delta. The deterministic coefficients $\hat{u}_{\mathbf{\kappa}}(t, x)$ can be approximated by exploiting the orthonormality of the basis function and projecting $u(t, x, \mathbf{\Phi})$ onto each basis function $\mathbf{\Psi}_k(\mathbf{\Phi})$ to obtain the representation

$$\hat{u}_{\boldsymbol{\kappa}}(t,x) = \langle u(t,\mathrm{x},\boldsymbol{\Phi}), \boldsymbol{\Psi}_{\boldsymbol{\kappa}}(\boldsymbol{\Phi})\rangle_{\rho} = \int_{\Gamma} u(t,x,\boldsymbol{\Phi})\boldsymbol{\Psi}_{\boldsymbol{\kappa}}(\boldsymbol{\Phi})\rho_{\boldsymbol{\Phi}}(\varphi)d\varphi\,. \qquad \textit{Eq. 7.15}$$

7.2.3.2 Pseudospectral collocation approach

We use the pseudospectral approach as a solution technique to estimate multidimensional integral that describes $\hat{u}_{\boldsymbol{\kappa}}(t,x)$. It is a discrete collocation method that relies on quadrature techniques to calculate $\hat{u}_{\boldsymbol{\kappa}}(t,x)$ at selected quadrature nodes $\mathbf{g^q} = \{g_1^{q_1}, \dots, g_d^{q_d}\} \in \mathbb{R}$ defined on Γ with the associated weights $w_{\mathbf{q}} = \{w_{q_1}, \dots, w_{q_d}\} \in \mathbb{R}$. Therefore, the deterministic solvers that describe the groundwater flow and the topological responses of the aquifer are not modified (i.e., non-intrusive spectral projection) because it is only required to evaluate $u(t,x,\mathbf{g^q})$ at the given $\mathbf{g^q}$. We employ Gaussian quadrature rules (Golub and Welsch, 1968) over a full tensor product grid to distribute $\mathbf{g^q}$ according to the probability density functions $\rho_{\Phi_i}(\varphi_i)$. Using $\mathcal{Q}$ to represent the quadrature integration, the extension of the univariate Gaussian quadrature yields to the summation over all possible combinations over m_i nodes

$$\begin{aligned}\mathcal{Q}[u(t,x,\cdot)] &= \left(\mathcal{Q}_{m_1} \otimes \dots \otimes \mathcal{Q}_{m_d}\right)[u(t,x,\cdot)] \\ &= \sum_{q_1=1}^{m_1} \dots \sum_{q_d=1}^{m_d} u\left(t,x,g_1^{q_1},\dots,g_d^{q_d}\right) w_{q_1} \dots w_{q_d}\,,\end{aligned} \qquad \textit{Eq. 7.16}$$

that can be recast for the sake of simplicity to the multi-index approximation

$$\hat{u}_{\boldsymbol{\kappa}}(t,x) \asymp \mathcal{Q}[u(t,x,\cdot)\boldsymbol{\Psi}_{\boldsymbol{\kappa}}(\cdot)] = \sum_{\mathbf{q}=1}^{M} u(t,x,\mathbf{g^q})\boldsymbol{\Psi}_{\boldsymbol{\kappa}}(\mathbf{g^q})w_{\mathbf{q}}\,, \qquad \textit{Eq. 7.17}$$

where the total number of grid points is $M = m^d$ given that we opt for $m_1 = \dots = m_d = m$.

The expected value of $u(t,x,\boldsymbol{\Phi})$ can be estimated from the polynomial chaos coefficients $\hat{u}_0(t,x)$, given that

$$\mu = \mathbb{E}[u(t,x,\boldsymbol{\Phi})] \approx \mathbb{E}\left[\sum_{\boldsymbol{\kappa}=0}^{K} \hat{u}_{\boldsymbol{\kappa}}(t,x)\boldsymbol{\Psi}_{\boldsymbol{\kappa}}(\boldsymbol{\Phi})\right]$$
$$= \hat{u}_0(t,x)\mathbb{E}[\boldsymbol{\Psi}_0(\boldsymbol{\Phi})] + \sum_{\boldsymbol{\kappa}=1}^{K} \hat{u}_{\boldsymbol{\kappa}}(t,x)\mathbb{E}[\boldsymbol{\Psi}_{\boldsymbol{\kappa}}(\boldsymbol{\Phi})] \qquad \textit{Eq. 7.18}$$
$$= \hat{u}_0(t,x)\,.$$

Similarly, the variance $\sigma^2 = \mathbb{V}[u(t,x,\boldsymbol{\Phi})]$ and the standard deviation $\sigma = \sqrt[2]{\mathbb{V}[u(t,x,\boldsymbol{\Phi})]}$ are quantified following

$$\sigma^2 = \mathbb{V}[u(t,x,\boldsymbol{\Phi})] = \mathbb{E}[(u(t,x,\boldsymbol{\Phi}) - \mathbb{E}[u(t,x,\boldsymbol{\Phi})])^2]$$
$$\approx \mathbb{E}\left[\left(\sum_{\boldsymbol{\kappa}=0}^{K} \hat{u}_{\boldsymbol{\kappa}}(t,x)\boldsymbol{\Psi}_{\boldsymbol{\kappa}}(\boldsymbol{\Phi}) - \hat{u}_0(t,x)\right)^2\right]$$
$$= \mathbb{E}\left[\left(\sum_{\boldsymbol{\kappa}=1}^{K} \hat{u}_{\boldsymbol{\kappa}}(t,x)\boldsymbol{\Psi}_{\boldsymbol{\kappa}}(\boldsymbol{\Phi})\right)^2\right] \qquad \textit{Eq. 7.19}$$
$$= \sum_{\boldsymbol{\kappa}=1}^{K} \hat{u}_{\boldsymbol{\kappa}}^2(t,x)\boldsymbol{\Psi}_{\boldsymbol{\kappa}}\,.$$

7.2.4 Okubo-Weiss

We consider a flow deformation metric based on a two-dimensional velocity gradient tensor ϵ, to be

$$\epsilon(t) = \nabla v(x,y,t), \qquad \textit{Eq. 7.20}$$

where $v(x, y, t)$ is the velocity at the space coordinates x and y at time t and it is estimated with the calculated head gradient by solving Eq. 7.1.

The Okubo-Weiss function (Okubo, 1970; Weiss, 1991) is defined by

$$\xi = -4\det(\epsilon), \qquad \textit{Eq. 7.21}$$

which in the horizontal plane with coordinates x and y is written as

$$\xi = -4\det\begin{bmatrix} \frac{\partial v_x}{\partial x} & \frac{\partial v_x}{\partial y} \\ \frac{\partial v_y}{\partial x} & \frac{\partial v_y}{\partial y} \end{bmatrix}. \qquad \textit{Eq. 7.22}$$

We take the definition used by Okubo (1970) for stretching deformation $\hat{\alpha}$, vorticity $\hat{\omega}$, and shear deformation $\hat{\sigma}$

$$\hat{\alpha} = \frac{\partial v_x}{\partial x} - \frac{\partial v_y}{\partial y}, \qquad \hat{\omega} = \frac{\partial v_y}{\partial x} - \frac{\partial v_x}{\partial y}, \qquad \hat{\sigma} = \frac{\partial v_y}{\partial x} + \frac{\partial v_x}{\partial x}. \qquad \textit{Eq. 7.23}$$

By substituting Eq. 7.23 into Eq. 7.22, and following de Barros et al. (2012), in which for a two-dimensional transport scenario $\frac{\partial v_x}{\partial x} = -\frac{\partial v_y}{\partial y}$, and therefore stretching deformation $\hat{\alpha} = 2\frac{\partial v_x}{\partial x}$, the deformation tensor can be then rewritten as

$$\epsilon = \frac{1}{2}\begin{pmatrix} \hat{\alpha} & \hat{\sigma} - \hat{\omega} \\ \hat{\sigma} + \hat{\omega} & -\hat{\alpha} \end{pmatrix}, \qquad \textit{Eq. 7.24}$$

and the Okubo-Weiss function ξ [1/T^2] is calculated by

$$\xi = (\hat{\alpha}^2 + \hat{\sigma}^2) - \hat{\omega}^2 \, . \qquad \textit{Eq. 7.25}$$

Positive Okubo-Weiss values, $\xi > 0$, correspond to regions where shear and stretching forces dominate, and are associated to mixing hotspots (Engdahl et al., 2014; Wright et al., 2017). On the other hand, negative values, $\xi < 0$, correspond to regions dominated by vorticity and local mixing potential is low.

7.2.5 Algorithm implementation

We use MODFLOW-2005 as groundwater flow equation solver, and the time-variant specified-head boundary package (i.e., CHD package) was used to set the Dirichlet boundaries (Harbaugh, 2005). The model was built using FloPy (Bakker et al., 2016) and the polynomial chaos expansion approach was implemented using the Chaospy library (Feinberg, 2019). The Okubo-Weiss calculations, random field generator, wave functions, postprocessing scripts, and the code for coupling the polynomial expansions and the MODFLOW-2005 model were written in Python 3. The scripts and results are available in the online repository of the research (Merchán-Rivera et al., 2022).

7.3 Results and discussion

7.3.1 Deterministic scenarios

Figure 7.2 shows the spatial effect of the waveform on the groundwater heads at specific time steps $\tau/T \in \{60{,}80{,}86{,}100\}$. Steeper hydraulic gradients are observed in the trapezoidal wave, which significantly impact the flow field magnitude. These gradients occur in the trapezoidal wave due to two reasons. First, this wave exposes longer intervals of constant head at the wave crest and wave through. Second, the trapezoidal wave presents a sharp fluctuation from minimum to maximum stage. Furthermore, the behavior of the sine scenario is very similar to the triangular one. As expected, the porous medium acts as a damper that gradually moderates the propagation of groundwater head signals, converting all of them to sinusoidal patterns after travelling a certain distance and later vanishing them (see Figure 7.3). The dampening depends on the value of the hydraulic conductivity in accordance with the analytical solution for the head response in the semi-infinite aquifer presented by Singh (2004) and Sawyer et al., (2009) for the case of a homogeneous porous medium.

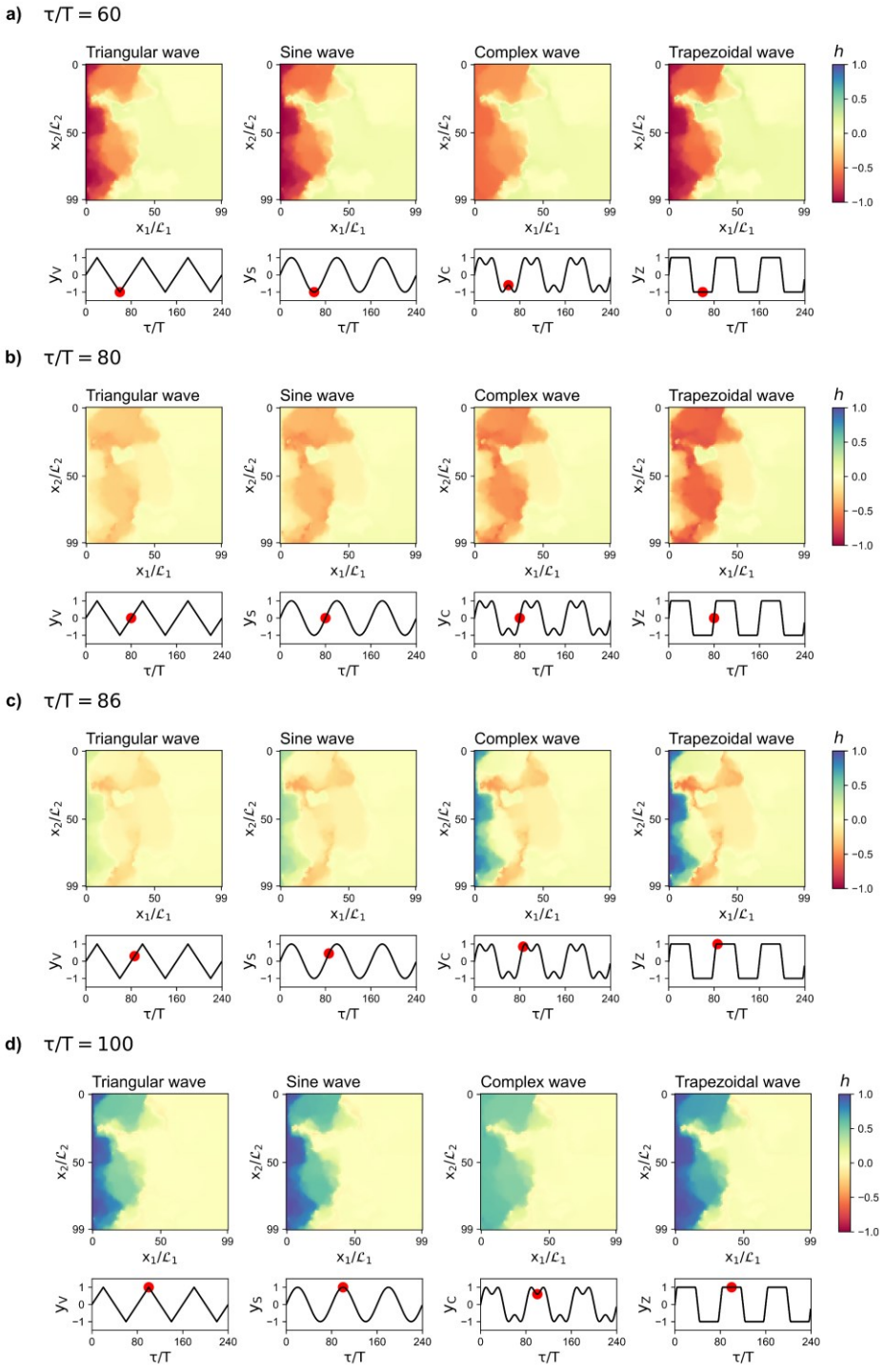

Figure 7.2. Groundwater head responses at different time steps: a) $\tau/T=60$, a) $\tau/T=80$, a) $\tau/T=86$, and d) $\tau/T=100$. The colored maps show the distribution of the groundwater heads, and the graph plot shows the imposed boundary conditions. The red dots show the time steps at which the snapshots were taken.

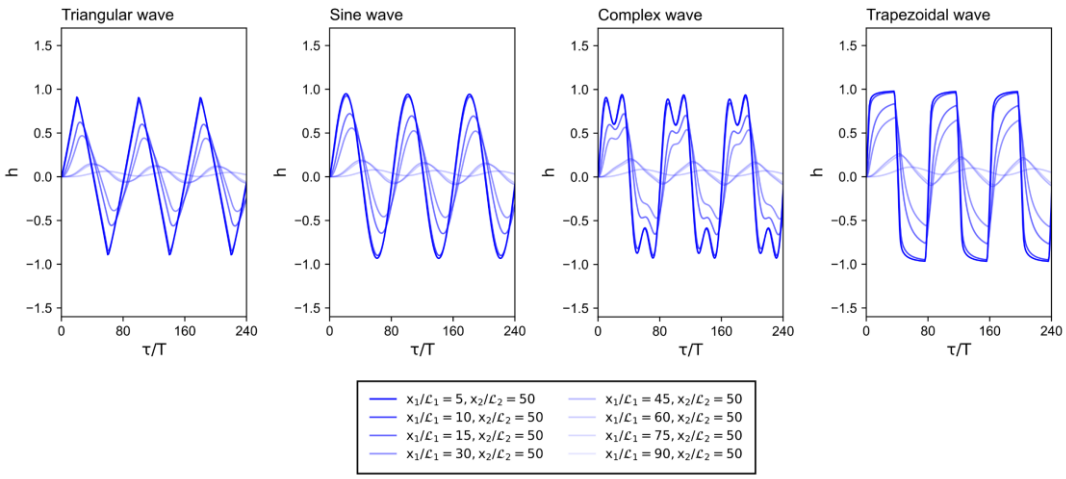

Figure 7.3. Dampening of the head signals from the different scenarios. The groundwater head values are extracted at various distances from the wave-shaped boundaries, $x_1/\mathcal{L}_1 \in \{5,10,15,30,45,60,75,90\}$*, at the middle of the domain* $x_2/\mathcal{L}_2 = 50$

The outcomes from the deterministic scenarios show some remarkable differences in the mean variance of the groundwater heads and the Okubo-Weiss. In Figure 7.4a, we observe a larger $\bar{\sigma}_h^2$ from the trapezoidal wave scenario, followed by the complex wave scenario, which is also very similar to the sine one. This occurs due to the flux variations and the groundwater gradient differences among the cases. We also observe that the behavior of the four scenarios is very similar after $x_1/\mathcal{L}_1 = 40$ and that $\bar{\sigma}_h^2 \to 0$ after $x_1/\mathcal{L}_1 = 60$. Figure 7.4b shows the mean variance in the results of the Okubo-Weiss metric. We see that ξ may vary by several orders of magnitude depending on the wave used as boundary condition. Similar to $\bar{\sigma}_h^2$, we see larger variations in $\bar{\sigma}_\xi^2$ in the trapezoidal and complex scenarios.

We show the spatial and temporal pattern of the Okubo-Weiss metric in Figure 7.5. We observe regions where the Okubo-Weiss metric is very high $\xi > 0.1e^{-6}$, when the flow is dominated by stretching and strain and very low $\xi < -0.1e^{-6}$, when vorticity dominates. These regions correspond to areas of high hydraulic conductivity and high conductivity contrasts (see Figure 7.1b), where also flow focusing may occur. Hence, the location of these spots is fully controlled by the configuration of heterogeneous field in all the scenarios. In temporal terms, the most remarkable discrepancies in ξ among the four scenarios occur during the sharp ramp upwards and the sharp drop of the trapezoidal wave. In a lower magnitude, this is also visible in the complex wave. Highest positive and lower negative values of ξ are found in these two scenarios. Furthermore, it is possible to observe cells changing from positive ξ to negative ξ, and vice versa, in all the scenarios. This can be observed before and

after the apexes of the trapezoidal wave (Figure 7.5b and Figure 7.5c), the peak of the triangular wave (Figure 7.5c and Figure 7.5d), the local maximum and local minimum of the complex wave (Figure 7.5b and Figure 7.5c). This swap of dominance is transitory and can be repeatedly observed in all the scenarios at critical points of the wave-shaped boundaries, such as stationarity points (i.e., constant value), inflection points, local maxima, and local minima. This could occur due to flow reversal caused by the deacceleration of the transient boundary signal into the aquifer. Overall, this behavior gives evidence of the waveform's role in the temporal dynamics of the topology of the flow field.

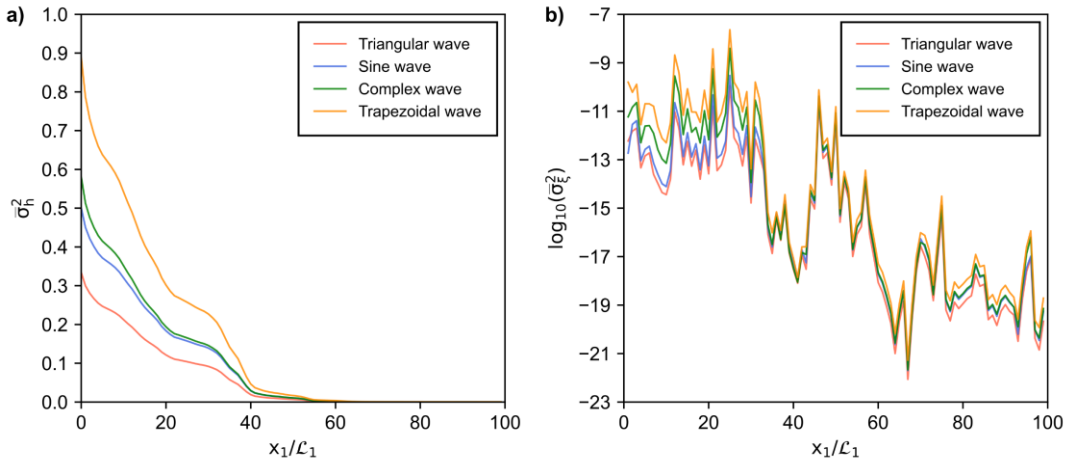

Figure 7.4. Spread of deterministic results at different distances $x_1/\mathcal{L}_1$ from the boundary conditions: a) mean variance of the groundwater heads $\bar{\sigma}_h^2$, and b) logarithm of the mean variance of the Okubo-Weiss $\bar{\sigma}_\xi^2$

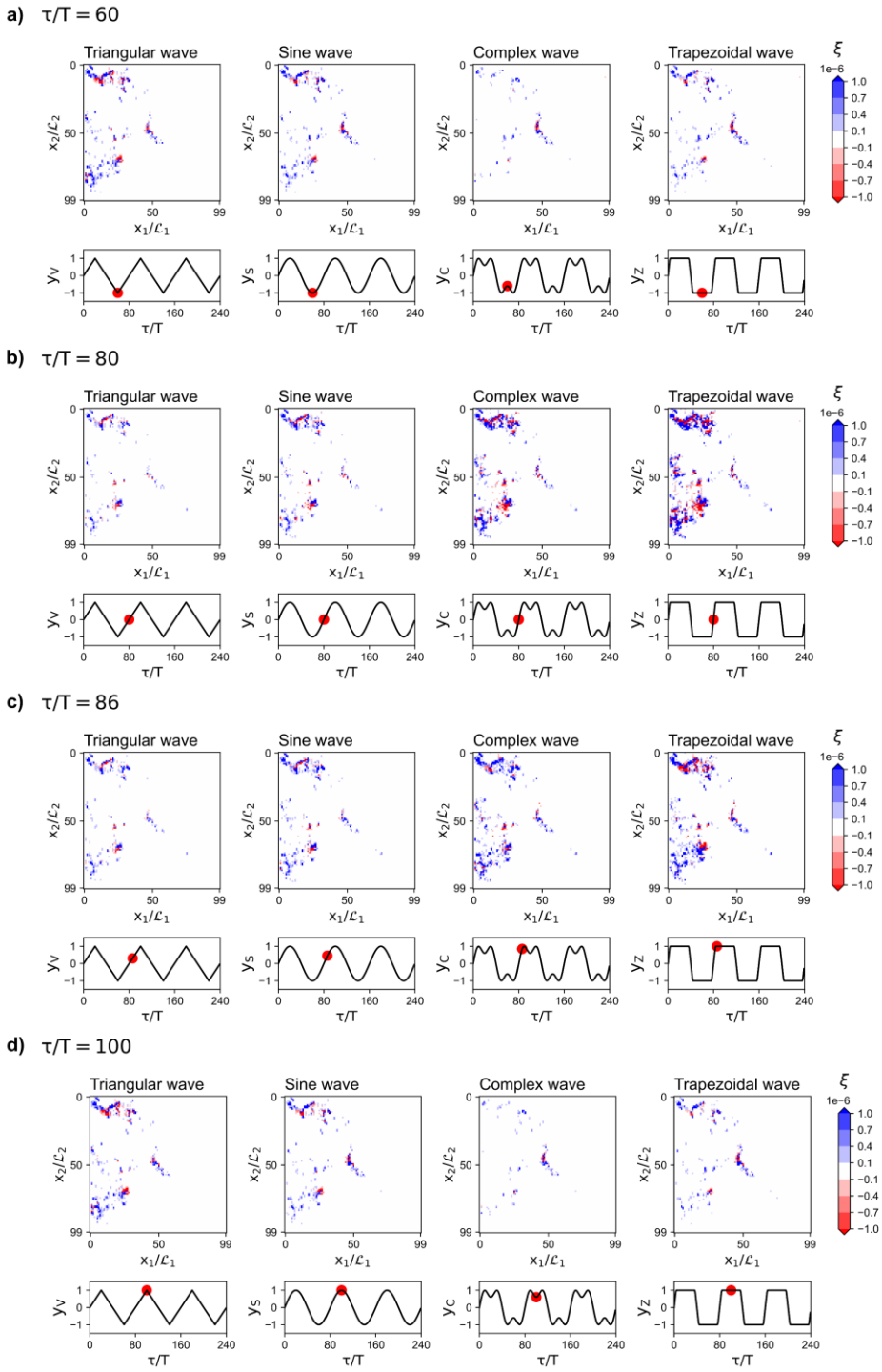

Figure 7.5. Okubo-Weiss values at different time steps: a) $\tau/T = 60$, b) $\tau/T = 80$, c) $\tau/T = 86$, and d) $\tau/T = 100$. The colored maps show the distribution of the groundwater heads, and the graph plot shows the imposed boundary conditions. The red dots show the time steps at which the snapshots were taken.

7.3.2 Stochastic scenarios

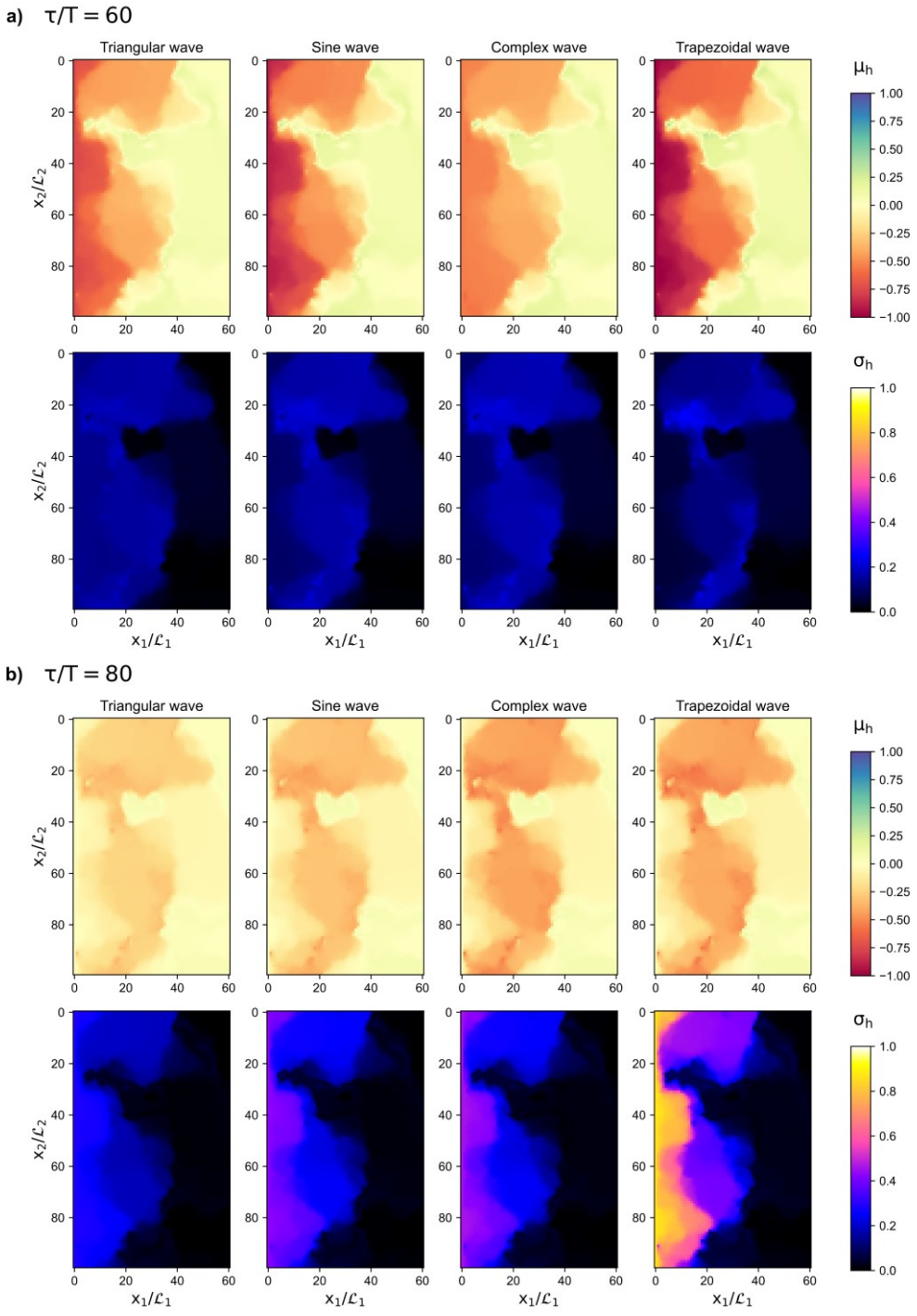

Figure 7.6. Propagation of the uncertainty into the groundwater head responses represented by the expected value μ_h and the standard deviation σ_h into the groundwater head responses at a) $\tau/T = 60$, and b) $\tau/T = 80$

The uncertainty in the amplitude and phase of the waves propagates in the groundwater head following different patterns (see Figure 7.6). The results of μ_h are similar to the results of h in the deterministic scenarios. Regarding the standard deviation, in Figure 7.6a, we see at $\tau/T = 60$ that all scenarios present similar snapshots, with slightly higher σ_h close to the left boundary for the triangular wave. In contrast, in Figure 7.6b, a significant difference in σ_h can be observed at $\tau/T = 80$ in the complex and trapezoidal wave as compared to the triangular and sine waves. This time step corresponds to the change between low and high river stage.

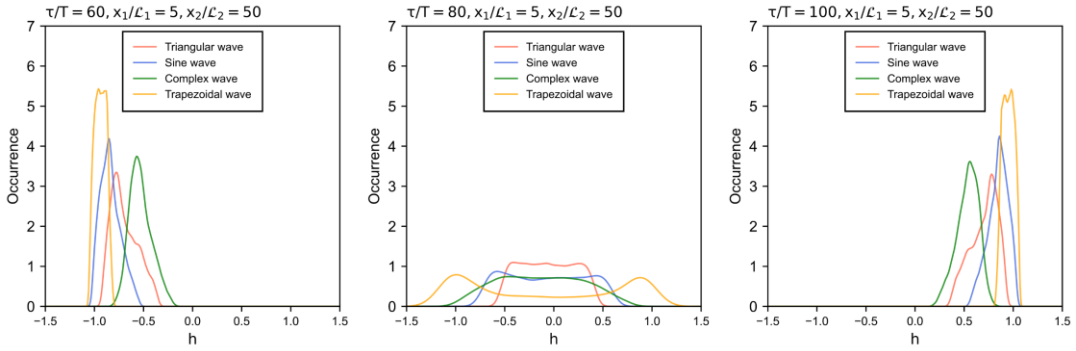

Figure 7.7. Posterior probability density functions of the groundwater heads at $\tau/T \in \{60,80,100\}$ at specific location $x_1/\mathcal{L}_1 = 5$ and $x_2/\mathcal{L}_2 = 50$

We also computed the probability density functions from the output expansions of the groundwater heads. The results are shown in Figure 7.7. We observe small uncertainties at high and low values of the groundwater heads, which are depicted by the high occurrence values in the probability density functions, when $\tau/T = 60$ and $\tau/T = 100$ (see Figure 7.7a and Figure 7.7c). Larger uncertainties are observed when $\mu_h \approx 0$, when $\tau/T = 80$ (see Figure 7.7b). These behaviors occur in all the scenarios. However, two peaks of high probability are observed in Figure 7.7b in the trapezoidal scenario due to the rapid fluctuation of the heads in the transient boundary conditions. The trapezoidal scenario also shows the smallest uncertainty at $\tau/T = 60$ and $\tau/T = 100$, because of the low influence of the phase uncertainty in the points where the heads in the boundaries are constant (i.e, minimum and maximum).

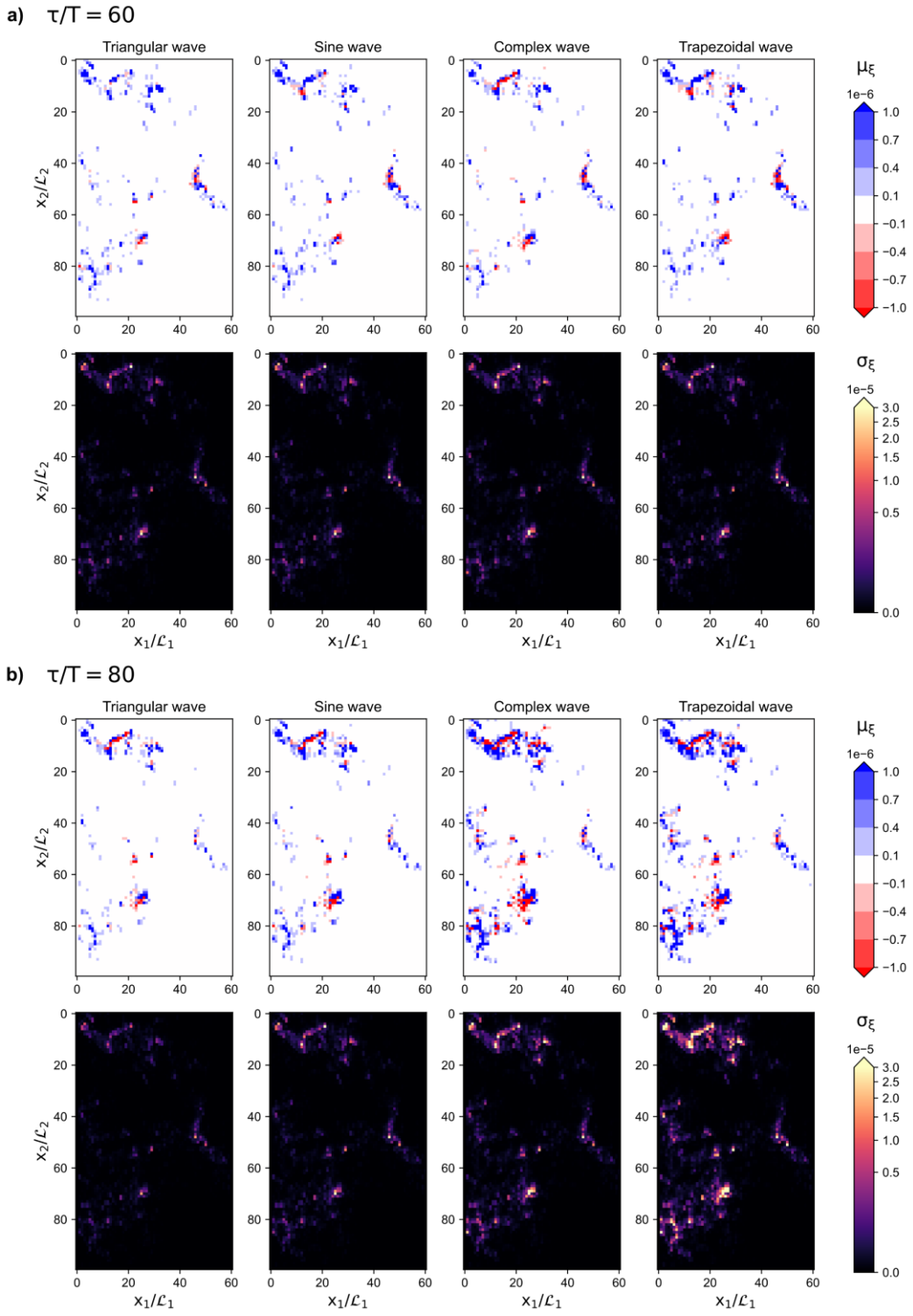

Figure 7.8. Propagation of the uncertainty into the Okubo-Weiss metric represented by the expected value μ_h and the standard deviation σ_h into the groundwater head responses at different times.

The influence of the uncertain transient boundary conditions is also reflected in the Okubo-Weiss values shown in Figure 7.8. As expected, the spots with large uncertainty appear in the regions with high hydraulic conductivity contrast and large hydraulic conductivity. Specifically, we allocate large uncertainties in the complex and trapezoidal scenarios at $\tau/T = 80$ (Figure 7.8b). This is a consequence of the large uncertainty in the groundwater heads observed previously (Figure 7.6b), which occur due to the effect of the phase shift over the sharp movements in the boundary conditions. The steepness of the slopes in these waves creates a wide range of variability when we introduced the offset uncertainty. Moreover, the magnitude of the μ_ξ values vary depending on the scenario, finding larger values in the trapezoidal and complex scenarios. Similar to the outcomes of the deterministic scenarios, the results of μ_ξ also reveal spots with variable dominances of the deformation and rotational forces of the flow field.

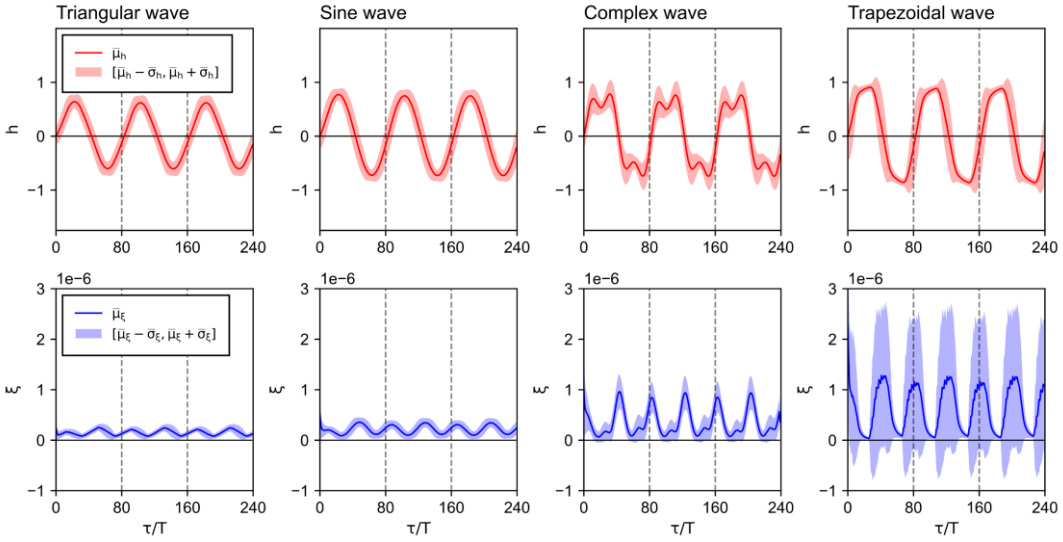

Figure 7.9. Uncertainty propagation into the groundwater heads and the Okubo-Weiss metric at a distance $\lambda/2$ from the boundary conditions ($x_1/\mathcal{L}_1 = 5$): a) mean expected value of the groundwater heads and interval $[\bar{\mu}_h - \bar{\sigma}_h, \bar{\mu}_h + \bar{\sigma}_h]$, and b) mean expected value of the Okubo-Weiss metric and interval $[\bar{\mu}_\xi - \bar{\sigma}_\xi, \bar{\mu}_\xi + \bar{\sigma}_\xi]$.

The responses of both h and ξ, as well as the statistics that define their uncertainty, follow periodic patterns. To evaluate the average behavior of the statistics of h and ξ at a certain distance from the boundaries and their differences, we chose a relatively close distance to the

stream, at distance $\lambda/2$ (i.e., $x_1/\mathcal{L}_1 = 5$), where the propagation of the signal is clear. We computed the arithmetic means of the uncertainty statistics at a distance $x_1/\mathcal{L}_1 = 5$, which are shown in Figure 7.9. We see that $\bar{\mu}_h$ is highly fluctuating in the trapezoidal and the complex scenario. Moreover, according to the interval $[\bar{\mu}_\xi - \bar{\sigma}_\xi, \bar{\mu}_\xi + \bar{\sigma}_\xi]$, the trapezoidal scenario exhibits the highest uncertainty in ξ, followed by the complex wave. The results also indicate that it is more likely to find rotation properties dominating in the flow field under the trapezoidal scenario conditions than to find them under the conditions of the other scenarios. On the other hand, we see smaller variability of $\bar{\sigma}_h$ and $\bar{\sigma}_\xi$ in the sine wave scenario, showing a similar spread in the outputs along the whole simulation period. While the behavior of the triangular wave is similar to the sine wave, the complex wave is comparable with the trapezoidal wave.

Overall, our results from the deterministic and stochastic scenarios show that wave-shaped boundary conditions can influence not only the magnitude of the deformation and rotational forces of the flow field (i.e., shear, stretching, and vorticity) but also the temporal dynamics of dominance between local strain and rotation properties. Although our results show that their location is determined by the areas with high hydraulic conductivity contrast, as can be seen in Figure 7.1b, we provide evidence that the mixing potential in these areas is significantly affected by highly transient boundary conditions. This occurs due to the variety of hydraulic gradient responses as a consequence of the highly fluctuating head boundary conditions. To observe in detail the temporal variation and the two-dimensional distribution of the groundwater heads, the Okubo-Weiss values, and the statistical moments that describe the uncertainty, we refer to a series of videos included as part of the Supplementary Material of this research.

7.4 Conclusions

We studied the effect of the periodic stage conditions due to hydropeaking events on the groundwater flow topology in terms of the Okubo-Weiss metric. We imposed Dirichlet boundary conditions in the form of wave-shaped specified-heads with four types of waveforms: triangular, sine, complex, and trapezoidal. The formulation of the system considers a deterministic solution of the heterogeneous hydraulic conductivity field for all the scenarios. The first part of our analysis was done assuming no input uncertainty over the four waves that define the transient boundary conditions. The second part of the study approached the problem as a stochastic system with uncertainty in the parameterization of the transient boundary conditions. Here, the wave amplitude and phase were considered uncertain and treated as mutually independent random variables. These variables introduced the uncertainty

related to unknown fluctuations in the discharge volume and discharge duration and temporal uncertainty due to energy market demands and powerplant management. The application of polynomial expansions and pseudo-spectral collocation method allowed us to estimate the statistical moments (i.e., mean, and standard deviation) of the outputs of interest (i.e., groundwater heads and Okubo-Weiss metric). The method was convenient to extract the required spatial and temporal detail with low computational effort.

One of the main messages that the Okubo-Weiss metric can provide us is the identification of reaction hotspots. The spatial distribution of the Okubo-Weiss responses is fundamentally controlled by the hydraulic conductivity. In accordance, our results show that their location is determined by the areas with high hydraulic conductivity contrast. However, we also provide evidence that the mixing potential in these areas is significantly affected by the highly transient boundary conditions. The magnitude and temporal behavior of this topological indicator of mixing significantly vary according to the impose boundary conditions. Different highly transient boundary conditions influenced in different degree the temporal dynamics of dominance between local strain and rotation properties and the magnitude of the deformation and rotational forces of the flow field. Therefore, given the dynamic responses of the flow field to the time-variant head boundary conditions, the detailed temporal characterization of this metric is important to reliably predict, for instance, mixing-driven reactions.

The evaluation of hydropeaking impacts on subsurface flow requires to characterize the management of the surface water system and the intensity of the impact (e.g., shape, amplitude, and periodicity of the wave). Hence, we think it is essential to estimate hydropeaking effects on flow and transport processes in aquifers using a stochastic approach, not only due to the essential uncertainty in the aquifer heterogeneity but also due to the uncertain stream stages. The statistical moments that describe the propagation of the uncertainty show a periodic behavior and a varying degree of uncertainty depending on the applied wave-shaped boundary. Further work should focus on the characterization of real hydropeaking events to explicitly acknowledge the inherit uncertainty of these systems and its effect in the estimation of topological descriptors.

8 Conclusions

This dissertation addressed the interaction between rivers and aquifers during extreme events. The main objective was to characterize flow and transport processes in the groundwater under the effect of the uncertain river boundary conditions that arise during extreme events. The analyzed river-aquifer interactions involved morphological, climatic, and anthropogenic approximations that describe the events of groundwater flooding and hydropeaking. These extreme events were selected due to the highly fluctuating river stages and the associated uncertainty in the water level and the riverbed properties. Overall, this dissertation covered comprehensively the following areas:

- The quantification of uncertainty employing deterministic scenario modeling and formal stochastic approaches, specifically Bayesian inference and spectral expansions;
- The spatial and temporal responses of the groundwater flow and the flow field to the dynamics of the river boundary conditions and the description of the spatiotemporal evolution of the uncertainty; and,
- The characterization of flow and transport processes in the subsurface in probabilistic terms by creating stochastic frameworks for the identification of non-trivial flow features and the description of mixing predictors.

For clarity, Table 8.1 includes a summary of the answers to the research questions defined in this dissertation. In addition, the specific conclusive remarks are articulated in the following sections. Deeper explanations of the responses and findings related to Q1 are presented in Section 8.1, while those related to Q2 and Q3 are developed together in Section 8.2.

Table 8.1. Summary of answers to the research questions

Research Question		Answer
Q1.	What is the role of highly transient river boundary conditions during extreme events, such as groundwater flooding and hydropeaking, on the responses of the flow and transport processes in the subsurface?	• Changes between low and high river stages modifies the dynamics of the groundwater introducing variations in the hydraulic gradients and the exchange flux between the rivers and the aquifer. • Responses in the flow field can significantly vary depending on the evolution of the wave that represents the river boundary conditions, particularly in the regions close to the streams. A detailed temporal and spatial characterization of the metrics that described the flow field is hence important to reliably predict mixing-driven reactions. • Fluctuations in the river stage substantially influenced the dynamics of the flow field, including the magnitude and direction of the flow, the dominance between local strain and rotation properties and the magnitude of the deformation and rotational forces.
Q2.	How can uncertainties during extreme events, such as groundwater flooding and hydropeaking, propagate and affect the flow and transport processes in the subsurface?	• Uncertainty in the river boundary conditions affects the water flux and the flow paths in the stream-aquifer system. The propagation is relative to the spatial location, the temporal evolution of the wave and the hydrogeological conditions. The shape, peak amplitude, and periodicity of the river stage during the extreme events affect the propagation of the uncertainty due to the fluctuations on the hydraulic gradients. • The propagation of uncertainty significantly varies in space and time, which is reflected in the understanding and predictability of the groundwater flow, the transport of solutes and the description of mixing processes. The quantification of the flow field magnitude and direction may be affected in various orders of magnitude and several degrees, respectively, with a consequently major impact in the description of transport processes and mixing conditions in the subsurface at the meter-scale. • Due to the large propagation of uncertainty, the description of river-aquifer systems and the responses of the flow field demands the application of formal stochastic methods not only for improving the model reliability but also for assessing risk accurately.
Q3.	How can stochastic approaches be used to identify the spatial distribution and temporal variability of relevant flow conditions in the subsurface?	• Stochastic frameworks can assess the flow field characteristics for the identification of non-trivial flow features (i.e., stagnation zones and reverse flow) and the description of topological metrics (i.e., Okubo-Weiss) in probabilistic terms. Model outputs can be represented in terms of probabilities to identify subsurface flow features that can would be unfeasible to recognize from a pure deterministic approach. • The definitions of the susceptible zones and the evolution in spatial and temporal terms can be easily constructed from a probabilistic perspective, and the accuracy of the simulations can be updated with new evidence data. • Polynomial chaos expansions techniques are efficient methods to quantify uncertainty due to river boundary conditions, particularly in pre-existing models, where the dimensionality of the models can be enclosed to the river description.

8.1 Spatiotemporal responses due to river-aquifer dynamics

Along all the components of this dissertation, we have seen the importance of evaluating the extreme events at the different temporal phases that characterize them. The changes between low and high river stages modifies the dynamics of the groundwater introducing variations in the hydraulic gradients and the exchange flux between the river and the aquifer. Therefore, a single temporal snapshot can be fairly imprecise for a general diagnosis of the groundwater flow and flow field responses. Likewise, the results of this dissertation strengthen the idea that the description of the flow field requires to consider the spatial characteristics of the area of study. The influence of transient boundary conditions in the aquifer also depends on the specific geological and hydrological settings of the case study, doing the mapping of the spatial distribution of the inputs and the responses a valuable subject when complex hydrodynamic features, such as various surface streams, are involved. In these regards, these works provided a deeper insight to characterize the flow and transport processes in the subsurface because all of them considered these temporal and spatial complexity.

For analyzing the groundwater flooding event, it was convenient to separate the different phases of the flood events in order to recognize the temporal effect of the river-aquifer interactions. Four specific time steps were used to represent the model responses before the event, at the peak-flow, at the recession phase, and after the flood event. The surface streams are hydraulically connected to the aquifer and infiltration occurs from precipitation ad river leakage. As consequence, different groundwater head gradients and different river discharges into the saturated zone were observed. All the modeling exercises described in Chapter 4, 5, and 6 gave evidence of the temporal influence of the input variables (i.e., river stage and riverbed conductance) that describe the river boundary conditions on the groundwater responses. Indeed, the flow responses in the proximities of the streams are driven by the river boundary conditions. The hydraulic conductivity plays a fundamental role by itself as well as a factor of interaction with other model variables. In the particular case of the valley of the Alz River, due to the high hydraulic conductivity of the alluvial plain (formed by gravels and sands), the groundwater heads near to the river and the canal showed rapid responses and similar fluctuation patterns to the stream stages. To what concerns the risk assessment of groundwater flooding event, heavy rainfall precipitation may trigger the affections from groundwater flooding, but they can occur due to the accumulation of water in the aquifer for long periods.

For the study of hydropeaking, it was required to use a high temporal resolution to understand the dynamic effect of the river boundary conditions. Thanks to this temporal discretization, the variations and progression of the hydraulic heads from the different wave-shaped boundaries were clearly distinguished. In addition, the high temporal resolution support to avoid numerical and convergence errors. In Chapter 7, we observe that the characterization of hydropeaking impacts on the groundwater flow implies the management of the energy infrastructure and the market demand. Due to the steepness of the hydraulic gradients and the exposure to different intervals of constant heads at the wave crest and wave through, the responses in the aquifer can dramatically vary depending on the wave-shaped boundary conditions. The Okubo-Weiss responses are primarily controlled by the hydraulic conductivity and the model outcomes are sensitive to the field, analogous to what is observed in the evaluation of the groundwater flooding case. However, the evidence observed in Chapter 7 suggests that mixing potential is also significantly affected by the highly transient boundary conditions. The study showed that the magnitude and temporal behavior of this topological indicator of mixing significantly vary according to the boundary condition that represent the river. The fluctuation in the river stage substantially influenced the dynamics of dominance between local strain and rotation properties and the magnitude of the deformation and rotational forces of the flow field.

8.2 The role of uncertainty

The driving premise undergirding this dissertation is truly straightforward: river boundary conditions contain uncertainties because they attempt to capture the complexity river-aquifer interactions and these uncertainties can be particularly significant due to disruptive and/or unexpected conditions during events of groundwater flooding and hydropeaking. Hence, the uncertainty in the river-aquifer continuum is primarily introduced in the predictive modeling process because the numerical representation of the rivers under extreme conditions contains largely unknown parameters and imprecise approximations of the physical processes underlying the aforementioned events. Although the aftermath of groundwater flooding may not be as hazardous as fluvial or pluvial floods, the events are harmful and the occurrence is unanticipated. Hydropeaking events may have a tendency to recur at certain interval, and they can indeed be described in terms of their periodicity. However, these events are disruptive because they break the usual behavior of the hydrological system and the significance in the aquifer responses is hard to anticipate. In addition, the magnitude of the impact is largely unknown, particularly when deviations from the average tendency occur due to the dependency on energy market factors.

Initial and boundary conditions are meant to obtain a unique solution to the differential equations that govern the groundwater flow. The application of basic uncertainty analysis techniques then suggests to combine the relevant parameters using the minimum and maximum expectation values or the best- and worst-case states to catch the uncertainty of extreme events. The theory behind them is relatively simple and their implementation is extremely cheap with regard to computational demand. Unfortunately, they neglect the existence of equifinal models and assume absolute confidence in the base model. This approach can still be valuable under simple circumstances with relatively stable systems with not highly fluctuating boundary conditions. However, it may be reckless to describe extreme events with explicit deterministic valuations because, by definition, extreme events are disruptive or unexpected. In the deterministic scenarios in Chapter 4, we observed that the variation in the stage and riverbed conductance can highly affect the transport of the solute. The influence of the temporality flood wave propagation within the aquifer is particularly perceptible in the advective-dispersive transport when we observe the different timing in the changes in concentration. Chapter 4 was a first approximation to the understanding of the temporal and spatial effects of the uncertain river boundary conditions, as seen in the outcomes of the breakthrough curve of the solute concentration. This study was an initial interpretation of the system and showed that the event in the valley of the Alz River was a suitable groundwater flooding case for the further experimentation, later done in the research presented in Chapter 5 and Chapter 6.

8.2.1 Embracing the unknown

The most noteworthy contributions of this dissertation indeed derive from the application of probabilistic techniques and the creation of various products built over the representation of the problems as stochastic systems. These contributions include:

1) The formal quantification of spatiotemporal propagation of uncertainty in the flow field components and flow topological descriptors during the selected extreme events (Chapter 6 and 7);
2) The application of a Bayesian framework for assessing risk of groundwater flooding (Chapter 5); and,
3) The definition of a stochastic framework for identifying elusive and non-trivial flow features and mixing descriptors (Chapter 6 and 7).

The findings of this dissertation provide spatially and temporally distributed probabilistic information from groundwater models. In this line, the results characterize the uncertainty in hydrogeological systems affected by extreme events with a high level of temporal and spatial detail. Overall, the results of the dissertation show that the propagation of uncertainty also vary in space and time, which is reflected in the understanding and predictability of the

groundwater flow and the transport of solutes. The temporal and spatial dependencies of the uncertainty are reflected in the functional relations of model inputs (Chapter 5), in the temporal and spatial uncertainties in the groundwater flow (Chapter 5 and 6), in the flow field magnitude and direction (Chapter 6), in the appearance of stagnation points and reverse flow (Chapter 6), and in the responses of the Okubo-Weiss metric (Chapter 7). Then, a general remark of these studies is that the explicit quantification of uncertainty in river-aquifer systems should embrace the temporal and spatial detail for understanding the transport and fate of solutes. This remark is important given that some properties of the input variables that define the boundaries of the modeled system are going to be unavoidably unknown and there is a strict spatiotemporal dependency in the aquifer responses.

A broader image of the parameter uncertainty is captured in Chapter 5, where the quantification of uncertainty involves not only the river boundary conditions but also hydraulic parameters such as hydraulic conductivity, specific yield, specific storage, and recharge into the saturated zone. In this study, the sensitivity in the input variables and the parameters also presents temporal variations. This means that the allocation of uncertainties in the output of the models vary depending on the evaluation time steps. The omission of the temporality of the fluctuating events will reveal an incomplete image of the reality and affect the understanding of the system's dynamics. This study also identified that the non-linearity, non-monotonicity, and interactions between model parameters vary depending on the phase of the groundwater flood event. It was observed that the functional relationships between the inputs and outputs tend to high non-linearity, high non-monotonicity, and larger interactions during the peak-flow and the recession phase while these relationships decrease before and after the event. One of the advantages of addressing the problem from the notion of stochasticity is found in this study. The susceptibility to groundwater flooding is explained and communicated with probability maps. Such strategy gives not only a clear impression of the model reliability but also improves the accuracy of the message that is communicated to part-takers. Due to the nature of groundwater flooding, the presented Bayesian framework seem to be a viable method to assess exposure over one single event models and to efficiently create imagery products of flood risk.

The quantification of uncertainty is used to represent the model outputs in terms of probabilities, which supports the identification subsurface flow features that can be unfeasible to recognize from a pure deterministic perspective. This is clearly observed in Chapter 6. In a dynamic system, points where the velocity is equal to zero are likely to occur, but extremely complicated to identify by specific realizations of numerical models. In this work, the identification of stagnation points is actually possible because the method is constructed over the probability of occurrence. Here, the maps of probability are created with the statistical moments of the flow field magnitude, which are obtained from the quantification of uncertainty with polynomial expansions. Similarly, in Chapter 7, we observe that the

dynamics of dominance between local strain and rotation properties can be identified by mapping the statistical moments of the outputs that define the flow field. This supportive probabilistic approach is important because the uncertainty that propagates from hydropeaking waves, which depend on operation and management of hydropower plants, can largely vary from one wave shape to another.

8.3 Recommendations and outlook

It is worth noting that the quantification of uncertainties is more challenging in coupled system, such as river-aquifer models and transport simulations, in comparison to single system solvers. This occurs due to the multiple interacting phenomena and the multiple scale representations required to assemble different systems. In practice, the challenge is reflected in the propagation of uncertainty through several linked simulations. A series of simulation codes must be coupled to connect the hydrological models with the mathematical tools that are required to quantify the uncertainty. Although this creates a multi-compound system, there is no need of any edition of the internal workings of the elementary hydrological solvers. Furthermore, the success of the techniques applied in Chapter 5, 6, and 7 will also depend on the proper prior representation of the probability density function. Any interpretation of the resulting posterior probabilities of the models should be attached to the understanding initial parameterization of the uncertainties. Furthermore, parameters can be correlated or not follow a Gaussian or uniform distribution. This can be a major issue in applying the methods because the efficiency can be compromised by the construction of the joint probability distribution. However, it is reasonable to assume that the river stage and the hydraulic conductivity of the riverbed material are mutually independent parameters, which makes possible the direct application of the marginal distributions for sampling methods or spectral expansions. Similarly, the wave amplitude and phase that describe the dynamics of the water level in hydropeaking events can be treated as mutually independent random variables. This is an important reflection of this work because it may motivate and ease the application of these techniques in similar models where uncertain river boundary conditions play a major.

Additional applications of polynomial chaos expansions can be developed for the hydrological modeling of real case scenarios. Although, spectral techniques are an attractive option for quantifying uncertainty, the literature review of this dissertation revealed that most of the implementations of spectral expansions had been done in simplified analytical problems. New applications will spread the knowledge to the hydrological community and facilitate the process of learning. Furthermore, a similar exercise with polynomial chaos expansions can be applied to study the boundary conditions for the solution of the advection-dispersion-reaction equation for the solute transport. Stochastic methods have been largely

used for the understanding of solute transport. Naturally, they mainly focus on the variation of the hydraulic conductivity values due to their significant influence on the solute spreading. However, similar to the groundwater flow, mass transport requires fixed concentration, fixed gradient, or variable flux boundary conditions, which may be considerably uncertain and can be analyzed by spectral expansions with a relatively low number of model realizations. The latter is one of the most attractive potentials of spectral applications because transport model simulations regularly require a long time.

The application of formal stochastic methods can be extended to understand groundwater flooding and hydropeaking. The susceptibility to inundation due to the rising of the groundwater table can be identified in other regions affected by these events. Studies with this purpose can be valuable and suitable for other regions that have been affected by groundwater flooding in the past. With these applications, the use of single-event groundwater models with large temporal scales and high spatial resolution can be validated to detect exposure to groundwater. Uncertainty quantification in real hydropeaking cases is still an open matter. Probability density functions related to the periodic behavior of these events can be derived from field data to construct the basis for quantifying uncertainties. The explicit computation of the uncertainty of the hydrological systems affected by hydropeaking can also be used to estimate and understand topological descriptors beyond the Okubo-Weiss metric.

Finally, several issues remain open for study concerning the representation of the river boundary conditions in numerical models. The representation of the spatial extent and river geometry, which is often represented within the limits of modeling grids, often requires details at the meter-scale. Additionally, the conceptual representations of the rivers often neglect the complexity of the river geometry and the effect of lateral fluxes. Systematic errors in the estimation of exchange fluxes can emerge due to these inadequate representations, introducing uncertainties in the simulation of solute fate and transport. Then, research addressing the epistemic uncertainty in the river geometry representation can be characterized and quantified to understand its impact on solute transport and mixing processes in the subsurface.

9 References

Abboud, J.M., Ryan, M.C., Osborn, G.D., 2018. Groundwater flooding in a river-connected alluvial aquifer. J Flood Risk Management 11, e12334. https://doi.org/10.1111/jfr3.12334

Allocca, V., Di Napoli, M., Coda, S., Carotenuto, F., Calcaterra, D., Di Martire, D., De Vita, P., 2021. A novel methodology for Groundwater Flooding Susceptibility assessment through Machine Learning techniques in a mixed-land use aquifer. Science of The Total Environment 790, 148067. https://doi.org/10.1016/j.scitotenv.2021.148067

Anderson, M.P., Munter, J.A., 1981. Seasonal reversals of groundwater flow around lakes and the relevance to stagnation points and lake budgets. Water Resour. Res. 17, 1139–1150. https://doi.org/10.1029/WR017i004p01139

Anderson, M.P., Woessner, W.W., Hunt, R.J., 2015. Applied groundwater modeling: simulation of flow and advective transport, Second edition. ed. Academic Press, London; San Diego, CA.

Andrade, L., O'Dwyer, J., O'Neill, E., Hynds, P., 2018. Surface water flooding, groundwater contamination, and enteric disease in developed countries: A scoping review of connections and consequences. Environmental Pollution 236, 540–549. https://doi.org/10.1016/j.envpol.2018.01.104

Aquanty Inc., 2015. HGS Theory Manual, HydroGeoSphere (HGS) version 2301. Waterloo, Ontario.

Arrigoni, A.S., Poole, G.C., Mertes, L.A.K., O'Daniel, S.J., Woessner, W.W., Thomas, S.A., 2008. Buffered, lagged, or cooled? Disentangling hyporheic influences on temperature cycles in stream channels. Water Resour. Res. 44. https://doi.org/10.1029/2007WR006480

Ascott, M.J., Marchant, B.P., Macdonald, D., McKenzie, A.A., Bloomfield, J.P., 2017. Improved understanding of spatio-temporal controls on regional scale groundwater flooding using hydrograph analysis and impulse response functions. Hydrological Processes 31, 4586–4599. https://doi.org/10.1002/hyp.11380

Bachmat, Y., Robert S. Kerr Environmental Research Laboratory, Holcomb Research Institute, 1978. Utilization of Numerical Groundwater Models for Water Resource Management, EPA 600/8. Environmental Protection Agency, Office of Research and Development, Robert S. Kerr Environmental Research Laboratory.

Baioni, E., Mousavi Nezhad, M., Porta, G.M., Guadagnini, A., 2021. Modeling solute transport and mixing in heterogeneous porous media under turbulent flow conditions. Physics of Fluids 33, 106604. https://doi.org/10.1063/5.0065734

Bakker, M., Post, V., Langevin, C.D., Hughes, J.D., White, J.T., Starn, J.J., Fienen, M.N., 2016. Scripting MODFLOW Model Development Using Python and FloPy. Groundwater 54, 733–739. https://doi.org/10.1111/gwat.12413

Barker, K., Haimes, Y.Y., 2009. Assessing uncertainty in extreme events: Applications to risk-based decision making in interdependent infrastructure sectors. Reliability Engineering & System Safety 94, 819–829. https://doi.org/10.1016/j.ress.2008.09.008

Bayerisches Landesamt für Umwelt, 2020. Haupttabelle für Grundwasserstände.

Bayerisches Landesamt für Umwelt, 2017. UmweltAtlas Bayern.

Bear, J., 2012. Hydraulics of Groundwater. Dover Publications.

Bear, J., 1979. Hydraulics of groundwater, McGraw-Hill series in water resources and environmental engineering. McGraw-Hill International Book Co, London ; New York.

Bear, J., 1972. Dynamics of fluids in porous media, Environmental science series (New York, 1972-). American Elsevier Pub. Co, New York.

Bear, J.J., Cheng, H.-D.A., 2010. Modeling Under Uncertainty, in: Modeling Groundwater Flow and Contaminant Transport. Springer Netherlands, Dordrecht, pp. 637–693. https://doi.org/10.1007/978-1-4020-6682-5_10

Bedekar, V., Morway, E.D., Langevin, C.D., Tonkin, M.J., 2016. MT3D-USGS version 1: A U.S. Geological Survey release of MT3DMS updated with new and expanded transport capabilities for use with MODFLOW (USGS Numbered Series No. 6-A53), MT3D-USGS version 1: A U.S. Geological Survey release of MT3DMS updated with new and expanded transport capabilities for use with MODFLOW, Techniques and Methods. U.S. Geological Survey, Reston, VA. https://doi.org/10.3133/tm6A53

Bernard-Jannin, L., Brito, D., Sun, X., Jauch, E., Neves, R., Sauvage, S., Sánchez-Pérez, J.-M., 2016. Spatially distributed modelling of surface water-groundwater exchanges during overbank flood events – a case study at the Garonne River. Advances in Water Resources 94, 146–159. https://doi.org/10.1016/j.advwatres.2016.05.008

Beven, K., 2016. Facets of uncertainty: epistemic uncertainty, non-stationarity, likelihood, hypothesis testing, and communication. Hydrological Sciences Journal 61, 1652–1665. https://doi.org/10.1080/02626667.2015.1031761

Beven, K., Binley, A., 1992. The future of distributed models: Model calibration and uncertainty prediction. Hydrol. Process. 6, 279–298. https://doi.org/10.1002/hyp.3360060305

Beven, K., Freer, J., 2001. Equifinality, data assimilation, and uncertainty estimation in mechanistic modelling of complex environmental systems using the GLUE methodology. Journal of Hydrology 249, 11–29. https://doi.org/10.1016/S0022-1694(01)00421-8

Bhaskar, A.S., Harvey, J.W., Henry, E.J., 2012. Resolving hyporheic and groundwater components of streambed water flux using heat as a tracer. Water Resour. Res. 48. https://doi.org/10.1029/2011WR011784

Bhola, P.K., Leandro, J., Disse, M., 2020. Building hazard maps with differentiated risk perception for flood impact assessment. Nat. Hazards Earth Syst. Sci. 20, 2647–2663. https://doi.org/10.5194/nhess-20-2647-2020

Bittner, D., Engel, M., Wohlmuth, B., Labat, D., Chiogna, G., 2021. Temporal Scale-Dependent Sensitivity Analysis for Hydrological Model Parameters Using the Discrete Wavelet Transform and Active Subspaces. Water Res 57. https://doi.org/10.1029/2020WR028511

Boano, F., Harvey, J.W., Marion, A., Packman, A.I., Revelli, R., Ridolfi, L., Wörman, A., 2014. Hyporheic flow and transport processes: Mechanisms, models, and biogeochemical implications. Rev. Geophys. 52, 603–679. https://doi.org/10.1002/2012RG000417

Boano, F., Revelli, R., Ridolfi, L., 2013. Modeling hyporheic exchange with unsteady stream discharge and bedform dynamics: Unsteady Hyporheic Exchange with Moving Bed Forms. Water Resour. Res. 49, 4089–4099. https://doi.org/10.1002/wrcr.20322

Boisson, A., de Anna, P., Bour, O., Le Borgne, T., Labasque, T., Aquilina, L., 2013. Reaction chain modeling of denitrification reactions during a push–pull test. Journal of Contaminant Hydrology 148, 1–11. https://doi.org/10.1016/j.jconhyd.2013.02.006

Booth, E.G., Zipper, S.C., Loheide, S.P., Kucharik, C.J., 2016. Is groundwater recharge always serving us well? Water supply provisioning, crop production, and flood attenuation in conflict in Wisconsin, USA. Ecosystem Services 21, 153–165. https://doi.org/10.1016/j.ecoser.2016.08.007

Boulton, A.J., Datry, T., Kasahara, T., Mutz, M., Stanford, J.A., 2010. Ecology and management of the hyporheic zone: stream–groundwater interactions of running waters and their floodplains. Journal of the North American Benthological Society 29, 26–40. https://doi.org/10.1899/08-017.1

Box, G.E.P., Tiao, G.C., 2011. Bayesian Inference in Statistical Analysis. John Wiley & Sons.

Boyce, S.E., Yeh, W.W.-G., 2014. Parameter-independent model reduction of transient groundwater flow models: Application to inverse problems. Advances in Water Resources 69, 168–180. https://doi.org/10.1016/j.advwatres.2014.04.009

BP p.l.c., 2021. BP Statistical Review of World Energy 2021. BP.

Bresciani, E., Gleeson, T., Goderniaux, P., de Dreuzy, J.R., Werner, A.D., Wörman, A., Zijl, W., Batelaan, O., 2016. Groundwater flow systems theory: research challenges beyond the specified-head top boundary condition. Hydrogeol J 24, 1087–1090. https://doi.org/10.1007/s10040-016-1397-8

Bresciani, E., Kang, P.K., Lee, S., 2019. Theoretical Analysis of Groundwater Flow Patterns Near Stagnation Points. Water Resour. Res. 55, 1624–1650. https://doi.org/10.1029/2018WR023508

British Geological Survey, 2006. Groundwater Flooding Susceptibility (Metadata Catalogue). British Geological Survey, United Kingdom.

Bruder, A., Tonolla, D., Schweizer, S.P., Vollenweider, S., Langhans, S.D., Wüest, A., 2016. A conceptual framework for hydropeaking mitigation. Science of The Total Environment 568, 1204–1212. https://doi.org/10.1016/j.scitotenv.2016.05.032

Brunner, P., Simmons, C.T., Cook, P.G., Therrien, R., 2010. Modeling Surface Water-Groundwater Interaction with MODFLOW: Some Considerations. Ground Water 48, 174–180. https://doi.org/10.1111/j.1745-6584.2009.00644.x

Brunner, P., Therrien, R., Renard, P., Simmons, C.T., Franssen, H.-J.H., 2017. Advances in understanding river-groundwater interactions: River-Groundwater Interactions. Rev. Geophys. 55, 818–854. https://doi.org/10.1002/2017RG000556

Cameron, R.H., Martin, W.T., 1947. The Orthogonal Development of Non-Linear Functionals in Series of Fourier-Hermite Functionals. The Annals of Mathematics 48, 385. https://doi.org/10.2307/1969178

Campolongo, F., Cariboni, J., Saltelli, A., 2007. An effective screening design for sensitivity analysis of large models. Environmental Modelling & Software, Modelling, computer-assisted simulations, and mapping of dangerous phenomena for hazard assessment 22, 1509–1518. https://doi.org/10.1016/j.envsoft.2006.10.004

Carabin, G., Dassargues, A., 2000. Coupling of parallel river and groundwater models to simulate dynamic groundwater boundary conditions. Proc. of Computational Methods in Water Resources 2000.

Cardenas, M.B., 2015. Hyporheic zone hydrologic science: A historical account of its emergence and a prospectus: Hyporheic zone hydrologic science: a historical account. Water Resour. Res. 51, 3601–3616. https://doi.org/10.1002/2015WR017028

Cardenas, M.B., 2008. Surface water-groundwater interface geomorphology leads to scaling of residence times. Geophys. Res. Lett. 35, L08402. https://doi.org/10.1029/2008GL033753

Cardenas, M.B., Zlotnik, V.A., 2003. Three-dimensional model of modern channel bend deposits: 3D model of channel bend deposit. Water Resour. Res. 39. https://doi.org/10.1029/2002WR001383

Carroll, R.J., Carroll, R.J. (Eds.), 2006. Measurement error in nonlinear models: a modern perspective, 2nd ed. ed, Monographs on statistics and applied probability. Chapman & Hall/CRC, Boca Raton, FL.

Casas-Mulet, R., Alfredsen, K., Hamududu, B., Timalsina, N.P., 2015. The effects of hydropeaking on hyporheic interactions based on field experiments. Hydrol. Process. 29, 1370–1384. https://doi.org/10.1002/hyp.10264

Casella, E., Molcard, A., Provenzale, A., 2011. Mesoscale vortices in the Ligurian Sea and their effect on coastal upwelling processes. Journal of Marine Systems 88, 12–19. https://doi.org/10.1016/j.jmarsys.2011.02.019

Castagna, M., Bellin, A., Chiogna, G., 2015. Uncertainty Estimation and Evaluation of Shallow Aquifers' Exploitability: The Case Study of the Adige Valley Aquifer (Italy). Water 7, 3367–3395. https://doi.org/10.3390/w7073367

Chapman, R.E., 1981. Geology and water: an introduction to fluid mechanics for geologists, Developments in applied earth sciences. Nijhoff ; Distributed by Kluwer Boston, The Hague ; Boston : Hingham, MA.

Cheng, A.H.-D., Cheng, D.T., 2005. Heritage and early history of the boundary element method. Engineering Analysis with Boundary Elements 29, 268–302. https://doi.org/10.1016/j.enganabound.2004.12.001

Chiang, W.-H., 2012. Processing Modflow. An Integrated Modeling Environment for the Simulation of Groundwater Flow, Transport and Reactive Processes. Simcore Software.

Chiogna, G., Hochstetler, D.L., Bellin, A., Kitanidis, P.K., Rolle, M., 2012. Mixing, entropy and reactive solute transport. Geophys. Res. Lett. 39, 2012GL053295. https://doi.org/10.1029/2012GL053295

Chiogna, G., Marcolini, G., Liu, W., Pérez Ciria, T., Tuo, Y., 2018. Coupling hydrological modeling and support vector regression to model hydropeaking in alpine catchments. Science of The Total Environment 633, 220–229. https://doi.org/10.1016/j.scitotenv.2018.03.162

Cho, M.S., Solano, F., Thomson, N.R., Trefry, M.G., Lester, D.R., Metcalfe, G., 2019. Field Trials of Chaotic Advection to Enhance Reagent Delivery. Groundwater Monit R 39, 23–39. https://doi.org/10.1111/gwmr.12339

Chow, R., Bennett, J., Dugge, J., Wöhling, T., Nowak, W., 2020. Evaluating Subsurface Parameterization to Simulate Hyporheic Exchange: The Steinlach River Test Site. Groundwater 58, 93–109. https://doi.org/10.1111/gwat.12884

Cirpka, O.A., Valocchi, A.J., 2016. Debates-Stochastic subsurface hydrology from theory to practice: Does stochastic subsurface hydrology help solving practical problems of contaminant hydrogeology? Water Resour. Res. 52, 9218–9227. https://doi.org/10.1002/2016WR019087

Coduto, D.P., 1999. Geotechnical engineering: principles and practices. Prentice Hall, Upper Saddle River, NJ.

Coles, S., 2001. Introduction, in: An Introduction to Statistical Modeling of Extreme Values, Springer Series in Statistics. Springer London, London, pp. 1–17. https://doi.org/10.1007/978-1-4471-3675-0_1

Collins, S.L., Christelis, V., Jackson, C.R., Mansour, M.M., Macdonald, D.M.J., Barkwith, A.K.A.P., 2020. Towards integrated flood inundation modelling in groundwater-dominated catchments. Journal of Hydrology 591, 125755. https://doi.org/10.1016/j.jhydrol.2020.125755

Colombo, L., Gattinoni, P., Scesi, L., 2018. Stochastic modelling of groundwater flow for hazard assessment along the underground infrastructures in Milan (northern Italy). Tunnelling and Underground Space Technology 79, 110–120. https://doi.org/10.1016/j.tust.2018.05.007

Conant, B., Robinson, C.E., Hinton, M.J., Russell, H.A.J., 2019. A framework for conceptualizing groundwater-surface water interactions and identifying potential impacts on water quality, water quantity, and ecosystems. Journal of Hydrology 574, 609–627. https://doi.org/10.1016/j.jhydrol.2019.04.050

Cools, R., Nuyens, D., 2016. Monte Carlo and Quasi-Monte Carlo Methods.

Cousquer, Y., Pryet, A., Flipo, N., Delbart, C., Dupuy, A., 2017. Estimating River Conductance from Prior Information to Improve Surface-Subsurface Model Calibration. Groundwater 55, 408–418. https://doi.org/10.1111/gwat.12492

Cui, G., Su, X., Liu, Y., Zheng, S., 2020. Effect of riverbed sediment flushing and clogging on river-water infiltration rate: a case study in the Second Songhua River, Northeast China. Hydrogeol J. https://doi.org/10.1007/s10040-020-02218-7

Daniluk, T.L., Lautz, L.K., Gordon, R.P., Endreny, T.A., 2013. Surface water-groundwater interaction at restored streams and associated reference reaches. Hydrol. Process. 27, 3730–3746. https://doi.org/10.1002/hyp.9501

Darcy, H., 1856. Les fontaines publiques de la ville de Dijon, Les fontaines publiques de la ville de Dijon. Exposition et application des principes à suivre et des formules à employer dans les questions de distribution d'eau: ouvrage terminé par un appendice relatif aux fournitures d'eau de plusieurs villes au filtrage des eaux et à la fabrication des tuyaux de fonte, de plomb, de tole et de bitume. V. Dalmont.

Dassargues, A., 2020. Hydrogeology: groundwater science and engineering, First issued in paperback. ed. CRC Press, Taylor & Francis Group, Boca Raton London New York.

Davis, J.H., 2003. Fate and transport modeling of selected chlorinated organic compounds at Hangar 1000, U.S. Naval Air Station, Jacksonville, Florida. U.S. Geological Survey, Branch of Information Services.

de Anna, P., Dentz, M., Tartakovsky, A., Le Borgne, T., 2014a. The filamentary structure of mixing fronts and its control on reaction kinetics in porous media flows. Geophys. Res. Lett. 41, 4586–4593. https://doi.org/10.1002/2014GL060068

de Anna, P., Jimenez-Martinez, J., Tabuteau, H., Turuban, R., Le Borgne, T., Derrien, M., Méheust, Y., 2014b. Mixing and Reaction Kinetics in Porous Media: An Experimental Pore Scale Quantification. Environ. Sci. Technol. 48, 508–516. https://doi.org/10.1021/es403105b

de Barros, F.P.J., Dentz, M., Koch, J., Nowak, W., 2012. Flow topology and scalar mixing in spatially heterogeneous flow fields. Geophys. Res. Lett. 39, n/a-n/a. https://doi.org/10.1029/2012GL051302

Deman, G., Konakli, K., Sudret, B., Kerrou, J., Perrochet, P., Benabderrahmane, H., 2016. Using sparse polynomial chaos expansions for the global sensitivity analysis of groundwater lifetime expectancy in a multi-layered hydrogeological model. Reliability Engineering & System Safety 147, 156–169. https://doi.org/10.1016/j.ress.2015.11.005

Demeritt, D., Nobert, S., 2014. Models of best practice in flood risk communication and management. Environmental Hazards 13, 313–328. https://doi.org/10.1080/17477891.2014.924897

Derx, J., Blaschke, A.P., Blöschl, G., 2010. Three-dimensional flow patterns at the river–aquifer interface — a case study at the Danube. Advances in Water Resources 33, 1375–1387. https://doi.org/10.1016/j.advwatres.2010.04.013

DHI, 2017. MIKE SHE. Volume 2: Reference Guide., Reference Manual for Water Movement. DHI.

DHI, 2013. The MIKE SHE user and technical reference manual. Danish Hydraulic Institute, Copenhagen.

Di Baldassarre, G., Montanari, A., 2009. Uncertainty in river discharge observations: a quantitative analysis. Hydrol. Earth Syst. Sci. 13, 913–921. https://doi.org/10.5194/hess-13-913-2009

Di Baldassarre, G., Schumann, G., Bates, P.D., Freer, J.E., Beven, K.J., 2010. Flood-plain mapping: a critical discussion of deterministic and probabilistic approaches.

Hydrological Sciences Journal 55, 364–376. https://doi.org/10.1080/02626661003683389

Di Ciacca, A., Leterme, B., Laloy, E., Jacques, D., Vanderborght, J., 2019. Scale-dependent parameterization of groundwater–surface water interactions in a regional hydrogeological model. Journal of Hydrology 576, 494–507. https://doi.org/10.1016/j.jhydrol.2019.06.072

Dingman, S.L., 2015. Physical Hydrology: Third Edition. Waveland Press.

Disse, M., Keilholz, P., Bhola, P., 2015. Die Grundhochwasser - Problematik in der Gemeinde Tacherting und Untersuchung von Gegenmaßnahmen. Chair of Hydrology and River Basin Management, Technical University of Munich, Munich.

Doherty, J., 2010. Methodologies and software for PEST-based model predictive uncertainty analysis. Watermark Numerical Computing.

Doherty, J.E., Hunt, R.J., Tonkin, M.J., 2010. Approaches to Highly Parameterized Inversion: A Guide to Using PEST for Model-Parameter and Predictive-Uncertainty Analysis, Scientific Investigations Report 2010–5211. U.S. Geological Survey.

Doppler, G., Kroemer, E., Rögner, K., Wallner, J., Jerz, H., Grottenthaler, W., 2011. Quaternary Stratigraphy of Southern Bavaria. https://doi.org/10.23689/FIDGEO-1763

Dudley-Southern, M., Binley, A., 2015. Temporal responses of groundwater-surface water exchange to successive storm events. Water Resour. Res. 51, 1112–1126. https://doi.org/10.1002/2014WR016623

Dutta, D., 2013. Hydrodynamic Dispersion, in: Li, D. (Ed.), Encyclopedia of Microfluidics and Nanofluidics. Springer US, Boston, MA, pp. 1–14. https://doi.org/10.1007/978-3-642-27758-0_660-3

Elliott, A.H., Brooks, N.H., 1997. Transfer of nonsorbing solutes to a streambed with bed forms: Laboratory experiments. Water Resour. Res. 33, 137–151. https://doi.org/10.1029/96WR02783

Engdahl, N.B., Benson, D.A., Bolster, D., 2014. Predicting the enhancement of mixing-driven reactions in nonuniform flows using measures of flow topology. Phys. Rev. E 90, 051001. https://doi.org/10.1103/PhysRevE.90.051001

Erdal, D., Cirpka, O.A., 2019. Global sensitivity analysis and adaptive stochastic sampling of a subsurface-flow model using active subspaces. Hydrol. Earth Syst. Sci. 23, 3787–3805. https://doi.org/10.5194/hess-23-3787-2019

Esfandiar, B., Porta, G., Perotto, S., Guadagnini, A., 2015. Impact of space-time mesh adaptation on solute transport modeling in porous media. Water Resour. Res. 51, 1315–1332. https://doi.org/10.1002/2014WR016569

Esri, 2017. ArcGIS. Features. Esri.

Essouayed, E., Annable, M.D., Momtbrun, M., Atteia, O., 2019. An innovative tool for groundwater velocity measurement compared with other tools in laboratory and field tests. Journal of Hydrology X 2, 100008. https://doi.org/10.1016/j.hydroa.2018.100008

Feinberg, J., 2019. ChaosPy – Uncertainty Quantification Library [WWW Document]. ChaosPy – Uncertainty Quantification Library. URL https://chaospy.readthedocs.io/en/master/

Feinberg, J., Langtangen, H.P., 2015. Chaospy: An open source tool for designing methods of uncertainty quantification. Journal of Computational Science 11, 46–57. https://doi.org/10.1016/j.jocs.2015.08.008

Feng, K., Lu, Z., Yang, C., 2019. Enhanced Morris method for global sensitivity analysis: good proxy of Sobol' index. Struct Multidisc Optim 59, 373–387. https://doi.org/10.1007/s00158-018-2071-7

Ferencz, S.B., Cardenas, M.B., Neilson, B.T., 2019. Analysis of the Effects of Dam Release Properties and Ambient Groundwater Flow on Surface Water-Groundwater Exchange Over a 100-km-Long Reach. Water Resour. Res. 55, 8526–8546. https://doi.org/10.1029/2019WR025210

Fetter, C.W., 1999. Contaminant hydrogeology, 2nd ed. ed. Prentice Hall, Upper Saddle River, NJ.

Fetter, C.W., Boving, T., Kreamer, D., 2017. Contaminant Hydrogeology: Third Edition. Waveland Press.

Findlay, S., 1995. Importance of surface-subsurface exchange in stream ecosystems: The hyporheic zone. Limnol. Oceanogr. 40, 159–164. https://doi.org/10.4319/lo.1995.40.1.0159

Fiori, A., de Barros, F.P.J., 2015. Groundwater flow and transport in aquifers: Insights from modeling and characterization at the field scale. Journal of Hydrology 531, 1. https://doi.org/10.1016/j.jhydrol.2015.11.001

Fornasini, P., 2008. The uncertainty in physical measurements: an introduction to data analysis in the physics laboratory. Springer, New York, N.Y.

Francis, B.A., Francis, L.K., Cardenas, M.B., 2010. Water table dynamics and groundwater-surface water interaction during filling and draining of a large fluvial island due to dam-induced river stage fluctuations. Water Resour. Res. 46. https://doi.org/10.1029/2009WR008694

Franke, O.L., Reilly, T.E., Bennett, G.D., 1987. Definition of boundary and initial conditions in the analysis of saturated ground-water flow systems - An introduction (USGS Numbered Series No. 03-B5), Definition of boundary and initial conditions in the analysis of saturated ground-water flow systems - An introduction, Techniques of Water-Resources Investigations. U.S. G.P.O.,. https://doi.org/10.3133/twri03B5

Fürst, J., Bichler, A., Konecny, F., 2015. Regional Frequency Analysis of Extreme Groundwater Levels. Groundwater 53, 414–423. https://doi.org/10.1111/gwat.12223

Garcia Sanchez, D., Lacarrière, B., Musy, M., Bourges, B., 2014. Application of sensitivity analysis in building energy simulations: Combining first- and second-order elementary effects methods. Energy and Buildings 68, 741–750. https://doi.org/10.1016/j.enbuild.2012.08.048

Gattinoni, P., Scesi, L., 2017. The groundwater rise in the urban area of Milan (Italy) and its interactions with underground structures and infrastructures. Tunnelling and

Underground Space Technology 62, 103–114. https://doi.org/10.1016/j.tust.2016.12.001

Gautschi, W., 1968. Construction of Gauss-Christoffel quadrature formulas. Math. Comp. 22, 251–251. https://doi.org/10.1090/S0025-5718-1968-0228171-0

Gelman, A., Rubin, D.B., 1992. Inference from Iterative Simulation Using Multiple Sequences. Statist. Sci. 7. https://doi.org/10.1214/ss/1177011136

Geng, X., Michael, H.A., Boufadel, M.C., Molz, F.J., Gerges, F., Lee, K., 2020. Heterogeneity Affects Intertidal Flow Topology in Coastal Beach Aquifers. Geophys. Res. Lett. 47. https://doi.org/10.1029/2020GL089612

Georgakakos, K.P., Seo, D.-J., Gupta, H., Schaake, J., Butts, M.B., 2004. Towards the characterization of streamflow simulation uncertainty through multimodel ensembles. Journal of Hydrology 298, 222–241. https://doi.org/10.1016/j.jhydrol.2004.03.037

Gerecht, K.E., Cardenas, M.B., Guswa, A.J., Sawyer, A.H., Nowinski, J.D., Swanson, T.E., 2011. Dynamics of hyporheic flow and heat transport across a bed-to-bank continuum in a large regulated river. Water Resour. Res. 47. https://doi.org/10.1029/2010WR009794

Ghaith, M., Li, Z., 2020. Propagation of parameter uncertainty in SWAT: A probabilistic forecasting method based on polynomial chaos expansion and machine learning. Journal of Hydrology 586, 124854. https://doi.org/10.1016/j.jhydrol.2020.124854

Ghysels, G., Benoit, S., Awol, H., Jensen, E.P., Debele Tolche, A., Anibas, C., Huysmans, M., 2018. Characterization of meter-scale spatial variability of riverbed hydraulic conductivity in a lowland river (Aa River, Belgium). Journal of Hydrology 559, 1013–1027. https://doi.org/10.1016/j.jhydrol.2018.03.002

Ghysels, G., Mutua, S., Veliz, G.B., Huysmans, M., 2019. A modified approach for modelling river–aquifer interaction of gaining rivers in MODFLOW, including riverbed heterogeneity and river bank seepage. Hydrogeol J 27, 1851–1863. https://doi.org/10.1007/s10040-019-01941-0

Gibson, N.L., Gifford-Miears, C., Leon, A.S., Vasylkivska, V.S., 2014. Efficient computation of unsteady flow in complex river systems with uncertain inputs. International Journal of Computer Mathematics 91, 781–797. https://doi.org/10.1080/00207160.2013.854336

Golub, G.H., Welsch, J.H., 1968. Calculation of Gauss quadrature rules. Math. Comp. 23, 221–221. https://doi.org/10.1090/S0025-5718-69-99647-1

Gomez, J.D., Wilson, J.L., 2013. Age distributions and dynamically changing hydrologic systems: Exploring topography-driven flow: Age Distributions for Hydrologic Systems. Water Resour. Res. 49, 1503–1522. https://doi.org/10.1002/wrcr.20127

González-Quirós, A., Fernández-Álvarez, J.P., 2019. Conceptualization and finite element groundwater flow modeling of a flooded underground mine reservoir in the Asturian Coal Basin, Spain. Journal of Hydrology 578, 124036. https://doi.org/10.1016/j.jhydrol.2019.124036

Götzinger, J., Bárdossy, A., 2008. Generic error model for calibration and uncertainty estimation of hydrological models. Water Resour. Res. 44. https://doi.org/10.1029/2007WR006691

Guillaume, J.H.A., Hunt, R.J., Comunian, A., Blakers, R.S., Fu, B., 2016. Methods for Exploring Uncertainty in Groundwater Management Predictions, in: Jakeman, A.J., Barreteau, O., Hunt, R.J., Rinaudo, J.-D., Ross, A. (Eds.), Integrated Groundwater Management. Springer International Publishing, Cham, pp. 711–737. https://doi.org/10.1007/978-3-319-23576-9_28

Halton, J.H., 1964. Algorithm 247: Radical-inverse quasi-random point sequence. Commun. ACM 7, 701–702. https://doi.org/10.1145/355588.365104

Harbaugh, A., 2005. MODFLOW-2005, The U.S. Geological Survey Modular Ground-Water Model—the Ground-Water Flow Process, U.S. Geological Survey Techniques and Methods 6-A16. U.S. Geological Survey.

Harbaugh, A.W., Banta, E.R., Hill, M.C., McDonald, M.G., 2000. MODFLOW-2000, The U.S. Geological Survey Modular Ground-Water Model - User Guide to Modularization Concepts and the Ground-Water Flow Process (USGS Numbered Series No. 2000–92), MODFLOW-2000, The U.S. Geological Survey Modular Ground-Water Model - User Guide to Modularization Concepts and the Ground-Water Flow Process, Open-File Report. Geological Survey (U.S.). https://doi.org/10.3133/ofr200092

Harris, C.R., Millman, K.J., van der Walt, S.J., Gommers, R., Virtanen, P., Cournapeau, D., Wieser, E., Taylor, J., Berg, S., Smith, N.J., Kern, R., Picus, M., Hoyer, S., van Kerkwijk, M.H., Brett, M., Haldane, A., del Río, J.F., Wiebe, M., Peterson, P., Gérard-Marchant, P., Sheppard, K., Reddy, T., Weckesser, W., Abbasi, H., Gohlke, C., Oliphant, T.E., 2020. Array programming with NumPy. Nature 585, 357–362. https://doi.org/10.1038/s41586-020-2649-2

Hatch, C.E., Fisher, A.T., Ruehl, C.R., Stemler, G., 2010. Spatial and temporal variations in streambed hydraulic conductivity quantified with time-series thermal methods. Journal of Hydrology 389, 276–288. https://doi.org/10.1016/j.jhydrol.2010.05.046

Hauer, C., Siviglia, A., Zolezzi, G., 2017. Hydropeaking in regulated rivers – From process understanding to design of mitigation measures. Science of The Total Environment 579, 22–26. https://doi.org/10.1016/j.scitotenv.2016.11.028

Helton, J.C., Johnson, J.D., Oberkampf, W.L., 2004. An exploration of alternative approaches to the representation of uncertainty in model predictions. Reliability Engineering & System Safety, Alternative Representations of Epistemic Uncertainty 85, 39–71. https://doi.org/10.1016/j.ress.2004.03.025

Henstra, D., Minano, A., Thistlethwaite, J., 2019. Communicating disaster risk? An evaluation of the availability and quality of flood maps. Nat. Hazards Earth Syst. Sci. 19, 313–323. https://doi.org/10.5194/nhess-19-313-2019

Herman, J., Usher, W., 2017. SALib: An open-source Python library for Sensitivity Analysis. Journal of Open Source Software 2, 97. https://doi.org/10.21105/joss.00097

Heße, F., Comunian, A., Attinger, S., 2019. What We Talk About When We Talk About Uncertainty. Toward a Unified, Data-Driven Framework for Uncertainty

Characterization in Hydrogeology. Front. Earth Sci. 7, 118. https://doi.org/10.3389/feart.2019.00118

Hester, E.T., Santizo, K.Y., Nida, A.A., Widdowson, M.A., 2021. Hyporheic transverse mixing zones and dispersivity: Laboratory and numerical experiments of hydraulic controls. Journal of Contaminant Hydrology 243, 103885. https://doi.org/10.1016/j.jconhyd.2021.103885

Hidalgo, J.J., Dentz, M., 2018. Mixing across fluid interfaces compressed by convective flow in porous media. J. Fluid Mech. 838, 105–128. https://doi.org/10.1017/jfm.2017.888

Hidalgo, J.J., Dentz, M., Cabeza, Y., Carrera, J., 2015. Dissolution patterns and mixing dynamics in unstable reactive flow. Geophys. Res. Lett. 42, 6357–6364. https://doi.org/10.1002/2015GL065036

Hintze, S., Glauser, G., Hunkeler, D., 2020. Influence of surface water – groundwater interactions on the spatial distribution of pesticide metabolites in groundwater. Science of The Total Environment 733, 139109. https://doi.org/10.1016/j.scitotenv.2020.139109

Houska, T., Kraft, P., Chamorro-Chavez, A., Breuer, L., 2015. SPOTting Model Parameters Using a Ready-Made Python Package. PLoS ONE 10, e0145180. https://doi.org/10.1371/journal.pone.0145180

Hubbs, S.A., 2006. Evaluating Streambed Forces Impacting the Capacity of Riverbed Filtration Systems, in: Hubbs, S.A. (Ed.), Riverbank Filtration Hydrology, Nato Science Series: IV: Earth and Environmental Sciences. Springer Netherlands, Dordrecht, pp. 21–42. https://doi.org/10.1007/978-1-4020-3938-6_2

Hunt, R.J., Strand, M., Walker, J.F., 2006. Measuring groundwater–surface water interaction and its effect on wetland stream benthic productivity, Trout Lake watershed, northern Wisconsin, USA. Journal of Hydrology 320, 370–384. https://doi.org/10.1016/j.jhydrol.2005.07.029

Hunter, J.D., 2007. Matplotlib: A 2D Graphics Environment. Comput. Sci. Eng. 9, 90–95. https://doi.org/10.1109/MCSE.2007.55

Jaffe, P.R., Kaplan, D.I., 2017. Fate of Uranium During Transport Across the Groundwater-Surface Water Interface (No. DOE-Princeton-SC0006847). Princeton Univ., NJ (United States). https://doi.org/10.2172/1367535

Jaxa-Rozen, M., Kwakkel, J., 2018. Tree-based ensemble methods for sensitivity analysis of environmental models: A performance comparison with Sobol and Morris techniques. Environmental Modelling & Software 107, 245–266. https://doi.org/10.1016/j.envsoft.2018.06.011

Jazayeri, A., Werner, A.D., 2019. Boundary Condition Nomenclature Confusion in Groundwater Flow Modeling. Groundwater 57, 664–668. https://doi.org/10.1111/gwat.12893

Jiang, X.-W., Wan, L., Wang, J.-Z., Yin, B.-X., Fu, W.-X., Lin, C.-H., 2014. Field identification of groundwater flow systems and hydraulic traps in drainage basins using a geophysical method: Jiang et al.: Identification of flow systems. Geophys. Res. Lett. 41, 2812–2819. https://doi.org/10.1002/2014GL059579

Jiang, X.-W., Wang, X.-S., Wan, L., Ge, S., 2011. An analytical study on stagnation points in nested flow systems in basins with depth-decaying hydraulic conductivity. Water Resour. Res. 47. https://doi.org/10.1029/2010WR009346

Jimenez-Martinez, J., Smith, M., Pope, D., 2015. Prediction of groundwater-induced flooding in a chalk aquifer for future climate change scenarios: Prediction of Groundwater-Induced Flooding in a Chalk Aquifer. Hydrol. Process. https://doi.org/10.1002/hyp.10619

Jones, J.B., Holmes, R.M., 1996. Surface-subsurface interactions in stream ecosystems. Trends in Ecology & Evolution 11, 239–242. https://doi.org/10.1016/0169-5347(96)10013-6

Joo, J., Tian, Y., 2021. Impact of Stream-Groundwater Interactions on Peak Streamflow in the Floods. Hydrology 8, 141. https://doi.org/10.3390/hydrology8030141

Kaipio, J., Somersalo, E., 2005. Statistical and Computational Inverse Problems, Applied Mathematical Sciences. Springer-Verlag, New York. https://doi.org/10.1007/b138659

Kaiser, M., Borga, M., Disse, M., 2020. Occurrence and Characteristics of Flash Floods in Bavaria (Germany), in: Leal Filho, W., Nagy, G.J., Borga, M., Chávez Muñoz, P.D., Magnuszewski, A. (Eds.), Climate Change, Hazards and Adaptation Options, Climate Change Management. Springer International Publishing, Cham, pp. 293–310. https://doi.org/10.1007/978-3-030-37425-9_16

Kang, P.K., Bresciani, E., An, S., Lee, S., 2019. Potential impact of pore-scale incomplete mixing on biodegradation in aquifers: From batch experiment to field-scale modeling. Advances in Water Resources 123, 1–11. https://doi.org/10.1016/j.advwatres.2018.10.026

Keilholz, P., Disse, M., Bhola, P., 2015. Integrierte Betrachtung der Grundhochwasser-Problematik in der Gemeinde Tacherting (Bayern). Hydrologie und Wasserbewirtschaftung 2015, 688–693. https://doi.org/10.3243/kwe2015.11.003

Khan, H.H., Khan, A., 2019. Groundwater and Surface Water Interaction, in: GIS and Geostatistical Techniques for Groundwater Science. Elsevier, pp. 197–207. https://doi.org/10.1016/B978-0-12-815413-7.00014-6

Kitanidis, P.K., McCarty, P.L. (Eds.), 2012. Delivery and Mixing in the Subsurface, SERDP/ESTCP Environmental Remediation Technology. Springer New York, New York, NY. https://doi.org/10.1007/978-1-4614-2239-6

Kløve, B., Ala-aho, P., Bertrand, G., Boukalova, Z., Ertürk, A., Goldscheider, N., Ilmonen, J., Karakaya, N., Kupfersberger, H., Kvœrner, J., Lundberg, A., Mileusnić, M., Moszczynska, A., Muotka, T., Preda, E., Rossi, P., Siergieiev, D., Šimek, J., Wachniew, P., Angheluta, V., Widerlund, A., 2011. Groundwater dependent ecosystems. Part I: Hydroecological status and trends. Environmental Science & Policy 14, 770–781. https://doi.org/10.1016/j.envsci.2011.04.002

Krause, S., Boano, F., Cuthbert, M.O., Fleckenstein, J.H., Lewandowski, J., 2014. Understanding process dynamics at aquifer-surface water interfaces: An introduction to the special section on new modeling approaches and novel experimental technologies: Introduction. Water Resour. Res. 50, 1847–1855. https://doi.org/10.1002/2013WR014755

Krause, S., Lewandowski, J., Grimm, N.B., Hannah, D.M., Pinay, G., McDonald, K., Martí, E., Argerich, A., Pfister, L., Klaus, J., Battin, T., Larned, S.T., Schelker, J., Fleckenstein, J., Schmidt, C., Rivett, M.O., Watts, G., Sabater, F., Sorolla, A., Turk, V., 2017. Ecohydrological interfaces as hot spots of ecosystem processes. Water Resour. Res. 53, 6359–6376. https://doi.org/10.1002/2016WR019516

Kreibich, H., Thieken, A.H., Grunenberg, H., Ullrich, K., Sommer, T., 2009. Extent, perception and mitigation of damage due to high groundwater levels in the city of Dresden, Germany. Nat. Hazards Earth Syst. Sci. 9, 1247–1258. https://doi.org/10.5194/nhess-9-1247-2009

Kuczera, G., Mroczkowski, M., 1998. Assessment of hydrologic parameter uncertainty and the worth of multiresponse data. Water Resour. Res. 34, 1481–1489. https://doi.org/10.1029/98WR00496

Kurowicka, D., Cooke, R., 2006. Uncertainty analysis with high dimensional modelling. John Wiley & Sons, Hoboken, NJ.

Laloy, E., Rogiers, B., Vrugt, J.A., Mallants, D., Jacques, D., 2013. Efficient posterior exploration of a high-dimensional groundwater model from two-stage Markov chain Monte Carlo simulation and polynomial chaos expansion: Speeding up MCMC Simulation of a Groundwater Model. Water Resour. Res. 49, 2664–2682. https://doi.org/10.1002/wrcr.20226

Lamontagne, S., Cosme, F., Minard, A., Holloway, A., 2018. Nitrogen attenuation, dilution and recycling in the intertidal hyporheic zone of a subtropical estuary. Hydrol. Earth Syst. Sci. 22, 4083–4096. https://doi.org/10.5194/hess-22-4083-2018

Le Gratiet, L., Marelli, S., Sudret, B., 2017. Metamodel-Based Sensitivity Analysis: Polynomial Chaos Expansions and Gaussian Processes, in: Ghanem, R., Higdon, D., Owhadi, H. (Eds.), Handbook of Uncertainty Quantification. Springer International Publishing, Cham, pp. 1289–1325. https://doi.org/10.1007/978-3-319-12385-1_38

Le Maitre, O.P., Knio, O.M., 2010. Spectral methods for uncertainty quantification: With applications to computational fluid dynamics, Scientific computation. Springer, Dordrecht.

Leake, S.A., Prudic, D.E., 1991. Documentation of a computer program to simulate aquifer-system compaction using the modular finite-difference ground-water flow model (No. 06-A2), Techniques of Water-Resources Investigations. U.S. Geological Survey.

Leek, R., Wu, J.Q., Wang, L., Hanrahan, T.P., Barber, M.E., Qiu, H., 2009. Heterogeneous characteristics of streambed saturated hydraulic conductivity of the Touchet River, south eastern Washington, USA. Hydrol. Process. 23, 1236–1246. https://doi.org/10.1002/hyp.7258

Lewandowski, J., Arnon, S., Banks, E., Batelaan, O., Betterle, A., Broecker, T., Coll, C., Drummond, J., Gaona Garcia, J., Galloway, J., Gomez-Velez, J., Grabowski, R., Herzog, S., Hinkelmann, R., Höhne, A., Hollender, J., Horn, M., Jaeger, A., Krause, S., Löchner Prats, A., Magliozzi, C., Meinikmann, K., Mojarrad, B., Mueller, B., Peralta-Maraver, I., Popp, A., Posselt, M., Putschew, A., Radke, M., Raza, M., Riml, J., Robertson, A., Rutere, C., Schaper, J., Schirmer, M., Schulz, H., Shanafield, M., Singh, T., Ward, A., Wolke, P., Wörman, A., Wu, L., 2019. Is the Hyporheic Zone

Relevant beyond the Scientific Community? Water 11, 2230. https://doi.org/10.3390/w11112230

Lewandowski, J., Meinikmann, K., Krause, S., 2020. Groundwater–Surface Water Interactions: Recent Advances and Interdisciplinary Challenges. Water 12, 296. https://doi.org/10.3390/w12010296

Li, T., Pasternack, G.B., 2021. Revealing the diversity of hydropeaking flow regimes. Journal of Hydrology 598, 126392. https://doi.org/10.1016/j.jhydrol.2021.126392

Liang, X., Zhan, H., Schilling, K., 2018. Spatiotemporal Responses of Groundwater Flow and Aquifer-River Exchanges to Flood Events. Water Resour. Res. 54, 1513–1532. https://doi.org/10.1002/2017WR022046

Litvinenko, A., Logashenko, D., Tempone, R., Wittum, G., Keyes, D., 2020. Solution of the 3D density-driven groundwater flow problem with uncertain porosity and permeability. Int J Geomath 11, 10. https://doi.org/10.1007/s13137-020-0147-1

Liu, Z., 2018. Multiphysics in Porous Materials. Springer International Publishing, Cham. https://doi.org/10.1007/978-3-319-93028-2

Lykkegaard, M.B., Dodwell, T.J., Moxey, D., 2021. Accelerating uncertainty quantification of groundwater flow modelling using a deep neural network proxy. Computer Methods in Applied Mechanics and Engineering 383, 113895. https://doi.org/10.1016/j.cma.2021.113895

Macdonald, D., Bloomfield, J.P., Hughes, A.G., MacDonald, A., Adams, B., McKenzie, A.A., 2008. Improving the understanding of the risk from groundwater flooding in the UK. Presented at the FLOODrisk 2008, European Conference on Flood Risk Management, CRC Press, The Netherlands.

Macdonald, D., Dixon, A., Newell, A., Hallaways, A., 2012. Groundwater flooding within an urbanised flood plain: Groundwater flooding within urbanised flood plain. J. Flood Risk Manage 5, 68–80. https://doi.org/10.1111/j.1753-318X.2011.01127.x

Magliozzi, C., Grabowski, R.C., Packman, A.I., Krause, S., 2018. Toward a conceptual framework of hyporheic exchange across spatial scales. Hydrol. Earth Syst. Sci. 22, 6163–6185. https://doi.org/10.5194/hess-22-6163-2018

Mahecha, M.D., Gans, F., Sippel, S., Donges, J.F., Kaminski, T., Metzger, S., Migliavacca, M., Papale, D., Rammig, A., Zscheischler, J., 2017. Detecting impacts of extreme events with ecological in situ monitoring networks. Biogeosciences 14, 4255–4277. https://doi.org/10.5194/bg-14-4255-2017

Maina, F.Z., Guadagnini, A., 2018. Uncertainty Quantification and Global Sensitivity Analysis of Subsurface Flow Parameters to Gravimetric Variations During Pumping Tests in Unconfined Aquifers. Water Resour. Res. 54, 501–518. https://doi.org/10.1002/2017WR021655

Malzone, J.M., Anseeuw, S.K., Lowry, C.S., Allen-King, R., 2016a. Temporal Hyporheic Zone Response to Water Table Fluctuations: J.M. Malzone. Groundwater 54, 274–285. https://doi.org/10.1111/gwat.12352

Malzone, J.M., Lowry, C.S., Ward, A.S., 2016b. Response of the hyporheic zone to transient groundwater fluctuations on the annual and storm event time scales: Transient model

of the hyporheic zone. Water Resour. Res. 52, 5301–5321. https://doi.org/10.1002/2015WR018056

Mancini, C.P., Lollai, S., Volpi, E., Fiori, A., 2020. Flood Modeling and Groundwater Flooding in Urbanized Reclamation Areas: The Case of Rome (Italy). Water 12, 2030. https://doi.org/10.3390/w12072030

Mara, T.A., Fajraoui, N., Guadagnini, A., Younes, A., 2017. Dimensionality reduction for efficient Bayesian estimation of groundwater flow in strongly heterogeneous aquifers. Stoch Environ Res Risk Assess 31, 2313–2326. https://doi.org/10.1007/s00477-016-1344-1

Marzadri, A., Tonina, D., Bellin, A., 2013. Effects of stream morphodynamics on hyporheic zone thermal regime: Stream Morphology Control on Hyporheic Temperature. Water Resour. Res. 49, 2287–2302. https://doi.org/10.1002/wrcr.20199

Marzadri, A., Tonina, D., Bellin, A., Valli, A., 2016. Mixing interfaces, fluxes, residence times and redox conditions of the hyporheic zones induced by dune-like bedforms and ambient groundwater flow. Advances in Water Resources 88, 139–151. https://doi.org/10.1016/j.advwatres.2015.12.014

Master, Y., Shavit, U., Shaviv, A., 2005. Modified Isotope Pairing Technique to Study N Transformations in Polluted Aquatic Systems: Theory. Environ. Sci. Technol. 39, 1749–1756. https://doi.org/10.1021/es049086c

Mays, D.C., Neupauer, R.M., 2012. Plume spreading in groundwater by stretching and folding: PLUME SPREADING IN GROUNDWATER. Water Resour. Res. 48. https://doi.org/10.1029/2011WR011567

McCallum, A.M., Andersen, M.S., Rau, G.C., Larsen, J.R., Acworth, R.I., 2014. River-aquifer interactions in a semiarid environment investigated using point and reach measurements. Water Resour. Res. 50, 2815–2829. https://doi.org/10.1002/2012WR012922

McCarty, P.L., Criddle, C.S., 2012. Chemical and Biological Processes: The Need for Mixing, in: Kitanidis, P.K., McCarty, P.L. (Eds.), Delivery and Mixing in the Subsurface, SERDP/ESTCP Environmental Remediation Technology. Springer New York, New York, NY, pp. 7–52. https://doi.org/10.1007/978-1-4614-2239-6_2

McKenzie, A.A., Rutter, H.K., Hulbert, A.G., 2010. The use of elevation models to predict areas at risk of groundwater flooding. Geological Society, London, Special Publications 345, 75–79. https://doi.org/10.1144/SP345.9

McMillan, H.K., Westerberg, I.K., Krueger, T., 2018. Hydrological data uncertainty and its implications. WIREs Water 5. https://doi.org/10.1002/wat2.1319

McPhillips, L.E., Chang, H., Chester, M.V., Depietri, Y., Friedman, E., Grimm, N.B., Kominoski, J.S., McPhearson, T., Méndez-Lázaro, P., Rosi, E.J., Shafiei Shiva, J., 2018. Defining Extreme Events: A Cross-Disciplinary Review. Earth's Future 6, 441–455. https://doi.org/10.1002/2017EF000686

Mehl, S., Hill, M.C., 2010. Grid-size dependence of Cauchy boundary conditions used to simulate stream–aquifer interactions. Advances in Water Resources 33, 430–442. https://doi.org/10.1016/j.advwatres.2010.01.008

Meile, T., Boillat, J.-L., Schleiss, A.J., 2011. Hydropeaking indicators for characterization of the Upper-Rhone River in Switzerland. Aquat Sci 73, 171–182. https://doi.org/10.1007/s00027-010-0154-7

Meng, J., Li, H., 2017. An efficient stochastic approach for flow in porous media via sparse polynomial chaos expansion constructed by feature selection. Advances in Water Resources 105, 13–28. https://doi.org/10.1016/j.advwatres.2017.04.019

Merchán-Rivera, P., 2021. Dataset and algorithms for the Bayesian framework to assess and create risk maps of groundwater flooding. Mendeley Data. https://doi.org/10.17632/2j8hy7jfr2.2

Merchán-Rivera, P., Basilio Hazas, M., Marcolini, G., Chiogna, G., 2022. Dataset for the research "Propagation of hydropeaking waves in heterogeneous aquifers: effects on flow topology and uncertainty quantification." Mendeley Data, V1. https://doi.org/10.17632/sk3my3mtd8.1

Merchán-Rivera, P., Chiogna, G., Disse, M., Bhola, P., 2018. Surface water and groundwater interaction during flood events in the Alz Valley: Numerical modeling and solute transport simulations, in: Agua Subterránea., Interacción de Agua Superficial y Agua Subterránea. Hidrogeología de Salares. Presented at the XIV Congreso Latinoamericano de Hidrogeología, Editorial de la Universidad Nacional de Salta, Salta, Argentina.

Merchán-Rivera, P., Wohlmuth, B., Chiogna, G., 2021. Identifying Stagnation Zones and Reverse Flow Caused by River-Aquifer Interaction: An Approach Based on Polynomial Chaos Expansions. Water Res. https://doi.org/10.1029/2021WR029824

Merz, B., Thieken, A.H., 2009. Flood risk curves and uncertainty bounds. Nat Hazards 51, 437–458. https://doi.org/10.1007/s11069-009-9452-6

Mohd Anuar, M.A., Mohd Adnan, M.S., Lim, F.H., 2022. Uncertainty in River Hydraulic Modelling: A Review for Fundamental Understanding, in: Mohamed Noor, N., Sam, S.T., Abdul Kadir, A. (Eds.), Proceedings of the 3rd International Conference on Green Environmental Engineering and Technology, Lecture Notes in Civil Engineering. Springer Singapore, Singapore, pp. 215–220. https://doi.org/10.1007/978-981-16-7920-9_25

Morel-Seytoux, H.J., 2019. MODFLOW's River Package: Part 1: A Critique. PSIJ 1–9. https://doi.org/10.9734/psij/2019/v22i230129

Morel-Seytoux, H.J., Miller, C.D., Miracapillo, C., Mehl, S., 2017. River Seepage Conductance in Large-Scale Regional Studies. Groundwater 55, 399–407. https://doi.org/10.1111/gwat.12491

Morris, M.D., 1991. Factorial Sampling Plans for Preliminary Computational Experiments. Technometrics 33, 161–174. https://doi.org/10.1080/00401706.1991.10484804

Morris, S.E., Cobby, D., Zaidman, M., Fisher, K., 2018. Modelling and mapping groundwater flooding at the ground surface in Chalk catchments: Modelling and mapping groundwater flooding. J. Flood Risk Manage 11, S251–S268. https://doi.org/10.1111/jfr3.12201

Morrissey, P., McCormack, T., Naughton, O., Meredith Johnston, P., William Gill, L., 2020. Modelling groundwater flooding in a lowland karst catchment. Journal of Hydrology 580, 124361. https://doi.org/10.1016/j.jhydrol.2019.124361

Moslehi, M., de Barros, F.P.J., 2017. Uncertainty quantification of environmental performance metrics in heterogeneous aquifers with long-range correlations. Journal of Contaminant Hydrology 196, 21–29. https://doi.org/10.1016/j.jconhyd.2016.12.002

Mustafa, S.Md.T., Nossent, J., Ghysels, G., Huysmans, M., 2018. Estimation and Impact Assessment of Input and Parameter Uncertainty in Predicting Groundwater Flow With a Fully Distributed Model. Water Resour. Res. 54, 6585–6608. https://doi.org/10.1029/2017WR021857

Neupauer, R.M., Meiss, J.D., Mays, D.C., 2014. Chaotic advection and reaction during engineered injection and extraction in heterogeneous porous media. Water Resour. Res. 50, 1433–1447. https://doi.org/10.1002/2013WR014057

Nowak, W., de Barros, F.P.J., Rubin, Y., 2010. Bayesian geostatistical design: Task-driven optimal site investigation when the geostatistical model is uncertain. Water Resour. Res. 46. https://doi.org/10.1029/2009WR008312

Okubo, A., 1970. Horizontal dispersion of floatable particles in the vicinity of velocity singularities such as convergences. Deep Sea Research and Oceanographic Abstracts 17, 445–454. https://doi.org/10.1016/0011-7471(70)90059-8

Oladyshkin, S., de Barros, F.P.J., Nowak, W., 2012. Global sensitivity analysis: A flexible and efficient framework with an example from stochastic hydrogeology. Advances in Water Resources 37, 10–22. https://doi.org/10.1016/j.advwatres.2011.11.001

Osman, K.T., 2013. Forest Soils: Properties and Management, 1st ed. 2013. ed. Springer International Publishing : Imprint: Springer, Cham. https://doi.org/10.1007/978-3-319-02541-4

Oyedele, K.F., Ayolabi, E.A., Adeoti, L., Adegbola, R.B., 2009. Geophysical and hydrogeological evaluation of rising groundwater level in the coastal areas of Lagos, Nigeria. Bull Eng Geol Environ 68, 137–143. https://doi.org/10.1007/s10064-008-0182-x

Pappenberger, F., Matgen, P., Beven, K.J., Henry, J.-B., Pfister, L., Fraipont, P., 2006. Influence of uncertain boundary conditions and model structure on flood inundation predictions. Advances in Water Resources 29, 1430–1449. https://doi.org/10.1016/j.advwatres.2005.11.012

Pérez Ciria, T., Labat, D., Chiogna, G., 2019. Detection and interpretation of recent and historical streamflow alterations caused by river damming and hydropower production in the Adige and Inn river basins using continuous, discrete and multiresolution wavelet analysis. Journal of Hydrology 578, 124021. https://doi.org/10.1016/j.jhydrol.2019.124021

Pérez Ciria, T., Puspitarini, H.D., Chiogna, G., François, B., Borga, M., 2020. Multi-temporal scale analysis of complementarity between hydro and solar power along an alpine transect. Science of The Total Environment 741, 140179. https://doi.org/10.1016/j.scitotenv.2020.140179

Peyrard, D., Sauvage, S., Vervier, P., Sanchez-Perez, J.M., Quintard, M., 2008. A coupled vertically integrated model to describe lateral exchanges between surface and subsurface in large alluvial floodplains with a fully penetrating river. Hydrol. Process. 22, 4257–4273. https://doi.org/10.1002/hyp.7035

Pfister, L., Kirchner, J.W., 2017. Debates-Hypothesis testing in hydrology: Theory and practice: HYPOTHESIS TESTING IN HYDROLOGY. Water Resour. Res. 53, 1792–1798. https://doi.org/10.1002/2016WR020116

Pinay, G., Peiffer, S., De Dreuzy, J.-R., Krause, S., Hannah, D.M., Fleckenstein, J.H., Sebilo, M., Bishop, K., Hubert-Moy, L., 2015. Upscaling Nitrogen Removal Capacity from Local Hotspots to Low Stream Orders' Drainage Basins. Ecosystems 18, 1101–1120. https://doi.org/10.1007/s10021-015-9878-5

Pollock, D.W., 2012. User Guide for MODPATH Version 6—A Particle-Tracking Model for MODFLOW, Open-File Report, U.S. Geological Survey Techniques and Methods 6–A41. The Survey ; U.S. Geological Survey, Earth Science Information Center [distributor],. https://doi.org/10.3133/ofr94464

Preene, M., Fisher, S., 2015. Impacts from groundwater control in urban areas 6.

Rajabi, M.M., 2019. Review and comparison of two meta-model-based uncertainty propagation analysis methods in groundwater applications: polynomial chaos expansion and Gaussian process emulation. Stoch Environ Res Risk Assess 33, 607–631. https://doi.org/10.1007/s00477-018-1637-7

Rajabi, M.M., Ataie-Ashtiani, B., 2016. Efficient fuzzy Bayesian inference algorithms for incorporating expert knowledge in parameter estimation. Journal of Hydrology 536, 255–272. https://doi.org/10.1016/j.jhydrol.2016.02.029

Rajabi, M.M., Ataie-Ashtiani, B., Simmons, C.T., 2015. Polynomial chaos expansions for uncertainty propagation and moment independent sensitivity analysis of seawater intrusion simulations. Journal of Hydrology 520, 101–122. https://doi.org/10.1016/j.jhydrol.2014.11.020

Raudkivi, A.J., 2014. Hydrology: an Advanced Introduction to Hydrological Processes and Modelling. Elsevier Science, Kent.

Reddy, P.J.R., 2005. A Text Book of Hydrology. Laxmi Publications.

Ren, J., Zhao, B., 2020. Model-Based Analysis of the Effects of Rippled Bed Morphologies on Hyporheic Exchange. J. Hydrol. Eng. 25, 04020023. https://doi.org/10.1061/(ASCE)HE.1943-5584.0001931

Roache, P.J., 1997. Quantification of uncertainty in computational fluid dynamics. Annu. Rev. Fluid Mech. 29, 123–160. https://doi.org/10.1146/annurev.fluid.29.1.123

Rocchetta, R., Broggi, M., Patelli, E., 2018. Do we have enough data? Robust reliability via uncertainty quantification. Applied Mathematical Modelling 54, 710–721. https://doi.org/10.1016/j.apm.2017.10.020

Rolle, M., Le Borgne, T., 2019. Mixing and Reactive Fronts in the Subsurface. Reviews in Mineralogy and Geochemistry 85, 111–142. https://doi.org/10.2138/rmg.2018.85.5

Ross, J.L., Ozbek, M.M., Pinder, G.F., 2009. Aleatoric and epistemic uncertainty in groundwater flow and transport simulation. Water Resources Research 45. https://doi.org/10.1029/2007WR006799

Roullet, G., Klein, P., 2010. Cyclone-Anticyclone Asymmetry in Geophysical Turbulence. Phys. Rev. Lett. 104, 218501. https://doi.org/10.1103/PhysRevLett.104.218501

Saidi, H., Ciampittiello, M., Dresti, C., Turconi, L., 2014. Extreme rainfall events: evaluation with different instruments and measurement reliability. Environ Earth Sci 72, 4607–4616. https://doi.org/10.1007/s12665-014-3358-7

Saltelli, A., 2002. Sensitivity Analysis for Importance Assessment. Risk Analysis 22, 579–590. https://doi.org/10.1111/0272-4332.00040

Saltelli, A., Aleksankina, K., Becker, W., Fennell, P., Ferretti, F., Holst, N., Li, S., Wu, Q., 2019. Why so many published sensitivity analyses are false: A systematic review of sensitivity analysis practices. Environmental Modelling & Software 114, 29–39. https://doi.org/10.1016/j.envsoft.2019.01.012

Saltelli, A., Tarantola, S., Campolongo, F., Ratto, M., 2004. Sensitivity Analysis in Practice: A Guide to Assessing Scientific Models. John Wiley & Sons.

Sanchez-Vila, X., Fernàndez-Garcia, D., 2016. Debates-Stochastic subsurface hydrology from theory to practice: Why stochastic modeling has not yet permeated into practitioners? Water Resour. Res. 52, 9246–9258. https://doi.org/10.1002/2016WR019302

Santizo, K.Y., Widdowson, M.A., Hester, E.T., 2020. Abiotic Mixing-Dependent Reaction in a Laboratory Simulated Hyporheic Zone. Water Resour. Res. 56. https://doi.org/10.1029/2020WR027090

Sawyer, A., Bayani Cardenas, M., Bomar, A., Mackey, M., 2009. Impact of dam operations on hyporheic exchange in the riparian zone of a regulated river. Hydrol. Process. 23, 2129–2137. https://doi.org/10.1002/hyp.7324

Scheibe, T.D., Murphy, E.M., Chen, X., Rice, A.K., Carroll, K.C., Palmer, B.J., Tartakovsky, A.M., Battiato, I., Wood, B.D., 2015. An Analysis Platform for Multiscale Hydrogeologic Modeling with Emphasis on Hybrid Multiscale Methods. Groundwater 53, 38–56. https://doi.org/10.1111/gwat.12179

Schmadel, N.M., Ward, A.S., Lowry, C.S., Malzone, J.M., 2016. Hyporheic exchange controlled by dynamic hydrologic boundary conditions: Dynamic Hyporheic Exchange. Geophys. Res. Lett. 43, 4408–4417. https://doi.org/10.1002/2016GL068286

Schoups, G., Vrugt, J.A., 2010. A formal likelihood function for parameter and predictive inference of hydrologic models with correlated, heteroscedastic, and non-Gaussian errors. Water Resour. Res. 46, 2009WR008933. https://doi.org/10.1029/2009WR008933

Scott, D.W., 2014. Multivariate density estimation: theory, practice, and visualization, Second edition. ed. Wiley, Hoboken, New Jersey.

Sharma, A.S., Bunde, A., Dimri, V.P., Baker, D.N., 2013. Extreme Events and Natural Hazards the Complexity Perspective. Wiley, Washington.

Silverman, B.W., 1998. Density estimation for statistics and data analysis, Monographs on statistics and applied probability. Chapman & Hall/CRC, Boca Raton.

Singh, S.K., 2004. Aquifer Response to Sinusoidal or Arbitrary Stage of Semipervious Stream. J. Hydraul. Eng. 130, 1108–1118. https://doi.org/10.1061/(ASCE)0733-9429(2004)130:11(1108)

Singh, T., Gomez-Velez, J.D., Wu, L., Wörman, A., Hannah, D.M., Krause, S., 2020. Effects of Successive Peak Flow Events on Hyporheic Exchange and Residence Times. Water Resour. Res. 56. https://doi.org/10.1029/2020WR027113

Singh, T., Wu, L., Gomez-Velez, J.D., Lewandowski, J., Hannah, D.M., Krause, S., 2019. Dynamic Hyporheic Zones: Exploring the Role of Peak Flow Events on Bedform-Induced Hyporheic Exchange. Water Resour. Res. 55, 218–235. https://doi.org/10.1029/2018WR022993

Sivakumar, B., 2017. Characteristics of Hydrologic Systems, in: Chaos in Hydrology. Springer Netherlands, Dordrecht, pp. 29–62. https://doi.org/10.1007/978-90-481-2552-4_2

Smith, R.C., 2013. Uncertainty Quantification: Theory, Implementation, and Applications, Computational Science and Engineering. SIAM.

Sochala, P., Le Maître, O.P., 2013. Polynomial Chaos expansion for subsurface flows with uncertain soil parameters. Advances in Water Resources 62, 139–154. https://doi.org/10.1016/j.advwatres.2013.10.003

Song, X., Chen, X., Zachara, J.M., Gomez-Velez, J.D., Shuai, P., Ren, H., Hammond, G.E., 2020. River Dynamics Control Transit Time Distributions and Biogeochemical Reactions in a Dam-Regulated River Corridor. Water Resour. Res. 56. https://doi.org/10.1029/2019WR026470

Sophocleous, M., 2002. Interactions between groundwater and surface water: the state of the science. Hydrogeology Journal 10, 52–67. https://doi.org/10.1007/s10040-001-0170-8

Soren, J., 1976. Basement flooding and foundation damage from water-table rise in the East New York section of Brooklyn, Long Island, New York (USGS Numbered Series No. 76–95), Basement flooding and foundation damage from water-table rise in the East New York section of Brooklyn, Long Island, New York, Water-Resources Investigations Report. U.S. Geological Survey. https://doi.org/10.3133/wri7695

Stanford, J.A., Ward, J.V., 1988. The hyporheic habitat of river ecosystems. Nature 335, 64–66. https://doi.org/10.1038/335064a0

Stanko, Z.P., Boyce, S.E., Yeh, W.W.-G., 2016. Nonlinear model reduction of unconfined groundwater flow using POD and DEIM. Advances in Water Resources 97, 130–143. https://doi.org/10.1016/j.advwatres.2016.09.005

Stewardson, M.J., Datry, T., Lamouroux, N., Pella, H., Thommeret, N., Valette, L., Grant, S.B., 2016. Variation in reach-scale hydraulic conductivity of streambeds. Geomorphology 259, 70–80. https://doi.org/10.1016/j.geomorph.2016.02.001

Sudret, B., 2008. Global sensitivity analysis using polynomial chaos expansions. Reliability Engineering & System Safety 93, 964–979. https://doi.org/10.1016/j.ress.2007.04.002

Sullivan, T.J., 2015. Introduction to Uncertainty Quantification, 1st ed. 2015. ed, Texts in Applied Mathematics. Springer International Publishing : Imprint: Springer, Cham. https://doi.org/10.1007/978-3-319-23395-6

Sund, N.L., Bolster, D., Dawson, C., 2015. Upscaling transport of a reacting solute through a peridocially converging–diverging channel at pre-asymptotic times. Journal of Contaminant Hydrology 182, 1–15. https://doi.org/10.1016/j.jconhyd.2015.08.003

Tabari, H., 2020. Climate change impact on flood and extreme precipitation increases with water availability. Sci Rep 10, 13768. https://doi.org/10.1038/s41598-020-70816-2

Tang, Q., Kurtz, W., Brunner, P., Vereecken, H., Hendricks Franssen, H.-J., 2015. Characterisation of river–aquifer exchange fluxes: The role of spatial patterns of riverbed hydraulic conductivities. Journal of Hydrology 531, 111–123. https://doi.org/10.1016/j.jhydrol.2015.08.019

Tang, Q., Kurtz, W., Schilling, O.S., Brunner, P., Vereecken, H., Hendricks Franssen, H.-J., 2017. The influence of riverbed heterogeneity patterns on river-aquifer exchange fluxes under different connection regimes. Journal of Hydrology 554, 383–396. https://doi.org/10.1016/j.jhydrol.2017.09.031

Tarantola, A., 2005. Inverse Problem Theory and Methods for Model Parameter Estimation. SIAM.

Teixeira Parente, M., Bittner, D., Mattis, S.A., Chiogna, G., Wohlmuth, B., 2019. Bayesian Calibration and Sensitivity Analysis for a Karst Aquifer Model Using Active Subspaces. Water Resour. Res. 55, 7086–7107. https://doi.org/10.1029/2019WR024739

Teng, J., Jakeman, A.J., Vaze, J., Croke, B.F.W., Dutta, D., Kim, S., 2017. Flood inundation modelling: A review of methods, recent advances and uncertainty analysis. Environmental Modelling & Software 90, 201–216. https://doi.org/10.1016/j.envsoft.2017.01.006

Texeira Parente, M., 2020. Active Subspaces in Bayesian Inverse Problems. Technische Universität München, Munich.

Tian, Y., Xiong, J., He, X., Pi, X., Jiang, S., Han, F., Zheng, Y., 2018. Joint Operation of Surface Water and Groundwater Reservoirs to Address Water Conflicts in Arid Regions: An Integrated Modeling Study. Water 10, 1105. https://doi.org/10.3390/w10081105

Tóth, J., 1963. A theoretical analysis of groundwater flow in small drainage basins. J. Geophys. Res. 68, 4795–4812. https://doi.org/10.1029/JZ068i016p04795

Traub, F., 1975. Quartärgeologische Beobachtungen zwischen Alz und Salzach. Geologica Bavarica.

Trauth, N., Fleckenstein, J.H., 2017. Single discharge events increase reactive efficiency of the hyporheic zone. Water Resour. Res. 53, 779–798. https://doi.org/10.1002/2016WR019488

Upton, K.A., Jackson, C.R., 2011. Simulation of the spatio-temporal extent of groundwater flooding using statistical methods of hydrograph classification and lumped parameter models. Hydrol. Process. 25, 1949–1963. https://doi.org/10.1002/hyp.7951

Valocchi, A.J., Bolster, D., Werth, C.J., 2019. Mixing-Limited Reactions in Porous Media. Transp Porous Med 130, 157–182. https://doi.org/10.1007/s11242-018-1204-1

Virtanen, P., Gommers, R., Oliphant, T.E., Haberland, M., Reddy, T., Cournapeau, D., Burovski, E., Peterson, P., Weckesser, W., Bright, J., van der Walt, S.J., Brett, M., Wilson, J., Millman, K.J., Mayorov, N., Nelson, A.R.J., Jones, E., Kern, R., Larson, E., Carey, C.J., Polat, İ., Feng, Y., Moore, E.W., VanderPlas, J., Laxalde, D., Perktold, J., Cimrman, R., Henriksen, I., Quintero, E.A., Harris, C.R., Archibald, A.M., Ribeiro, A.H., Pedregosa, F., van Mulbregt, P., 2020. SciPy 1.0: fundamental algorithms for scientific computing in Python. Nat Methods 17, 261–272. https://doi.org/10.1038/s41592-019-0686-2

Vrugt, J.A., 2016. Markov chain Monte Carlo simulation using the DREAM software package: Theory, concepts, and MATLAB implementation. Environmental Modelling & Software 75, 273–316. https://doi.org/10.1016/j.envsoft.2015.08.013

Vrugt, J.A., Gupta, H.V., Bouten, W., Sorooshian, S., 2003. A Shuffled Complex Evolution Metropolis algorithm for optimization and uncertainty assessment of hydrologic model parameters. Water Resour. Res. 39. https://doi.org/10.1029/2002WR001642

Vrugt, J.A., Ter Braak, C.J.F., 2011. DREAM(D): an adaptive Markov Chain Monte Carlo simulation algorithm to solve discrete, noncontinuous, and combinatorial posterior parameter estimation problems. Hydrol. Earth Syst. Sci. 15, 3701–3713. https://doi.org/10.5194/hess-15-3701-2011

Vrugt, J.A., ter Braak, C.J.F., Clark, M.P., Hyman, J.M., Robinson, B.A., 2008. Treatment of input uncertainty in hydrologic modeling: Doing hydrology backward with Markov chain Monte Carlo simulation. Water Resour. Res. 44. https://doi.org/10.1029/2007WR006720

Vrugt, J.A., ter Braak, C.J.F., Diks, C.G.H., Robinson, B.A., Hyman, J.M., Higdon, D., 2009. Accelerating Markov Chain Monte Carlo Simulation by Differential Evolution with Self-Adaptive Randomized Subspace Sampling. International Journal of Nonlinear Sciences and Numerical Simulation 10. https://doi.org/10.1515/IJNSNS.2009.10.3.273

Wagner, B., Hauer, C., Schoder, A., Habersack, H., 2015. A review of hydropower in Austria: Past, present and future development. Renewable and Sustainable Energy Reviews 50, 304–314. https://doi.org/10.1016/j.rser.2015.04.169

Wallace, C.D., Tonina, D., McGarr, J.T., Barros, F.P.J., Soltanian, M.R., 2021. Spatiotemporal Dynamics of Nitrous Oxide Emission Hotspots in Heterogeneous Riparian Sediments. Water Resources Research 57. https://doi.org/10.1029/2021WR030496

Wand, M.P., Jones, M.C., 1995. Kernel smoothing, 1st ed. ed, Monographs on statistics and applied probability. Chapman & Hall, London ; New York.

Wang, X.-S., Wan, L., Jiang, X.-W., Li, H., Zhou, Y., Wang, J., Ji, X., 2017. Identifying three-dimensional nested groundwater flow systems in a Tóthian basin. Advances in Water Resources 108, 139–156. https://doi.org/10.1016/j.advwatres.2017.07.016

Ward, A.D., Trimble, S.W., Burckhard, S.R., Lyon, J.G., 2016. Environmental hydrology, Third edition. ed. CRC Press, Taylor & Francis Group, Boca Raton, FL.

Weiss, J., 1991. The dynamics of enstrophy transfer in two-dimensional hydrodynamics. Physica D: Nonlinear Phenomena 48, 273–294. https://doi.org/10.1016/0167-2789(91)90088-Q

Welch, C., Cook, P.G., Harrington, G.A., Robinson, N.I., 2013. Propagation of solutes and pressure into aquifers following river stage rise: PROPAGATION OF SOLUTES AND PRESSURE INTO AQUIFERS. Water Resour. Res. 49, 5246–5259. https://doi.org/10.1002/wrcr.20408

Willems, W., 2011. Unsicherheit von Wasserstands- und Abflussmessungen an A-Pegeln des Landes Bayern, Auftragsstudie für das Bayerische Landesamt für Umwelt. LfU Bayern.

Willems, W., Stricker, K., 2012. Bewertung der Qualität von Abflusszeitreihendaten anhand eines mathematisch/statistisch ermittelten Unsicherheitskriteriums, Auftragsstudie für das Bayerische Landesamt für Umwelt. LfU Bayern.

Winsemius, H.C., Aerts, J.C.J.H., van Beek, L.P.H., Bierkens, M.F.P., Bouwman, A., Jongman, B., Kwadijk, J.C.J., Ligtvoet, W., Lucas, P.L., van Vuuren, D.P., Ward, P.J., 2016. Global drivers of future river flood risk. Nature Clim Change 6, 381–385. https://doi.org/10.1038/nclimate2893

Winter, T.C., 1999. Relation of streams, lakes, and wetlands to groundwater flow systems. Hydrogeology Journal 7, 28–45. https://doi.org/10.1007/s100400050178

Winter, T.C. (Ed.), 1998. Ground water and surface water: a single resource, U.S. Geological Survey circular. U.S. Geological Survey, Denver, Colo.

Winter, T.C., 1976. Numerical simulation analysis of the interaction of lakes and ground water (USGS Numbered Series No. 1001), Numerical simulation analysis of the interaction of lakes and ground water, Professional Paper. U.S. Government Printing Office, Washington, D.C. https://doi.org/10.3133/pp1001

Woessner, W.W., 2000. Stream and Fluvial Plain Ground Water Interactions: Rescaling Hydrogeologic Thought. Ground Water 38, 423–429. https://doi.org/10.1111/j.1745-6584.2000.tb00228.x

Wondzell, S.M., Swanson, F.J., 1999. Floods, channel change, and the hyporheic zone. Water Resour. Res. 35, 555–567. https://doi.org/10.1029/1998WR900047

Wright, E.E., Richter, D.H., Bolster, D., 2017. Effects of incomplete mixing on reactive transport in flows through heterogeneous porous media. Phys. Rev. Fluids 2, 114501. https://doi.org/10.1103/PhysRevFluids.2.114501

Wu, L., Singh, T., Gomez-Velez, J., Nützmann, G., Wörman, A., Krause, S., Lewandowski, J., 2018. Impact of Dynamically Changing Discharge on Hyporheic Exchange Processes Under Gaining and Losing Groundwater Conditions. Water Resour. Res. 54. https://doi.org/10.1029/2018WR023185

Xiu, D., 2010. Numerical methods for stochastic computations: a spectral method approach. Princeton University Press, Princeton, N.J.

Xiu, D., 2009. Fast Numerical Methods for Stochastic Computations: A Review. Communications in Computational Physics.

Xiu, D., 2007. Efficient collocational approach for parametric uncertainty analysis. Commun. Comput. Phys 293–309.

Xiu, D., Karniadakis, G.E., 2002. The Wiener-Askey Polynomial Chaos for Stochastic Differential Equations. SIAM J. Sci. Comput. 24, 619–644. https://doi.org/10.1137/S1064827501387826

Xu, T., Valocchi, A.J., Ye, M., Liang, F., Lin, Y., 2017. Bayesian calibration of groundwater models with input data uncertainty. Water Resour. Res. 53, 3224–3245. https://doi.org/10.1002/2016WR019512

Yu, X., Moraetis, D., Nikolaidis, N.P., Li, B., Duffy, C., Liu, B., 2019. A coupled surface-subsurface hydrologic model to assess groundwater flood risk spatially and temporally. Environmental Modelling & Software 114, 129–139. https://doi.org/10.1016/j.envsoft.2019.01.008

Zeng, X., Wu, J., Wang, D., Zhu, X., Long, Y., 2016. Assessing Bayesian model averaging uncertainty of groundwater modeling based on information entropy method. Journal of Hydrology 538, 689–704. https://doi.org/10.1016/j.jhydrol.2016.04.038

Zhang, D., Lu, Z., 2004. An efficient, high-order perturbation approach for flow in random porous media via Karhunen–Loève and polynomial expansions. Journal of Computational Physics 194, 773–794. https://doi.org/10.1016/j.jcp.2003.09.015

Zhang, P., DeVries, S.L., Dathe, A., Bagtzoglou, A.C., 2009. Enhanced Mixing and Plume Containment in Porous Media under Time-Dependent Oscillatory Flow. Environ. Sci. Technol. 43, 6283–6288. https://doi.org/10.1021/es900854r

Zheng, C., Wang, P., 1999. MT3DMS: A modular three-dimensional multispecies transport model for simulation of advection, dispersion and chemical reactions of contaminants in groundwater systems. The University of Alabama. and U.S. Army Corps of Engineers.

Zhou, H., Gómez-Hernández, J.J., Li, L., 2014. Inverse methods in hydrogeology: Evolution and recent trends. Advances in Water Resources 63, 22–37. https://doi.org/10.1016/j.advwatres.2013.10.014

Ziliotto, F., Basilio Hazas, M., Rolle, M., Chiogna, G., 2021. Mixing Enhancement Mechanisms in Aquifers Affected by Hydropeaking: Insights From Flow-Through Laboratory Experiments. Geophys Res Lett 48. https://doi.org/10.1029/2021GL095336